BIOCHEMICAL CHARACTERIZATION OF THE WALKR AND THE LYTSR TWO COMPONENT SYSTEM OF *STAPHYLOCOCCUS AUREUS*

KEVIN PATEL

A THESIS SUBMITTED TO
THE FACULTY OF GRADUATE STUDIES
IN PARTIAL FULFULLMENT OF THE REQUIREMENTS
FOR THE DEGREE OF MASTER OF SCIENCE

GRADUATE PROGRAM IN CHMISTRY
YORK UNIVERSITY
TORONTO, ONTARIO

JANUARY 2014

© KEVIN PATEL 2014

ABSTRACT

Staphylococcus aureus is a major gram-positive pathogen, because of its remarkable capacity to develop resistance against different antimicrobial agents. It has been shown that in *S. aureus* two component systems (TCS) play an important role in responding to stress induced by antibiotics. Given the regulatory importance of TCS, herein we investigate *in vitro* the signal transduction mechanism of the WalKR, and the LytSR TCSs. These TCSs play a role in susceptibility towards cell wall active antibiotics and cationic antimicrobial agents, respectively. We found that both kinases, WalK and LytS, are active *in vitro* and capable of catalyzing ATP-dependent autophosphorylation and subsequent phosphoryl transfer reactions to their cognate response regulators WalR and LytR. In contrast to LytS, the autokinase activity of WalK is highly dependent on K^+ and Ca^{2+} ions. We found that LytR undergoes phosphorylation by small molecule phosphate donors such as acetyl phosphate. Phosphorylation of LytR leads to dimerization of the N-terminal domain. Furthermore, we show that LytR has the ability to bind to the promoter region of *lrgAB* in its unphosphorylated state. Taken together, these data provide *in vitro* proof of phosphorylation mediated signal flow in the WalKR and LytSR TCSs.

ACKNOWLEDGMENTS

Foremost, I would like to take this opportunity to express my special appreciation and thanks to my supervisor, Dr. Golemi-Kotra, who gave me an opportunity to work in her lab. She has been a great mentor for me throughout the last two years. I am truly thankful to her for encouraging my research and providing me with insightful guidance throughout the project. I enjoyed working in her lab and am proud of being her student.

Next, I would also like to thank the members of my examining committee, including Dr. Morin, Dr, Audette and Dr. Sheng for serving as my committee members and for taking their precious time to reflect on my research with constructive comments and suggestions.

Furthermore, a thank you to Martin Romero for all his help in the lab, to Preet Gill for all those coffee and chai tea runs to timmy's and to all of my friends who supported me during my writing.

Lastly, a special thanks to my mother and father for all of the sacrifices that you had to make on my behalf and for teaching me to strive towards my goal. And mother this thesis would not have been possible without your lunches. To you I dedicate this thesis.

TABLE OF CONTENTS

CHAPTER TWO: KINETIC CHARACTERIZATION OF THE WALKR TWO COMPONENT SYSTEM

CHAPTER THREE: *IN VITRO* CHARACTERIZATION AND PHOSPHRYLATION KINETICS OF THE LYTSR TWO COMPONENT SYSTEM

APPENDICES:

LIST OF FIGURES

CHAPTER ONE

CHAPTER TWO

CHAPTER THREE

LIST OF ABBREVIATIONS

Ala – Alanine

Asp – Aspartic acid

ATP – Adenosine triphosphate

Da – Dalton

EMSA – Electro-mobility shoft assay

ESI-MS – Electrospray ionization mass spectrometry

FPLC – Fast protein liquid chromatography

GST – Glutathione S-transferase

His – Histidine

HPLC – High performance liquid chromatography

IPTG – Isopropyl β-D-1-thiogalactopyranoside

LB – Luria bertani

LC MS – Liquid chromatography mass spectrommetry

MIC – Minimum inhibitory concentration

MRSA – Methicillin resistant staphylococcus aureus

NAG – N-Acetylglucosamine

NAM – N-Acetylmuramic acid

Ni-NTA – Nickel-nitrilotriacetic acid

PB – Phosphorylation buffer

PBP – Penicillin binidng protein

PCR – Polymerase chain reaction

PG – Peptidoglycan

PNK – poly nucletide kinase

RPM – Rotations per minute

SDS – Sodium dodecyl sulfate

SDS-PAGE – Sodium dodecyl sulfate-polyacrylamide gel electrophoresis

TCS – Two component system

TSB – Tryptic soy broth

VRSA – Vancomycin resistant staphylococcus aureus

CHAPTER ONE

INTRODUCTION

1.1 *Staphylococcus aureus*, the pathogen

The *Staphylococcus aureus* bacterium, commonly referred to as 'staph' was discovered in 1882 by a Scottish surgeon Alexander Ogston in his effort to identify the etiology of suppuration (formation of pus) in humans (Ogston 1882, Ogston 1984). The name "Staphylococci" was given to represent its round grape-like clustered morphology and "aureus" for its ability to form golden to yellow pigmented colonies (Ogston 1882, Baird-Parker 1990).

S. aureus is a facultative gram-positive bacterium that can thrive in the presence or absence of oxygen. It is both catalase- and coagulase- positive strain and this is used as one of the major criteria for identifying the organism in laboratory. Its ability to produce catalase, an enzyme that decomposes hydrogen peroxide to water and oxygen is used to distinguish it from other *Enterococci* and *Streptococci*. The presence of coagulase, used in conversion of fibrinogen to fibrin resulting in clotting of the blood, is a traditional marker used to discern the virulent pathogen, *S. aureus,* from less virulent coagulase-negative *Staphylococci* species (Kloos and Schleifer 1975).

S. aureus is nonmotile, non spore-forming and is widely distributed in nature. It is both a commensal, carried by 30% of healthy individuals in the anterior nares or skin and an extremely versatile pathogen. (Peacock, Curtis et al. 1999, Ozaki, Saito et al. 2013). It is an opportunistic pathogen with a high tendency to colonize abnormal skin surfaces and

open wounds, where it may merely reside asymptomatically for weeks without sourcing an active infection. In a hospital environment it is known to colonize inert medical objects such as surgical prosthetics and dialysis catheters and cause most of the nosocomial infections (Peacock, Curtis et al. 1999, Raad, Hanna et al. 2007, Deurenberg and Stobberingh 2008).

Its pathogencity precedes its reputation to pave its way into a systematic infection. In many cases, *S. aureus* first colonizes the host and given the opportunity it can enter the internal skin tissue or mucosal layer causing local infection such as boils or furonculosis (Archer 1998, Lowy 1998). Secondly, if the infection gains access into the bloodstream it can disseminate and cause a metastatic infection involving distant organ systems and ensuing septic shocks, meningitis (Arda, Yamazhan et al. 2005, Kallweit, Harzheim et al. 2007), endocarditis (Lodise, McKinnon et al. 2007), pneumonia (Rubinstein, Kollef et al. 2008, Ebert, Sheth et al. 2009) and other life threatening complications (Archer 1998). These infections are difficult to cure even with aggressive therapy with antimicrobial agents. The potency of *S. aureus* to cause such infections relies on its ability to swiftly control and produce an array of immune evading proteases and virulence factors (Kobayashi and DeLeo 2009). To name a few, it produces extracellular proteins for invasion of host tissues, metalloproteases that destroy host defense molecules (Banbula, Potempa et al. 1998) promoting the infection process and V8 protease (a serine protease) that helps protect against antimicrobial peptides (Prasad, Leduc et al. 2004). Moreover, it produces various toxins such as entrotoxins causing food poisoning and leukocidins, in particular the Panton-Valentine leukocidin (PVL) which is a pore forming toxin that

damages macrophages and neutrophils, thus weakening the host innate immune system (von Eiff, Friedrich et al. 2004, John and Lindsay 2008). However, in a recent study Thwaites and Gant proposed that phagocytes, especially neutrophils may act as privileged host to *S. aureus* in the blood stream, providing protection against popular antibiotics and a transport vehicle to travel and infect distant organs (Thwaites and Gant 2011). These findings are novel and perhaps paradigm shifting for future drug targets and treatment options for persistent bacteremia.

1.2 Antibiotic resistance in *Staphylococcus aureus* and the Evolution of MRSA, VISA and VRSA

1.2.1 History of antibiotic resistance

The origins of antibiotics and antibiotic-resistant in *S. aureus* dates back to 1941 when penicillin was first introduced to clinical practice. Penicillin, produced by *Penicillium*, a mold, was the first antibiotic discovered by a Scottish scientist Alexander Fleming in 1928. The following two decades marked the "era of antibiotic discovery" when more than half the present day antimicrobial drugs were discovered. This was the revolutionizing period in medicine during which time most of the major diseases known to mankind were brought more or less under control. In the "pre-antibiotic era", deaths associated with serious systemic *S. aureus* infection were over 80% and this rate had dropped to 25% by 1944 as a result of penicillin (Dancer 2008). However, this landmark event was short lasting and soon after two years strains of penicillin-resistant *S. aureus* had already emerged and within a decade the mortality rate rose back to 45 %. In

the following decade, these penicillin-resistant *S. aureus* strains became extremely prevalent in hospitals and by the 1960's the strains had spread into the community. To combat and treat infection caused by penicillin-resistant *S. aureus*, in 1960, methicillin, a semi-synthetic penicillin was introduced. However, within a year of methicillin reaching the clinics in 1961, the first documented methicillin-resistant *S. aureus* (MRSA) strain was discovered in the United Kingdom (Barber 1961, Eriksen 1961). As the use of methicillin and other similar penicillins increased, so did the incidence and prevalence of MRSA with MRSA bacteraemia mortality rate reaching 50 %. Subsequently, in the 1950s and early 1960s, many semi-synthetic derivatives of penicillin as well as new classes of antibiotics such as Macrolides, Lincosamides, Quinolones, and Glycopeptides, to name a few (Walsh 2003), were released in massive clinic use and similar resistant pattern in MRSA strains was noted.

As much as people have fueled the fire of antibiotic resistance through rampant overuse and misuse, antibiotic resistance is predominantly an evolution driven process. The prevalence of MRSA strains due to widespread use of antibiotics, suggested selection pressure from antibiotic use (i.e. antibiotics eradicate the methicillin-sensitive strains and leaving the resistant strains to flourish) was largely responsible. As a matter of fact, few years following widespread use of penicillin, a group of scientists discovered that penicillin resistant strains produced penicillinases, a beta-lactamase that can hydrolyze and deactivates penicillin, a beta-lactam antibiotic (Abraham and Chain 1988). By this time it was clear that half-century of antibiotic use undoubtedly modified all aspects of

microbial genetic ecology through mutation, and acquisition of resistance genes (through horizontal gene transfer) among microbes. Furthermore, decades of strong evolutionary pressure and extensive selection facilitated by microbes super-fast evolution rate has made antibiotic resistance inevitable.

Thus, the problem of antibiotic resistance is one of genetic ecology. The last few decades lacked discovery of new antibiotic and most of the available antibiotics today are outdated (Walsh 2003, Nathan 2004). This scarcity of antibiotics has attracted the attention of many scientists and has stimulated research towards deciphering the mechanisms of bacterial resistance, their origin, acquisition and dissemination for development of new drugs.

1.2.2 Evolution of MRSA, VISA and VRSA

S. aureus has always been a difficult pathogen to antimicrobial therapy and has overcome all the therapeutic drugs used to combat its infection in the last half century. MRSA emerged as a nosocomial pathogen in the early 1960s (Mulligan, Murray-Leisure et al. 1993). Since then several multi-drug resistant strains of MRSA arose and they rapidly spread and today they are found worldwide and has been the cause for numerous serious hospital outbreaks that have proved difficult to treat. The first reported United States outbreak of MRSA occurred in 1968 (Palavecino 2004). Subsequently after, Healthcare-associated MRSA (HA-MRSA) strains continued to spread throughout health care facilities but remained mostly confined to health care facilities until 1981(Ayliffe 1997). In 1981, first case of Community-associated MRSA (CA-MRSA) emerged from a Detroit, Michigan hospital (Saravolatz, Pohlod et al. 1982). Compared to HA-MRSA,

CA-MRSA are less resistant to most beta-lactams, however they are more virulent, highly invasive and capable of infecting young healthy people from sport teams, prisons, and military quarters with no hospital connection. This has made CA-MRSA more lethal and difficult to treat.

To combat the widespread of MRSA in both hospital and community facilities, in the late 80s and early 90s it led to the resurgence of Vancomycin, the antibiotic of last resort for MRSA infection. Vancomycin was first introduced in clinical practice in 1956 and since then has been effective in treatment of MRSA infections (Levine 2006). Vancomycin is naturally occurring in the microbe *Streptomyces orientalis* and it belongs to a glycopeptides group of antibiotics (Levine 2006). Most isolates of vancomycin susceptible *S. aureus* (VSSA) strains had a minimum inhibitory concentration (MIC) typically in the range of 0.5 and 2 μg/mL. However not long after strains of *S. aureus* emerged with reduced susceptibility towards vancomycin and other glycopeptides like teicoplanin. In 1996 two vancomycin resistant MRSA strains called MU50 and MU3 were identified in Japan with vancomycin MIC of 8 μg/mL (Hiramatsu, Hanaki et al. 1997). According to the Clinical and Laboratory Standards Institute (CLSI), *S. aureus* isolates for which vancomycin MICs are 8-16 μg/mL are classified as vancomycin intermediate (VISA), and isolates for which vancomycin MICs are ≥ 32 μg/mL are classified as vancomycin-resistant (VRSA) (Appelbaum, 2006). To date all the VISA and VRSA isolated strains have been MRSA with MICs to vancomycin well in to the resistant range, though their prevalence compared to MRSA strains remains very low (Hiramatsu, Hanaki et al. 1997, Hiramatsu, Cui et al. 2001). With the emergence of VRSA, the future

treatment for MRSA infection is blurred and much research is needed to help further understand all aspects of these organisms including their mechanism of resistance.

1.3 Mechanism of antibiotic resistance in MRSA, VISA and VRSA and involvement of peptidoglycan

Significant advancement has been made over the last decade in our understanding of how methicillin resistance is acquired by *S. aureus.* Thus far several mechanisms of resistance have been described, including active efflux of drugs, reduced permeability, alteration and or inactivation of drugs and creation of a decoy drug target (Mazel and Davies 1999). All these mechanism involve proteins that are encoded by clusters of different genes either endogenous or exogenous. Studies have identified two basic genetic mechanisms by which resistance determinants arise: mutation and acquisition of exogenous genes (Hiramatsu, Cui et al. 2001).

MRSA arose when it acquired a large genetic element known as the staphylococcal cassette chromosome (SCC) *mec*. SCC*mec* is a 21-67 kb DNA fragment that integrated in the chromosome of MRSA at a unique site near the origin of replication (Hiramatsu, Cui et al. 2001). Studies have proposed that positioning of SCC*mec* near the origin of replication might serve as strategic significance; enabling *S. aureus* to maintain increased copy number of useful antibiotic resistance genes imported in from other bacterial species (Hiramatsu, Cui et al. 2001). SCC*mec* is a unique class of mobile genetic element that lacks any phage-related genes or any specific transposases. Due to its large size it is regarded as an antibiotic resistance island that carries the *mec* gene complex responsible for encoding genes against most beta-lactam as well as non-beta-lactam

antibiotics. In *S. aureus*, most beta-lactams (penicillin and methicillin) and glycopeptides (vancomycin and teicoplanin) antibiotics exert bactericidal activity through inhibition of cell wall synthesis. To sustain internal osmotic pressure and cell integrity, *S. aureus* need to keep synthesizing a strong extracellular structure called peptidoglycan (PG, also known as murein). Briefly, PG is composed of alternating repeats of two monomeric sugar components, N-acetylglucosamine (NAG) and N-acetylmuramic acid (NAM) linked through a β-(1-4)-glycosidic bond (Fig.1.3.1) also known as the glycosylation reaction. Subsequent crosslinking of nascent PG chain to the already existing chain is achieved though a transpeptidation reaction catalyzed by penicillin binding proteins (PBPs). In this step, terminal $_{D}$-Ala from the pentapeptide chain ($_{L}$-Ala-$_{D}$-Glu-$_{L}$-Lys-$_{D}$-Ala-$_{D}$-Ala) attached to the NAM residues is cleaved off and the penultimate $_{D}$-Ala is ligated through a pentaglycine chain with the protruding $_{L}$-Lys residue of a different NAM unit from the pre-existing PG chain (Hiramatsu 2001), a simplified schematic is shown in Fig.1.3.1. The beta-lactam antibiotic, usually a structural analog of the two terminal $_{D}$-Ala-$_{D}$-Ala, binds covalently to the PBP active site in turn halting the transpeptidation reaction and formation of PG crosslinks (Hiramatsu 2001, Hiramatsu, Cui et al. 2001). This mechanism of action causes cell to rupture and leads to cell death. However, to become resistant, in addition to the four PBPs found in all *S. aureus* strains, MRSA strains produce PBP2a as a fifth PBP with a very low binding affinity for beta-lactam (Hartman and Tomasz 1984, Reynolds and Brown 1985). As a result, PBP2a continues synthesis of PG even in the presence of beta-lactam antibiotics. PBP2a is encoded by the *mec*A gene, an exogenous gene acquired by *S. aure*us though lateral gene transfer, carried by the

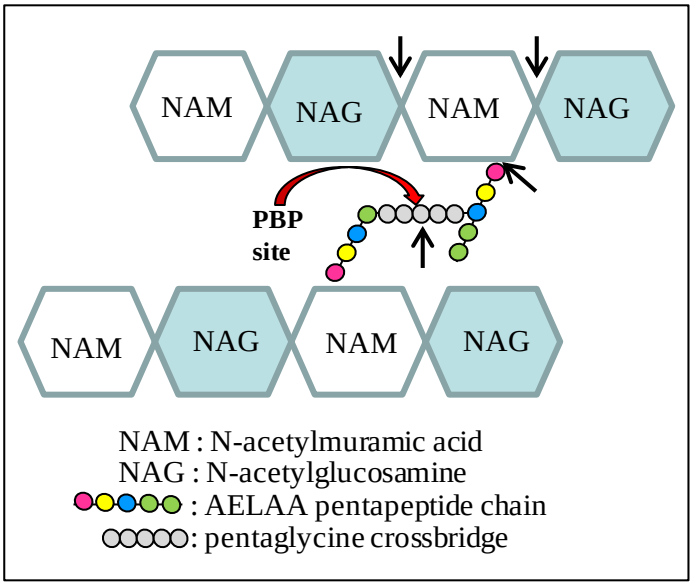

Figure 1.3.1 A schematic of peptidoglycan (PG) crosslinking, site of transpeptidation reaction and cleavage sites for murein hydrolases .

NAG-NAM glycosylation and PG csrosslinking . Red arrow shows PBP mediated transpeptidase reaction and black arrows with lettering points towards cleavage sites for WalKR regulated murein hydrolases.

SCC*mec* cassette (Katayama, Ito et al. 2000). Another way *S. aureus* develops resistant to most beta-lactam is though expression of blaZ, a beta-lactamase enzyme that can hydrolyze and deactivates beta-lactam antibiotic (Lowy 2003).

Mechanism of action and resistance for cell wall active glycopeptides such as vancomycin has also been extensively studied using the clinical isolate of VRSA strain MU50. In contrast to beta-lactam, vancomycin exerts pressure by binding directly to the terminal $_{D}$-Ala-$_{D}$-Ala of the pentapeptide chain (Williams and Kalman 1977). Vancomycin can bind to the $_{D}$-Ala-$_{D}$-Ala of the already existing or nascent PG chain and/or NAM monomers located in the cytoplasmic membrane (Hiramatsu 2001). The former, interferes with the formation of PG crosslinks mediated by PBPs but does not

inhibit nascent PG synthesis, however the latter completely inhibits PG synthesis in turn ceasing cell division. This mode of vancomycin action is only feasible if the molecules can penetrate the PG layers (approximately 20 layers) without being trapped in the first target. Contrary to beta-lactam resistance, vancomycin resistance is not achieved through acquisition of resistance genes, but more so thorough increased biosynthesis of PG and alteration in the NAM pentapeptide chain. As a mechanism of resistance, through biochemical and TEM studies it is revealed that VRSA strains produce thickened cell walls (> 40 layers of PG) whereby most vancomycin molecules are "affinity trapped" and "clogging" the PG mesh and compromising the therapeutic effects of vancomycin (Hiramatsu 2001). Several studies have proposed the regulation of this phenomenon of thickened cell wall through increased cell wall biosynthesis by the global regulatory systems Agr and the two component system VraSR along with their corresponding genes.

In addition to the above mentioned resistance mechanism, VRSA strains gain resistance though alerting the target, terminal $_{D}$-Ala-$_{D}$-Ala of the pentapetide chain. By employing an alternate pathway for nascent PG biosystnthesis, VRSA strains modify the vancomycin target $_{D}$-Ala-$_{D}$-Ala dipeptide of the nascent PG to a decoy $_{D}$-Ala-$_{D}$-Lac dipeptide with a 1000 fold decreased affinity for vancomycin (Bugg, Wright et al. 1991, González-Zorn and Courvalin 2003). This alternate pathway of nascent PG biosynthesis is encoded by the *vanA* operon located on the transposable element Tn1546, carried by a self transferable plasmid (González-Zorn and Courvalin 2003) and interestingly this operon is regulated by the VanSR TCS (Hong, Hutchings et al. 2008). Thus far, it has been an uphill battle against *S. aureus* as many other mechanism of resistance exists but

more research focused towards understating the underlying molecular mechanism of resistance may guide us towards discovering more potent drugs.

1.4 Role of Two component systems in *Staphylococcus aureus*

1.4.1 A brief overview of TCS

Two component systems (TCS) play a vital role in bacterial adaptation to their ever changing environment. They are the most widespread and highly sophisticated signaling mechanism capable of transducing external signal across the cell membrane to initiate specific gene expression or bacterial behavior. Briefly, a typical TCS is consisting of a membrane-bound Histidine Kinase (HK) that is capable of undergoing autophosphorylation at a conserved His residue upon sensing any environmental stimuli and a cytoplasmic Response Regulator (RR) protein, that is capable of receiving the phosphate molecule from its cognate HK and in turn regulating expression of target genes (West and Stock 2001, Laub and Goulian 2007). A schematic view of the TCS signal transduction pathway is shown in Fig. 1.4.1.

TCS are abundant in both gram positive and gram negative pathogenic bacteria where they typically constitute to 1% of the encoded proteins. In this environment they take part in regulating housekeeping genes, control expression of toxins and other protein essential for pathogensis. In MRSA strains, to date 16 TCS have been identified and some of which have been extensively characterized and implicated to affect their susceptibility to antimicrobial agents such as the VraSR (Belcheva and Golemi-Kotra 2008), BceRS (Kawada-Matsuo, Yoshida et al. 2011) and the GraSR (Falord, Mader et al. 2011,

Fridman, Williams et al. 2013). Others however require biochemical characterization and therefore as part of our study we undertook characterization of the WalKR TCS, and the LytSR TCS, implicated to play a role in susceptibility towards cell wall active antibiotics and cationic antimicrobial agents, respectively. A brief introduction for these systems follows.

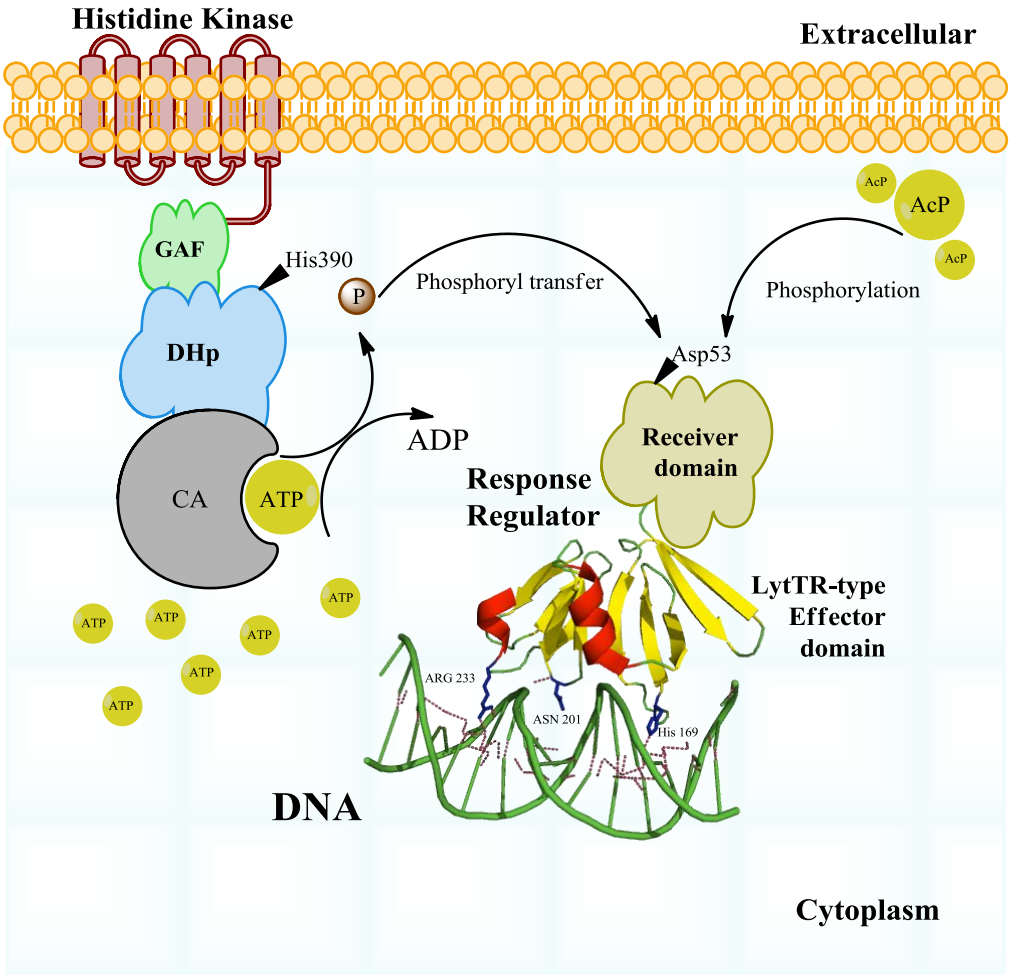

Figure 1.4.1 A schematic diagram of signal flow in a two component system (TCS)

Diagram of phosphoryl signal flow from Histidine kinase (HK) to Response regulator (RR) in a typical two component system leading to regulation of target gene expression

1.4.2 The WalKR system

The WalKR TCS was first discovered in *Bacillus subtilis* (Fabret and Hoch 1998), and since then this system has been widely studied and deemed "essential" for survival in *S. aureus* and several other pathogens (*Streptococcus pneumonia, S.mutans, S.pyogenes, Listeria monocytogenes*, *Enterococcis farcalis*) (Dubrac, Bisicchia et al. 2008). The WalKR system, formerly designated as the YycGF, VicKR or MicAB, was later renamed to reflect its function as the master regulatory system for cell wall metabolism. It is conserved throughout low G+C % gram positive bacteria where it is known to encode genes associated with murein hydrolases and biofilm formation (Fig 1.3.1). In *S. aureus* it is part of a five cistron operon that encodes other accessory proteins hypothesized to aid in its activity. The operons organization is shown in Fig. 1.4.2.

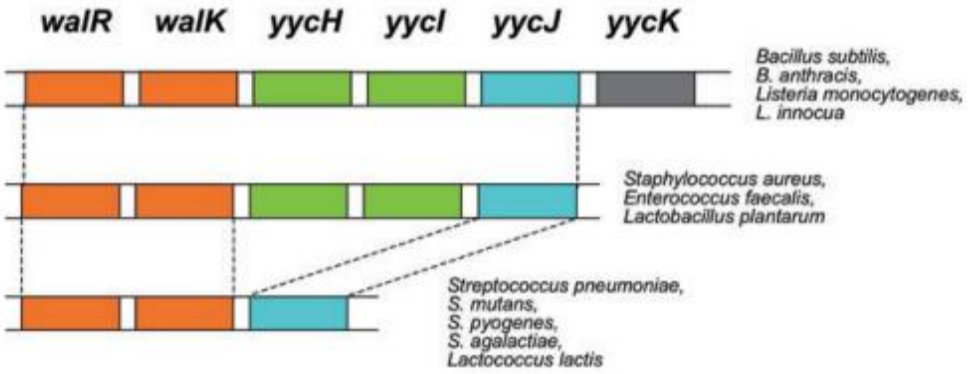

Figure 1.4.2 Organization of the *walKR* genetic operon . Image adopted from (Dubrac, Bisicchia et al. 2008)

A 3 to 6 cistronic operon encoding the WalKR two component system (TCS). Major bacterial species are indicated on the right.

WalK is a HK protein with two N-terminal transmembrane domain also known as the sensory domain and C-terminal cytoplasmic domain harboring the conserved histidine kinase box and ATP catalytic domain. WalR is typical cytoplasmic RR protein with N-terminal receiver domain and C-terminal effector domain capable of biding DNA.

1.4.3 The LytSR system

The LytSR TCS was first identified in 1996 through a PCR-based strategy used to identify sensor-like genes from *S. aureus* (Brunskill and Bayles 1996). The *lytS* and *lytR* gene are arranged in a dicistronic operon with their target gene of regulation *lrgAB* located downstream. The operons organization of the LytSR system is shown in Fig 1.4.3.

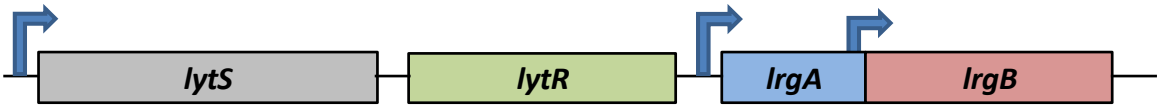

Figure 1.4.3 Organization of the *lytSR* genetic operon.

Arrangement of the *lrgAB* operon downstream of the *lytSR*. The arrows indicate the direction of transcription starts.

The gene product of *lytS* encodes the LytS HK protein with six N-terminal transmembrane domains also known as the sensory domain and C-terminal cytoplasmic domain harboring the conserved histidine kinase box and ATP catalytic domain. And the gene product of *lytR* encodes a typical cytoplasmic RR protein LytR with N-terminal receiver domain and C-terminal effector domain capable of biding DNA. Through sequence alignment, Brunskill and Bayles have shown that this system shares >50 % amino acid sequence similarity with the hypothetical YehUT system from *E. coli* (Brunskill and Bayles 1996). Through *in vivo* studies, it is reported that the LytSR

system is activated by cationic antimicrobial peptides (CAMP) and leading to regulation of genes associated with autolysis, cell growth and cell division (Brunskill and Bayles 1996, Yang, Xiong et al. 2013).

1.5 Objectives of this work

Thus far it is clear that *S. aureus* is a major human pathogen that is responsible for causing wider spectrum of infections mainly because of its adaptive potential to its surrounding environment. To date extensive studies are focused on deciphering the molecular mechanism through which they confer resistance genes. As part of our study, we focus on biochemical characterization of the WalKR and LytSR systems of *S. aureus.* In essence, our study shows the signal flow in the WalKR and LytSR systems leading to activation of resistance genes and sheds light on the importance of these systems as the choice of target by antimicrobial agents.

Firstly, we focus on *in vitro* characterization of the WalKR system. We compare ATP mediated autophosphorylation of two truncated version of WalK and their ability to transfer a phosphate group to its cognate response regulator WalR. We also look at whether WalK can dephosphorylate WalR confirming its phosphotase activity. As second part of the project we show kinetic characterization of LytS autophosphorylation, phosphotransfer and phosphotase activity. In addition, we investigate alternate ways of LytR phosphorylation *in vivo* by conducting *in vitro* acetyl phosphate mediated phosphorylation assays with LytR. Furthermore, the fact that RRs are also transcription factors, we investigate the DNA binding ability of LytR and look at genes it regulates.

Lastly, since most regulatory system in bacteria is based on the TCS “machinery”, an intriguing issue is whether cross-talk interconnects these pathways to form a network. Keeping this in mind another important goal of this project will be to investigate whether and to what extent these separate systems form an interacting network by conducting phosphotransfer experiments with other TCS being studied in the lab.

1.6 References

Abraham, E. P. and E. Chain (1988). "An enzyme from bacteria able to destroy penicillin. 1940." Rev Infect Dis **10**(4): 677-678.

Appelbaum, P. C. (2006). "The emergence of vancomycin-intermediate and vancomycin-resistant *Staphylococcus aureus*." Clin Microbiol Infect **12 Suppl 1**: 16-23.

Archer, G. L. (1998). "*Staphylococcus aureus*: a well-armed pathogen." Clin Infect Dis **26**(5): 1179-1181.

Arda, B., T. Yamazhan, O. R. Sipahi, S. Islekel, Ç. Buke and S. Ulusoy (2005). "Meningitis due to methicillin-resistant *Staphylococcus aureus* (MRSA): Review of 10 cases." International Journal of Antimicrobial Agents **25**(5): 414-418.

Ayliffe, G. A. (1997). "The progressive intercontinental spread of methicillin-resistant *Staphylococcus aureus*." Clin Infect Dis **24 Suppl 1**: S74-79.

Baird-Parker, A. C. (1990). "The staphylococci: an introduction." Soc Appl Bacteriol Symp Ser **19**: 1S-8S.

Banbula, A., J. Potempa, J. Travis, C. Fernandez-Catalan, K. Mann, R. Huber, W. Bode and F. Medrano (1998). "Amino-acid sequence and three-dimensional structure of the *Staphylococcus aureus* metalloproteinase at 1.72 A resolution." Structure **6**(9): 1185-1193.

Barber, M. (1961). "Methicillin-resistant staphylococci." J Clin Pathol **14**: 385-393.
Belcheva, A. and D. Golemi-Kotra (2008). "A close-up view of the VraSR two-component system. A mediator of *Staphylococcus aureus* response to cell wall damage." J Biol Chem **283**(18): 12354-12364.

Brunskill, E. W. and K. W. Bayles (1996). "Identification and molecular characterization of a putative regulatory locus that affects autolysis in *Staphylococcus aureus*." Journal of Bacteriology **178**(3): 611-618.

Brunskill, E. W. and K. W. Bayles (1996). "Identification of LytSR-regulated genes from *Staphylococcus aureus*." J Bacteriol **178**(19): 5810-5812.

Bugg, T. D., G. D. Wright, S. Dutka-Malen, M. Arthur, P. Courvalin and C. T. Walsh (1991). "Molecular basis for vancomycin resistance in Enterococcus faecium BM4147: biosynthesis of a depsipeptide peptidoglycan precursor by vancomycin resistance proteins VanH and VanA." Biochemistry **30**(43): 10408-10415.

Chambers, H. F. and F. R. Deleo (2009). "Waves of resistance: *Staphylococcus aureus* in the antibiotic era." Nat Rev Microbiol **7**(9): 629-641.

Dancer, S. J. (2008). "The effect of antibiotics on methicillin-resistant *Staphylococcus aureus*." J Antimicrob Chemother **61**(2): 246-253.

Delaune, A., O. Poupel, A. Mallet, Y. M. Coic, T. Msadek and S. Dubrac (2011). "Peptidoglycan crosslinking relaxation plays an important role in *Staphylococcus aureus* WalKR-dependent cell viability." PLoS One **6**(2): e17054.

Deurenberg, R. H. and E. E. Stobberingh (2008). "The evolution of *Staphylococcus aureus*." Infect Genet Evol **8**(6): 747-763.

Dubrac, S., P. Bisicchia, K. M. Devine and T. Msadek (2008). "A matter of life and death: cell wall homeostasis and the WalKR (YycGF) essential signal transduction pathway." Mol Microbiol **70**(6): 1307-1322.

Ebert, M. D., S. Sheth and E. K. Fishman (2009). "Necrotizing pneumonia caused by community-acquired methicillin-resistant *Staphylococcus aureus*: an increasing cause of "mayhem in the lung"." Emerg Radiol **16**(2): 159-162.

Eriksen, K. R. (1961). "["Celbenin"-resistant staphylococci]." Ugeskr Laeger **123**: 384-386.

Fabret, C. and J. A. Hoch (1998). "A two-component signal transduction system essential for growth of *Bacillus subtilis*: implications for anti-infective therapy." J Bacteriol **180**(23): 6375-6383.

Falord, M., U. Mader, A. Hiron, M. Debarbouille and T. Msadek (2011). "Investigation of the *Staphylococcus aureus* GraSR regulon reveals novel links to virulence, stress response and cell wall signal transduction pathways." PLoS One **6**(7): e21323.

Fridman, M., G. D. Williams, U. Muzamal, H. Hunter, K. W. Siu and D. Golemi-Kotra (2013). "Two Unique Phosphorylation-Driven Signaling Pathways Crosstalk in *Staphylococcus aureus* to Modulate the Cell-Wall Charge: Stk1/Stp1 Meets GraSR." Biochemistry **52**(45): 7975-7986.

González-Zorn, B. and P. Courvalin (2003). "vanA-mediated high level glycopeptide resistance in MRSA." The Lancet Infectious Diseases **3**(2): 67-68.

Hartman, B. J. and A. Tomasz (1984). "Low-affinity penicillin-binding protein associated with beta-lactam resistance in *Staphylococcus aureus*." J Bacteriol **158**(2): 513-516.

Hiramatsu, K. (2001). "Vancomycin-resistant *Staphylococcus aureus*: a new model of antibiotic resistance." Lancet Infect Dis **1**(3): 147-155.

Hiramatsu, K., L. Cui, M. Kuroda and T. Ito (2001). "The emergence and evolution of methicillin-resistant *Staphylococcus aureus*." Trends Microbiol **9**(10): 486-493.

Hiramatsu, K., H. Hanaki, T. Ino, K. Yabuta, T. Oguri and F. C. Tenover (1997). "Methicillin-resistant *Staphylococcus aureus* clinical strain with reduced vancomycin susceptibility." J Antimicrob Chemother **40**(1): 135-136.

Hong, H. J., M. I. Hutchings, M. J. Buttner, Biotechnology and U. K. Biological Sciences Research Council (2008). "Vancomycin resistance VanS/VanR two-component systems." Adv Exp Med Biol **631**: 200-213.

John, J. F., Jr. and J. A. Lindsay (2008). "Clones and drones: do variants of Panton-Valentine leukocidin extend the reach of community-associated methicillin-resistant *Staphylococcus aureus*?" J Infect Dis **197**(2): 175-178.

Kallweit, U., M. Harzheim, G. Marklein, T. Welt and D. Pohlau (2007). "Successful treatment of methicillin-resistant *Staphylococcus aureus* meningitis using linezolid without removal of intrathecal infusion pump. Case report." J Neurosurg **107**(3): 651-653.

Katayama, Y., T. Ito and K. Hiramatsu (2000). "A new class of genetic element, staphylococcus cassette chromosome mec, encodes methicillin resistance in *Staphylococcus aureus*." Antimicrob Agents Chemother **44**(6): 1549-1555.

Kawada-Matsuo, M., Y. Yoshida, N. Nakamura and H. Komatsuzawa (2011). "Role of two-component systems in the resistance of *Staphylococcus aureus* to antibacterial agents." Virulence **2**(5): 427-430.

Kloos, W. E. and K. H. Schleifer (1975). "Simplified scheme for routine identification of human Staphylococcus species." J Clin Microbiol **1**(1): 82-88.

Kobayashi, S. D. and F. R. DeLeo (2009). "An update on community-associated MRSA virulence." Curr Opin Pharmacol **9**(5): 545-551.

Laub, M. T. and M. Goulian (2007). "Specificity in two-component signal transduction pathways." Annu Rev Genet **41**: 121-145.

Levine, D. P. (2006). "Vancomycin: a history." Clin Infect Dis **42 Suppl 1**: S5-12.

Lodise, T. P., Jr., P. S. McKinnon, D. P. Levine and M. J. Rybak (2007). "Impact of empirical-therapy selection on outcomes of intravenous drug users with infective

endocarditis caused by methicillin-susceptible *Staphylococcus aureus*." Antimicrob Agents Chemother **51**(10): 3731-3733.

Lowy, F. D. (1998). "*Staphylococcus aureus* infections." N Engl J Med **339**(8): 520-532.

Lowy, F. D. (2003). "Antimicrobial resistance: the example of *Staphylococcus aureus*." J Clin Invest **111**(9): 1265-1273.

Mazel, D. and J. Davies (1999). "Antibiotic resistance in microbes." Cell Mol Life Sci **56**(9-10): 742-754.

Mulligan, M. E., K. A. Murray-Leisure, B. S. Ribner, H. C. Standiford, J. F. John, J. A. Korvick, C. A. Kauffman and V. L. Yu (1993). "Methicillin-resistant *Staphylococcus aureus*: A consensus review of the microbiology, pathogenesis, and epidemiology with implications for prevention and management." The American journal of medicine **94**(3): 313-328.

Nathan, C. (2004). "Antibiotics at the crossroads." Nature **431**: 899+.

Ogston, A. (1882). "Micrococcus Poisoning." J Anat Physiol **17**(Pt 1): 24-58.

Ogston, A. (1882). "Micrococcus Poisoning." J Anat Physiol **16**(Pt 4): 526-567.

Ogston, A. (1984). "Classics in infectious diseases. "On abscesses". Alexander Ogston (1844-1929)." Rev Infect Dis **6**(1): 122-128.

Ozaki, S., A. Saito, H. Nakaminami, M. Ono, N. Noguchi and N. Motomura (2013). "Comprehensive evaluation of fibrin glue as a local drug-delivery system-efficacy and safety of sustained release of vancomycin by fibrin glue against local methicillin-resistant *Staphylococcus aureus* infection." J Artif Organs.

Palavecino, E. (2004). "Community-acquired methicillin-resistant *Staphylococcus aureus* infections." Clin Lab Med **24**(2): 403-418.

Peacock, S. J., N. Curtis, A. R. Berendt, I. C. Bowler, C. G. Winearls and P. Maxwell (1999). "Outcome following haemodialysis catheter-related *Staphylococcus aureus* bacteraemia." J Hosp Infect **41**(3): 223-228.

Prasad, L., Y. Leduc, K. Hayakawa and L. T. Delbaere (2004). "The structure of a universally employed enzyme: V8 protease from *Staphylococcus aureus*." Acta Crystallogr D Biol Crystallogr **60**(Pt 2): 256-259.

Raad, I., H. Hanna and D. Maki (2007). "Intravascular catheter-related infections: advances in diagnosis, prevention, and management." Lancet Infect Dis **7**(10): 645-657.

Reynolds, P. E. and D. F. Brown (1985). "Penicillin-binding proteins of beta-lactam-resistant strains of *Staphylococcus aureus*. Effect of growth conditions." FEBS Lett **192**(1): 28-32.

Rubinstein, E., M. H. Kollef and D. Nathwani (2008). "Pneumonia caused by methicillin-resistant *Staphylococcus aureus*." Clin Infect Dis **46 Suppl 5**: S378-385.

Saravolatz, L. D., D. J. Pohlod and L. M. Arking (1982). "Community-acquired methicillin-resistant *Staphylococcus aureus* infections: a new source for nosocomial outbreaks." Ann Intern Med **97**(3): 325-329.

Thwaites, G. E. and V. Gant (2011). "Are bloodstream leukocytes Trojan Horses for the metastasis of *Staphylococcus aureus*?" Nat Rev Microbiol **9**(3): 215-222.

von Eiff, C., A. W. Friedrich, G. Peters and K. Becker (2004). "Prevalence of genes encoding for members of the staphylococcal leukotoxin family among clinical isolates of *Staphylococcus aureus*." Diagn Microbiol Infect Dis **49**(3): 157-162.

Walsh, C. (2003). "Where will new antibiotics come from?" Nature Reviews Microbiology **1**: 65+.

West, A. H. and A. M. Stock (2001). "Histidine kinases and response regulator proteins in two-component signaling systems." Trends Biochem Sci **26**(6): 369-376.

Williams, D. H. and J. Kalman (1977). "Structural and mode of action studies on the antibiotic vancomycin. Evidence from 270-MHz proton magnetic resonance." J Am Chem Soc **99**(8): 2768-2774.

Yang, S. J., Y. Q. Xiong, M. R. Yeaman, K. W. Bayles, W. Abdelhady and A. S. Bayer (2013). "Role of the LytSR two-component regulatory system in adaptation to cationic antimicrobial peptides in *Staphylococcus aureus*." Antimicrob Agents Chemother **57**(8): 3875-3882.

CHAPTER TWO

KINETIC CHARACTERIZATION OF THE WALKR TWO COMPONENT SYSTEM

2.1 Introduction

Since the discovery of antibiotic many resistance strains have emerged in growing numbers. Among these emerging resistant strains *Staphylococcus aureus* is considered as the pathogen of major concern. It is the leading cause of both hospital and community-acquired infections (Belcheva and Golemi-Kotra 2008). Understanding the underlying mechanism by which pathogens become resistant to and survive under antibiotic pressure has been the focus of present day's research. In bacteria, this is achieved by a two component system (TCS), where by a physical signal is integrated in to a chemical signal by a pair of proteins that communicate through a phosphorylation mediated signaling cascade.

TCSs play an important role in adaptation of bacterial metabolism to various environments. While TCSs are widely occurring in prokaryotes few to date have been identified as essential for cell viability (Bisicchia, Noone et al. 2007). Among these, the WalK/WalR (also known as YycG/YycF) TCS is a highly conserved and specific to low-G+C gram positive bacteria, such as *B. subtilis* and *S. aureus*, in which it exerts an effect as a master regulatory system for cell wall metabolism and is essential for cell viability (Dubrac, Boneca et al. 2007, Dubrac, Bisicchia et al. 2008, Dubrac and Msadek 2008).

In *S. aureus*, the first two genes located of a five gene WalKR operon encode the WalR response regulator (RR) and WalK the histidine kinase (HK) (Fig 1.1.1). The domain organization of WalK ortholog from *B. subtilis* is shown in Fig 2.1.1. The N-terminal of WalK is a membrane bound kinase consists of two transmembrane domains flanking an extracytoplasmic loop.

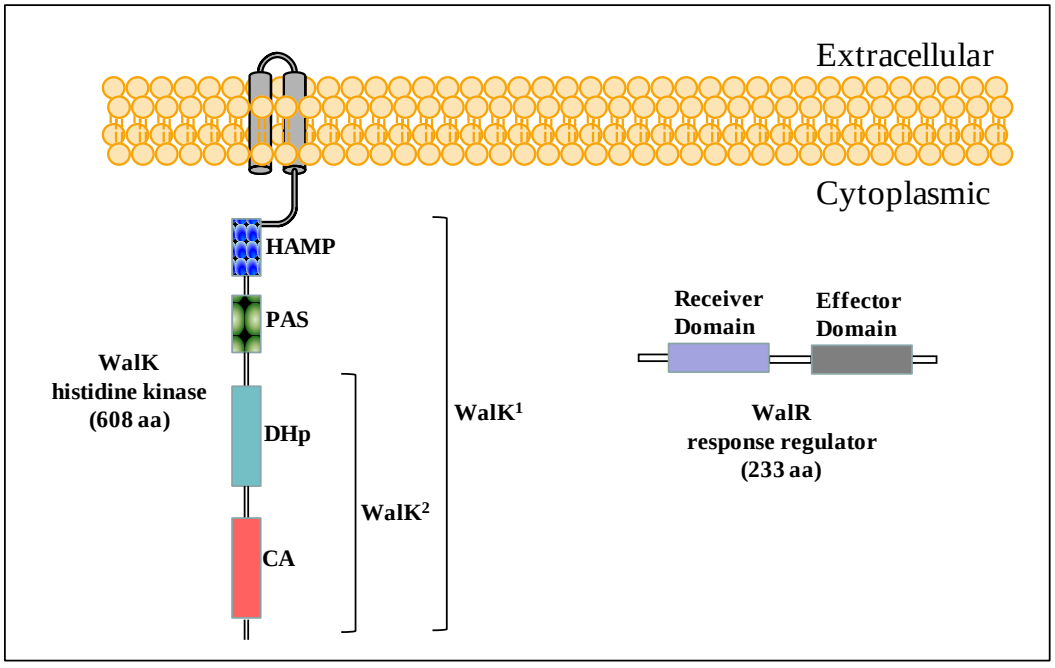

Figure 2.1.1. Domain organization of the WalKR TCS.

The domain designation for each domain are those of the prototypical *B.subtilis* WalK and WalR proteins. The HK, WalK is consist of two transmembrane helices , an extracytoplasmic loop, a Histidine kinases, Adenylyl cyclases, Methyl binding proteins, Phosphatases domain (HAMP linker), PER-ARNT-SIM and PAC sensor motif (PAS domain), the canonical dimerization and histidine phosphotransfer domain (DHp) and ATP catalytic domain (CA). The RR, WalR is consist of the receiver domain and the effector domain .

The C-terminal cytoplasmic domain consists of a HAMP linker: Histidine kinases, Adenylyl cyclases, Methyl binding proteins, Phosphatases domain; a PAS domain: PER-

ARNT-SIM and PAC sensor motif, as well as the canonical DHp: dimerization and histidine phosphotransfer domains and the CA: ATP catalytic domain. Although the N-terminal sensing domains of WalK are poorly conserved between bacterial species, the presence of internal PAS domain is a characteristic feature of all WalK orthologue (Dubrac and Msadek 2008). However, the precise role of this domain in WalK remains still unclear. WalR is a typical bipartite response regulatory protein belonging to the OmpR/PhoB family of RRs. The N-terminal receiver domain of WalR harbors all the invariant active site residues, as well as the conserved Asp53, presumed to be the phosphorylation site. The C-terminal effector domain harbors the characteristic winged helix-turn-helix DNA binding domain responsible for activating expression of target genes. Through sequence alignment it has been shown that all WalR orthologues display greater than 70% identity in amino acid sequence, mostly in their DNA binding domain (Dubrac and Msadek 2008). *In vitro* studies have shown that WalR, like most RRs from the OmpR/PhoB family, regulates gene expression by binding to a consensus sequence of 5′-TGTWAH-N5-TGTWAH-3′ (wherein W is A or T and H represent anything except G) consisting of two direct repeats of hexanucleotide separated by five nucleotides (Dubrac and Msadek 2004, Senadheera, Cordova et al. 2012).

The precise signal sensed by WalK is not yet known, however in the presence of a cell wall-active antibiotics Walk has been proposed to sense the accumulation of Lipid II, a peptidoglycan biosynthetic precursor (Dubrac, Bisicchia et al. 2008). In response, WalR has been shown to upregulate nine genes associated with cell wall metabolism including two major autolysins, AtlA and LytM, confirmed by both *in vitro* and *in vivo*

studies (Dubrac and Msadek 2004, Dubrac, Boneca et al. 2007, Dubrac, Bisicchia et al. 2008).

Taken together, the essentiality of WalKR system and its regulatory role in maintaining cell wall integrity, it is a great target for the development of novel antimicrobial compounds (Gotoh, Doi et al. 2010). To achieve this it is paramount to elucidate both the regulation and the signal transduction pathway of this system. Since its discovery it has been extensively characterized and the autophosphorylation and the phosphotransfer reaction of WalK has already been shown *in vitro* (Clausen, Bae et al. 2003, Dubrac and Msadek 2004). The reported autophosphorylation and phosphotransfer reactions have been shown using the highly truncated version of WalK, lacking the HAMP and the PAS domain. In this study, we compare the autophosphorylation, the phosphotransfer kinetics and the phosphotase activity of two truncated versions of WalK lacking their transmembrane regions. In particular, we look at the contribution of upstream domains HAMP and PAS, if any, in modulating the WalK kinase activity. In addition we explore the possibility of WalR phosphorylation by acetyl phosphate. Essentially the study will help illustrate the significance of this multi-domain TCS in activation of resistance genes and also shed light on the importance of both proteins as the choice of target by antimicrobial drugs.

2.2 Materials and methods

2.2.1 Chemicals

Chemicals and antibiotics were purchased from Sigma (Oakville, Canada) or Thermo-Fisher (Whitby, Canada), unless otherwise indicated. Chromatography media and columns were purchased from GE Healthcare (Quebec, Canada). Growth media were purchased from Fisher. *Escherichia coli* strains, NovaBlue and BL21 (DE3), and other expression plasmids were purchased from EMD4 Biosciences (New Jersey, USA). The pGEX-4T-1 vector was purchased from GE Healthcare (Quebec, Canada). All Restriction enzymes were obtained from New England Biolabs (NEB) Canada (Pickering, Canada) or Thermo-Fisher. The DNA polymerase *PfuTurbo*® and Phusion High-Fidelity were purchased from Agilent Technologies (Mississauga, Canada) and Thermo Scientific (Whitby, Canada), respectively. The [γ-^{32}P] ATP was purchased from Perkin Elmer LAS Canada Inc. (Toronto, Canada) and the cold ATP was purchased from NEB. The Proteo Extract All-in-One Trypsin Digestion Kit was purchased from EMD4 Bioscience. Genomic DNA of *S. aureus* strain Mu50 was obtained from Cedarlane (Burlington, Canada).

2.2.2 Cloning of the *walK* genes into expression plasmid

For the purpose of the *in vitro* experiments two truncated versions of WalK, lacking the transmembrane domain were cloned separately. Here in, the gene sequence of *walK* (SAV0019) will be divided in two, *walK*^{1}and *walK*^{2} translating into two proteins

WalK^1 and WalK^2. WalK^1 consisting of HAMP, PAS, PAC and the histidine kinase domain and WalK^2 consisting of only the histidine kinase domain.

2.2.2.1 Cloning of the *walK*^{2} genes into expression plasmid

The gene sequence of *walK*^{2} harboring the PAC and the histidine kinase domain (amino acid residues 370 - 608) was amplified from the genome *S. aureus* Mu50 using the following direct and reverse primers: Dir 5'- CG*GGATCC* GCTGTGTTACATGACGTTACTG -3' and Rev 5'- CCG*CTCGAG* TTATTATTCATCCCAATCACCG -3'. The primers were introduced with specific sites for *BamHI* and *XhoI* restriction enzymes (italicized sequence) at 5' and 3' ends respectively. PCR amplification of the 748 bp long gene was carried out by *pfu* Turbo high fidelity DNA polymerase. The thermal cycler conditions included: initial denaturation at 95^{o}C for 4 min, followed by 30 cycles of denaturation at 95^{o}C for 1 min, annealing at 55^{o}C for 1 min, extension at 58^{o}C for 1 min and final extension at 72^{o}C for 7 min. Following PCR amplification, the presence of PCR product was verified by 1 % agarose gel. The resulting blunt end amplicon was ligated to pSTblue blunt end vector. The construct *pSTBlue::walK* was further amplified in *E. coli* NovaBlue cells. The isolated plasmid carrying the construct, *pSTBlue::walK* and the host vector, pGEX4T-1 were digested with *BamH I* and *Xho I*. The resulting sticky end products were gel purified from 1% agarose gel using the QIAquick Gel Extraction Kit (Qiagen). Subsequent ligation reaction between *walK* and pGEX4T resulted in the construct *pGEX4T-1::walK*. The construct further amplified in *E. coli* NovaBlue cells. The correct sequence of the *walK* gene was confirmed by DNA sequencing (Core Facility in Department of Biology,

York University). As a final step, the construct harboring the *walK* gene was used to transform the *E. coli* BL21 (DE3) expression cells. This cloning strategy resulted in an introduction of N-terminal GST tag.

2.2.2.2 Cloning of the *walK*^{1} genes into expression plasmid

The gene sequence of *walK*^{1} harboring of HAMP, PAS and the histidine kinase domain (amino acid residues 203 - 608) was amplified from the genome *S. aureus* Mu50 using the following direct and reverse primers: Dir 5'- CG*GGATCC* CG*GGATCC* GCGCGAACGATTACCAAAC -3' and Rev 5'- CCG*CTCGAG* TTATTATTCATCCCAATCACCG -3'. The primers were introduced with specific sites for *BamHI* and *XhoI* restriction enzymes (italicized sequence) at 5' and 3' ends respectively. PCR amplification of 1201 bp long gene and successful cloning of the *walK*^{1} was achieved by employing the same cloning strategy used for *walK*^{2} resulting in an introduction of N-terminus GST tag

2.2.3 Cloning of the *walR* gene into expression plasmid

The gene sequence of *walR* (SAV0018) translating into full length protein was amplified from *S. aureus* MU50 genome using the primers: Dir 5'- CATG*CCATGG*CTAGAAAAGTTGTTGTAGTTGATG -3' and Rev 5'- CG*GGATCC*TTACTACTCATGTTGTTGGAGGAAAT -'3. The primers were designed to contain *NcoI* and *BamHI* restriction sites (italicized sequences) at 5' and 3' of *walR* ends respectively. PCR amplification of 702 bp *walR* gene was carried out using Phusion® High-Fidelity DNA polymerase. The thermal cycler conditions included: initial

denaturation at 98^{o}C for 3 min, followed by 30 cycles of denaturation at 98^{o}C for 10s, annealing at 61^{o}C for 30s, extension at 72^{o}C for 30s followed by final extension at 72^{o}C for 5 min. The resulting blunt end amplicon was ligated to pSTblue blunt end vector. The construct *pSTBlue::walR* was further amplified in *E. coli* NovaBlue cells. The isolated plasmid carrying the construct, *pSTBlue::walR* and the host vector, *pET24d* were digested with *NcoI* and *BamHI*. The resulting sticky end products were gel purified from 1% agarose gel using the QIAquick Gel Extraction Kit (Qiagen). Subsequent ligation reaction between *walR* and *pET24d* resulted in the construct *pET24d::walR*. The construct was further amplified in *E. coli* NovaBlue cells. The correct sequence of the *walR* gene was confirmed by DNA sequencing (Core Facility in Department of Biology, York University, shown in Appendix A, Fig A1). As a final step, the construct harboring the *walR* gene was used to transform the *E. coli* BL21 (DE3) expression cells. This cloning strategy did not result in the introduction of any tags or extra amino acids.

2.2.4 Expression and purification of GST-walK^{1} and GST-walK^{2}

A frozen glycerol stock of *E. coli* BL21 (DE3) cells carrying appropriate constructs were used to inoculate 5 ml of Luria Bertani (LB) medium in the presence of 100 µg/ml final concentration of ampicillin. An aliquot of 1 mL of the overnight grown seed culture was used to inoculate 1 L of Terrific Broth medium (TBM) supplemented with 100 µg/ml of ampicillin. The cells were allowed to grow to an optical density of 0.6-0.8 absorbance unit at 600 nm (OD_{600nm}) while shaking at 200 rpm at 37^{o}C. Once growth was achieved the media was cooled to 4 $^{\circ}$C, briefly. Overexpression of GST-WalK^{1} and GST-WalK^{2} was induced by adding 0.1 mM isopropyl β-D-1-thiogalactopyranoside

(IPTG) over 16 hrs at 18^{o}C and 1 mM IPTG, over 16 hrs at 22^{o}C, respectively. The cells were harvested by centrifugation at 3,300 x g for 20 min and the resulting pellet was stored at -80 $^{\circ}$C in aliquots of 3 g until time of purification. All purifications steps were carried out at 4^{o}C. For purification of GST-WalK^{1} and GST-WalK^{2}, the stored pellet at -80^{o}C was suspended in 1:10 (w/v) of 1X PBS buffer pH 7.4. The cellular contents were liberated by sonication while cooling on ice for 10 min (10s on/15s off) and cell debris was removed by centrifugation at 18,000 x g for 1 hour at 4^{o}C. The supernatant containing the protein was loaded on to a gravity column packed with 1 mL bed of Glutathione Sepharose 4B affinity resin equilibrated in 1X PBS. The flow by gravity allowed sufficient time for the protein to bind to the resin. Once all the input had passed through, the unbound proteins were removed by excessive washing with 1X PBS, pH 7.4 buffers and the protein of interest was eluted with 10mL of 50 mM Tris, pH 8.0 buffer supplemented with 10 mM Reduced Glutathione. One mililter fractions were collected and homogeneity of protein was assessed by 12.5% SDS-PAGE stained with Coomassie blue. The fractions containing the protein of interest were pooled and concentrated using Amicon Ultra- 10K concentrator (Millipore) followed by buffer exchange by dialysis into storage buffer (50 mM Tris pH 7.5, supplemented with 150 mM NaCl and 5 mM $MgCl_2$).

2.2.5 Expression and purification of walR

A frozen glycerol stock of *E. coli* BL21 (DE3) cells with the construct *pET24d::walR* was used to inoculate 5 ml of LB in the presence kanamycin at final concentration of 50 µg/mL final concentration. One milliliter aliquot of an overnight grown seed culture was used to inoculate 1 L of Terrific Broth medium supplemented

with 50 µg/mL of kanamycin. The cells were allowed to grow to an OD_{600nm} of 0.6-0.8 absorbance unit while shaking at 200 rpm at 37^{o}C. Once growth was achieved the media was cooled to 4^{o}C and protein expression was induced by adding IPTG to a final concentration of 0.1 mM at 18^{o}C for 16 hrs. The cells were harvested by centrifugation at 3,300 x g for 20 min and the resulting pellet was stored at -80 ^{o}C in aliquots of 3 g until time of purification. All purifications steps were carried out at 4 ^{o}C using the fast protein liquid chromatography (FPLC) AKTA purifier (Amersham Bioscience). For isolatation of WalR, the stored pellet at -80^{o}C was suspended in 1:10 (w/v) in 20 mM Tris, pH 7.0 supplemented with 5 mM $MgCl_{2.}$ The cellular content was liberated by sonication while cooling on ice for 10 min (10s on/15s off) and cell debris was removed by centrifugation at 18,000 x g for 1 hour at 4 ^{o}C. The resultant supernatant was loaded on to DEAE-Sepharose™ column. The protein was eluted over 8 column volume (CV) in a linear gradient (10% to 80%) of elution buffer (500 mM Tris, pH 7.0, 5 mM $MgCl_2$) at a flow rate of 2.5 mL/min. The impure WalR containing fractions were pooled and concentrated by centrifugation using Amicon Ultra-10K concentrator (Millipore) to a final volume of 15 mL and buffer exchanged into 20 mM Tris, pH 7.0, 5 mM $MgCl_{2.}$ For further purification the 15 mL sample was loaded on to Heparin-Sepharose™ column and protein of interest was eluted with similar program as the DEAE column. Fractions corresponding to elution peaks were analyzed by 15% SDS-PAGE for homogeneity. The fractions containing pure WalR were pooled and concentrated by centrifugation using Amicon Ultra-10K concentrator (Millipore). The identity of the protein was confirmed by Liquid Chromatography tandem Mass Spectrometry (LC-MS/MS).

2.2.6 Assessment of in-vitro autokinase activity of GST-WalK^1 and GST-WalK^2

GST-WalK^1 and GST-WalK^2 at 5 μM were equilibrated in phosphorylation buffer (PB: 50 mM Tris, 250 mM KCl, 5 mM $MgCl_2$, 5 mM $CaCl_2$, pH 7.4) individually. The autophosphorylation reaction was initiated by adding 1 μL of fresh high specificity [γ-^{32}P]-ATP (3000 Ci/mmol). Reaction was incubated at room temperature and samples were removed at different time intervals and quenched by adding 5 x SDS sample buffer (125 mM Tris, pH 6.8, 2.5% SDS, 25% glycerol, 100 mM DTT, 0.0025% bromophenol blue). Samples were analyzed by 12.5% SDS-PAGE. The radioactive gels were exposed to phosphor screen (GE healthcare) overnight and imaged using a Typhoon Trio$^+$ imager (GE healthcare). The radioactive gels were stained by Coomassie blue dye. Average band intensities of two trials were quantified using NIH ImageJ software (Version 1.45s). From the plot of intensity versus time, also known as the progress curve, initial rates of phosphorylation was calculated.

2.2.7 Effect of metal ions on phosphorylation of GST-WalK^1 and GST-WalK^2

GST-WalK^2 at 2 μM was equilibrated in phosphorylation buffer (PB: 50 mM Tris, 5 mM $MgCl_2$, 50 mM Tris, 10 mM $CaCl_2$, pH 7.4) supplemented with varying concentrations of KCl (50, 250 and 500 mM) and $CaCl_2$ (2, 4, 8 and 10 mM). The phosphorylation reaction was initiated by the addition of 1 μL of [γ-^{32}P]-ATP (3000 Ci/mmol). The reaction was incubated for 60 min at RT then quenched by adding 5X SDS sample buffer. Samples were loaded on to 12.5% SDS-PAGE. Similar

phosphorylation reactions with varying concentration of KCl was carried out with GST-WalK^{1}, GST-GraS, and GST-BceS. The radioactive gels were exposed to phosphor screen (GE Healthcare) overnight and the screen was imaged using a Typhoon Trio^{+} imager (GE Healthcare).

2.2.8 Investigating the stability of phosphoryalted histidine kinase domain (GST-walK^{2})

GST-WalK^{2} at 5 µM was phosphorylated for 40 min as above (2.2.6). Excess [γ-^{32}P]-ATP was removed by desalting using the Zeba Spin Desalting column (Pierce, Thermo Scientific) equilibrated with PB. The reaction mixture was further incubated at RT and aliquots were removed at different time intervals and quenched by adding 5X SDS sample buffer. Samples were analyzed by 15% SDS-PAGE. The radioactive gels were exposed to phosphor screen (GE Healthcare) overnight and the screen was imaged using a Typhoon Trio^{+} imager (GE Healthcare).

2.2.9 Phosphotransfer reaction from GST-WalK^{2} to WalR

GST-WalK^{2} at 15 µM was autophosphorylated as described above (2.2.6) for 60 min before removing excess [γ-^{32}P]-ATP by desalting using a Zeba Spin Desalting column (Pierce, Thermo Scientific) equilibrated in PB (PB: 50 mM Tris, pH 7.4, 50 mM KCl, 5 mM $MgCl_2$). The subsequent phosphotransfer reaction was initiated by mixing phosphoryalted GST-WalK^{2} at 3 µM to a master mixture containing WalR at 15 µM so to keep a ratio of 1:5 between the HK and RR. The final reaction was incubated at RT (25^{o}C) and quenched at different time intervals by removing aliquots of 10 µL and mixing with 10 µL of 5X SDS sample buffer. The samples were analyzed by 15 % SDS-

PAGE. The radioactive gels were exposed to phosphor screen (GE healthcare) overnight and imaged using a Typhoon Trio^{+} imager (GE healthcare). The radioactive gels were stained by Coomassie blue dye as well. These experiments were repeated multiple times to optimize reaction conditions. Average intensities over two trails, quantified using NIH ImageJ software (Version 1.45s), were normalized against GST-WalK^{2} and a progress curve of relative intensity versus time was plotted.

2.2.10 Investigating crosstalk between WalK and other response regulators

A phosphotransfer reaction from both variants of WalK to BceR and GraR was carried out. A similar protocol as that described above in 2.2.9 was followed. The progress of the reactions was observed over several time intervals.

2.2.11 Analysis of GST-WalK^{2} and WalR by native-PAGE

To determine the oligomerization state of the proteins varying concentration of GST-WalK^{2} and WalR were loaded on to a 10% native polyacrylamide gel electrophoresis (Native–PAGE). In further experiments, mixture of both proteins at different ratio (1:1 and 1:2) was incubated at RT and analyze by 10% native-PAGE to check for interactions between the two proteins.

2.3 Results

2.3.1 Cloning, expression and purification of WalR

Initially, the full length *walR* gene had been cloned into a pET26b vector however, the protein expression of WalR was nil since the cloning strategy employed resulted in deletion of the ribosomal binding site from the cloning and expression region of the vector. Therefore, primers were re-designed to incorporate *NcoI* and *BamHI* as the two respective restriction sites and w*alR* (residues 1 -233) was successfully cloned into

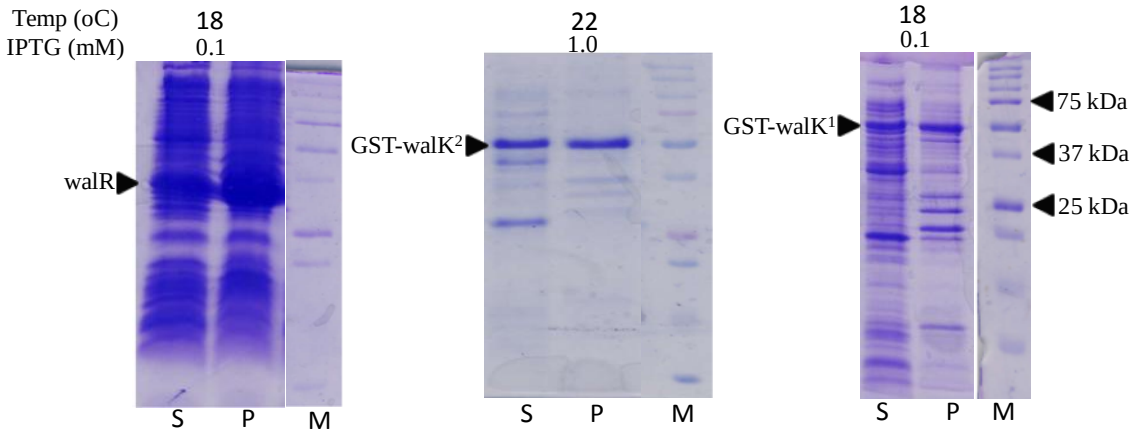

Figure 2.3.1. Optimization of protein overexpression for WalR, GST-WalK^1 and GST-WalK^2

The BL21 (DE3) cells carrying the appropriate construct were grown to OD_{600} equal to 0.6 in the presence of specific antibiotics. The overexpression of protein was probed at varying temperature and concentrations of IPTG. The supernatant (S) and pellet (P) were analyzed by SDS-PAGE and gels are stained with Coomassie blue. The best expression of A) WalR was achieved by induction with 0.1 mM IPTG for 16 hrs at 18^{o}C, B) GST-WalK^2 was achieved by induction with 1 mM IPTG for 16 hrs at 22^{o}C and C) GST-WalK^1 was achieved by induction with 0.1 mM IPTG for 16 hrs at 18^{o}C.

pET24d vector containing a T7 inducible promoter. Overexpression of WalR was achieved by induction with 0.1 mM IPTG over 16 hrs at 18^{o}C (Fig2.3.1A). The calculated molecular weight of WalR is 27,191 Da with a theoretical pI of 5.04.

Purification of WalR was carried out using the FPLC. Multiple chromatography steps were employed to obtain pure protein. Based on the theoretical pI of WalR, as a first step of purification, DEAE anion exchange column was used and protein of interest eluted at buffer conductivity between 15-16 mS/cm (Fig 2.3.2A). The resulting fractions,

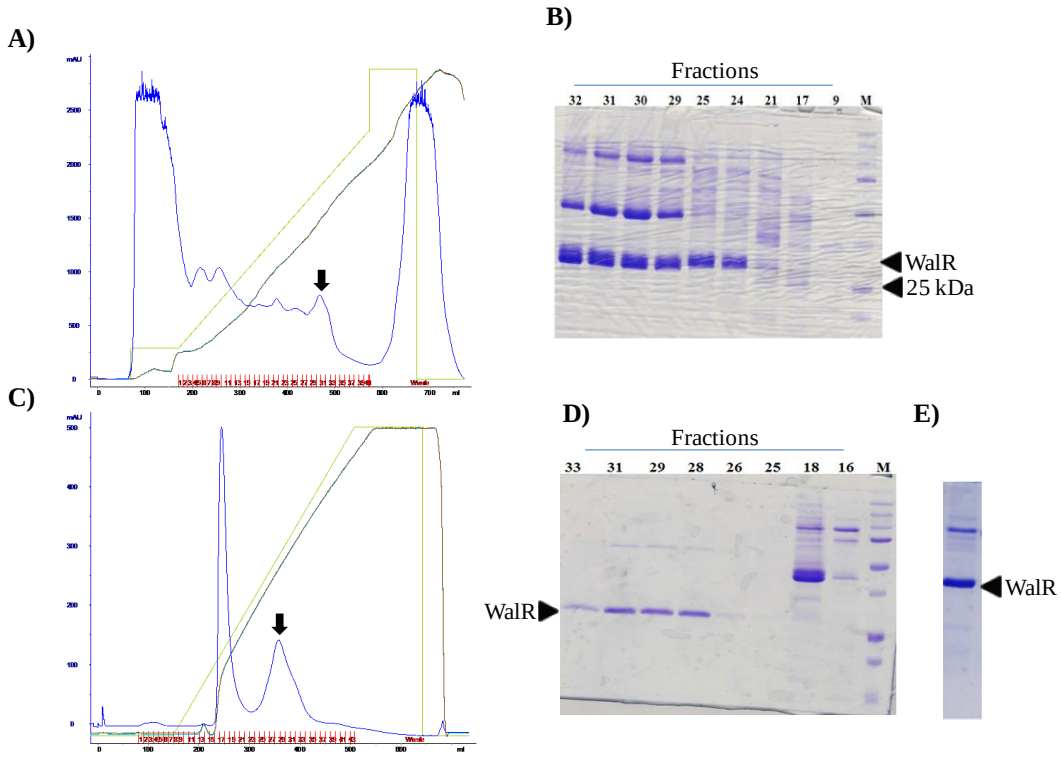

Figure 2.3.2: Purification chromatograms of WalR following DEAE column and Heparin column and analysis of concentrated WalR by 15% SDS-PAGE

A) FPLC chromatogram representing the elution profile of WalR from 80 mL DEAE column. B) Fractions corresponding to the elution peaks from DEAE column analyzed by 15% SDS-PAGE. C) FPLC chromatogram representing the elution profile of WalR from 40 mL Heparin column. D) Fractions corresponding to the elution peaks from Heparin column analyzed by 15% SDS-PAGE. E) Concentrated WalR following each purification was separated on an 15% SDS-PAGE to assess homogeneity. All gels were stained with Coomassie Blue for detection of protein bands. A pre-stained broad range protein marker was used from Bio-RAD (cat # 161-0374). On chromatograms the blue line represents the absorbance at 280 and the arrows indicate the elution peaks.

analyzed by 15% SDS-PAGE (Fig 2.3.2B) contained considerable amount of impurity requiring further purification. By taking advantage of strong DNA binding affinity of WalR, second purification step included the use of Heparin column. In brief, heparin is a molecule that resembles the structure of DNA backbone allowing many DNA binding proteins to bind and efficiently separated. WalR was eluted in a single peak at 50% concentration of the elution buffer (Fig 2.3.2C) from the heparin column. Analysis of fractions by 15% SDS-PAGE (Fig.2.3.2D) indicated that protein was purified to 90% homogeneity containing impurities of higher molecular weight. Per liter of cell culture, 5 mg of WalR was obtained on average. It is of note that during the process of concentrating significant precipitation was observed lowering the overall yield of WalR. Concentrated WalR, Fig 2.3.2E, was positively identified by in-gel trypsin digestion followed by LC-MS/MS (shown in Appendix A, Fig A3).

2.3.2 Cloning, expression and purification of GST-WalK^1 and GST-WalK^2

Two truncated versions of WalK: WalK^1 and WalK^2, lacking the transmembrane regions were cloned into pGEX4T-1 vector. The cloning strategy employed here resulted in a GST tag fused to the N-terminal of both proteins. Overproduction of GST-WalK^1 was achieved by induction with 0.1 mM IPTG for 16 hrs at 18^{o}C (Fig. 2.3.1C), and induction with 1 mM IPTG, over 16 hrs at 22^{o}C for GST-WalK^2 (Fig. 2.3.1B). These conditions yielded sufficient amount of soluble GST-WalK^1 and GST-WalK^2 for subsequent purification step. Purification of GST-WalK^1 and GST-WalK^2 was carried with Glutathione Sepharose 4B affinity resin. Using the technique of purification by gravity column, both proteins were purified to homogeneity with apparent impurities

resulting from the cleaved GST-tag (Fig.2.3.3) as analyzed by Coomassie blue staining. Attempts to overcome this issue were made by reducing the induction temperature and adding protease inhibitor (Roche) before cell lysis, however the problem still persisted. Usually the ratio between "tag" and "tag-protein" was quite low, freeing us to proceed with downstream experiments. Typically, 15 mg of GST-WalK^2 and 10 mg of GST-WalK^1 was obtained per liter of culture. The calculated molecular weight of GST-WalK^1 is 74, 704 Da with a pI of 5.41 and that of GST-WalK^2 is 54, 626 Da with a pI of 6.31.

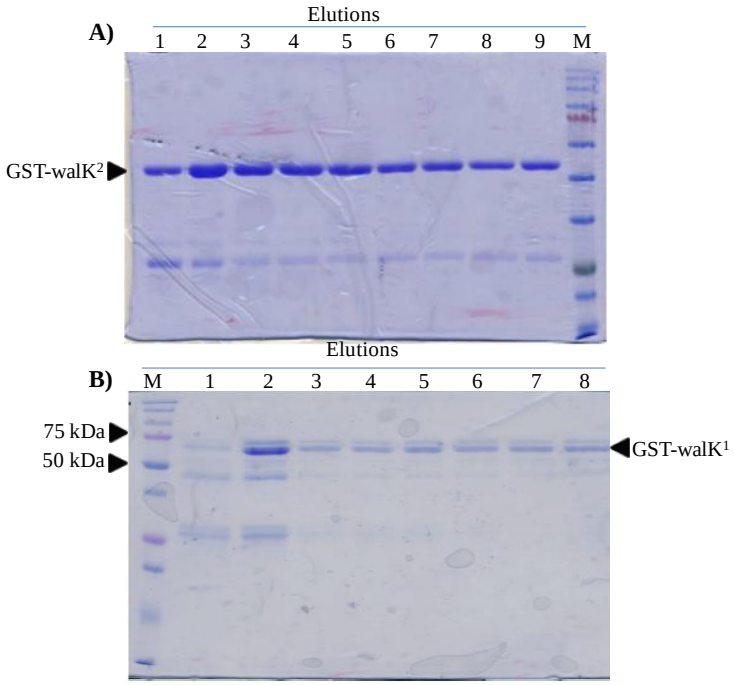

Figure 2.3.3. Gravity purification of GST-WalK^1 and GST-WalK^2

Purification of GST-WalK^1 and GST-WalK^2 using a gravity purification column. The protein of interest is eluted with 50 mM Tris, pH 8.0, 10 mM reduced glutathione buffer over 10 fractions of 1 mL each. Fractions corresponding to each elution are analyzed by 12.5 % SDS-PAGE.

2.3.3 GST-WalK^2 and WalR analysis by native-PAGE

Analysis of GST-WalK^2 and WalR by native-PAGE showed that both proteins have similar migration pattern and exist as monomeric species in solution, pH 7.0 (Fig.2.3.4). Furthermore, Fig.2.3.4B shows no alteration in the migration pattern of either proteins when incubated together, suggesting that there is no prolonged interaction between these cognate proteins under native conditions. However, this is not to say that a transient interaction might not exist in the presence of stimuli.

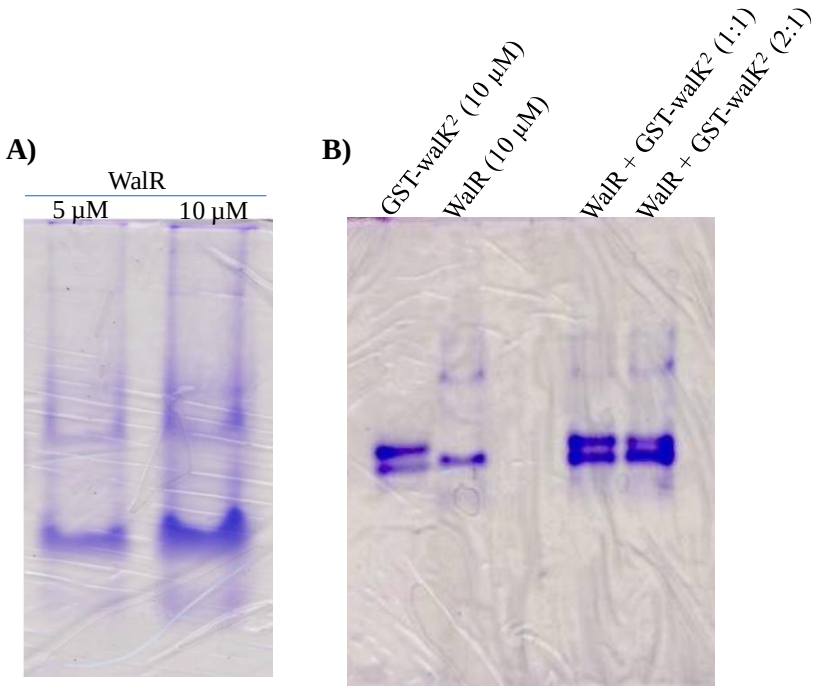

Figure 2.3.4. Native PAGE analysis of GST-WalK^2 and WalR

A) WalR at varying concentrations (5 and 10 µM) was loaded on to a 10% native PAGE for oligomerization state. B) Mixture of GST-WalK^2 and WalR incubated at different ratio (1:1 and1:2) to check protein interactions. However the migration pattern of both protein didn't change compare to the reference, suggesting no prolonged interaction between the two proteins

2.3.4 Autokinase activity of GST-WalK^1 and GST-WalK^2

Autophosphorylation of GST-WalK^1 and GST-WalK^2 in the presence of [γ-^{32}P]-ATP was observed *in vitro*. A time dependent autophosphorylation reaction with GST-WalK^2 at RT indicated a continuous increase in the phosphoryalted species for the first 30 min followed by saturation (Fig 2.3.5A&B).

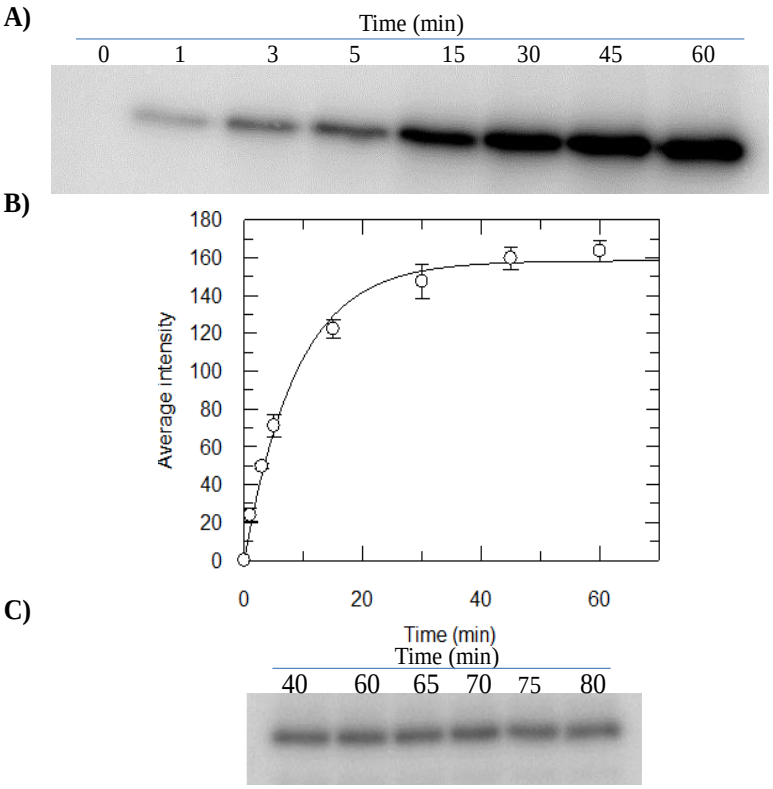

Figure 2.3.5 In vitro autokinase activity of GST-WalK^2

A) Time dependent autophosphorylation of GST-WalK^2. GST-WalK^2 at 5 µM was incubated with [γ-^{32}P]-ATP (1 µL) in PB at room temperature. Reaction was quenched at different time intervals and samples were analyzed by 12.5% SDS-PAGE . B) Progress curve of autophosphorylation reaction. The quantified band intensity of phosphorylation were plotted against time The data were fitted using Origin software to pseudo first order equation to calculate rate constant. The standard deviation represented as errors is averaged over two different trials. C) GST-WalK^2 at 5 µM was phosphoryalted for 40 min in PB at room temperature. Excessive ATP was removed by desalting and stability was monitored over 1 hour at different time intervals. Samples were analyzed by 15% SDS-PAGE. All gels were exposed to phosphor screen (GE Healthcare) overnight and imaged using a Typhoon Trio$^+$ imager (GE Healthcare).

In the case of GST-WalK^1, saturation was reached within the first 20 mins followed by sudden increase in phosphorylation after 40 min (Fig 2.3.6). The observed rate constant for phosphorylation of GST-WalK^1 was calculated (0.1809 ± 0.0289 with a $t_{1/2}$ = 6) to be higher than that of GST-WalK^2 (0.1127 ± 0.0093 min^{-1} with a $t_{1/2}$ = 9 min). The time for 50% of GST-WalK^1 is lower compare to the time for GST-WalK^2 making it a faster kinase. In addition, it was observed that following phosphorylation, the phosphorylated species of GST-WalK^2 was stable for at least 80 mins (Fig2.3.5C).

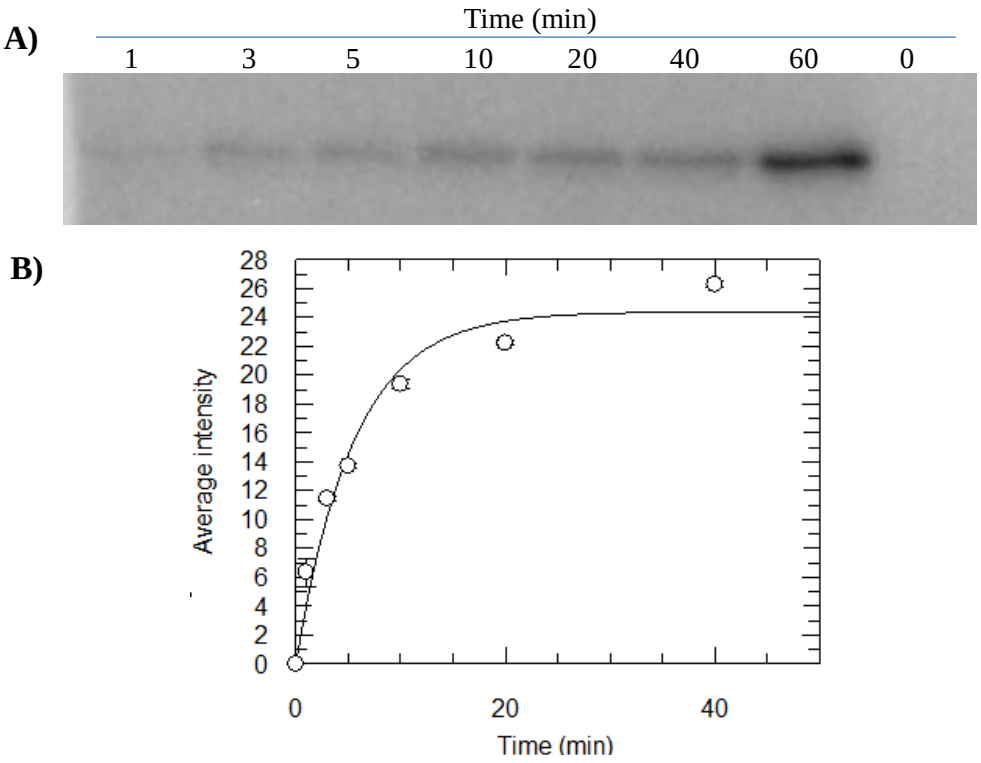

Figure 2.3.6 In vitro autokinase activity of GST-WalK^1

A) Time dependent autophosphorylation of GST-WalK^1. GST-WalK^1 at 5 µM was incubated with [γ-^{32}P]-ATP (1 µL) in PB at room temperature. Reaction was quenched at different time intervals and samples were analyzed by 12.5% SDS-PAGE. The gel was exposed to phosphor screen (GE Healthcare) overnight and imaged using a Typhoon Trio$^+$ imager (GE Healthcare). B) Progress curve of autophosphorylation reaction. The quantified band intensity of phosphorylation were plotted against time The data were fitted using Origin software to pseudo first order equation to calculate rate constant.

In further experiments, the effect of Ca^{2+} and K^{+} ions on autophosphorylation of WalK was investigated. The experiment revealed that phosphorylation of both GST-$WalK^{1}$ and GST-$WalK^{2}$ was highly dependent on the concentration of K^{+} ions. It was observed that increasing concentration of K^{+} ions upregulated the phosphorylation

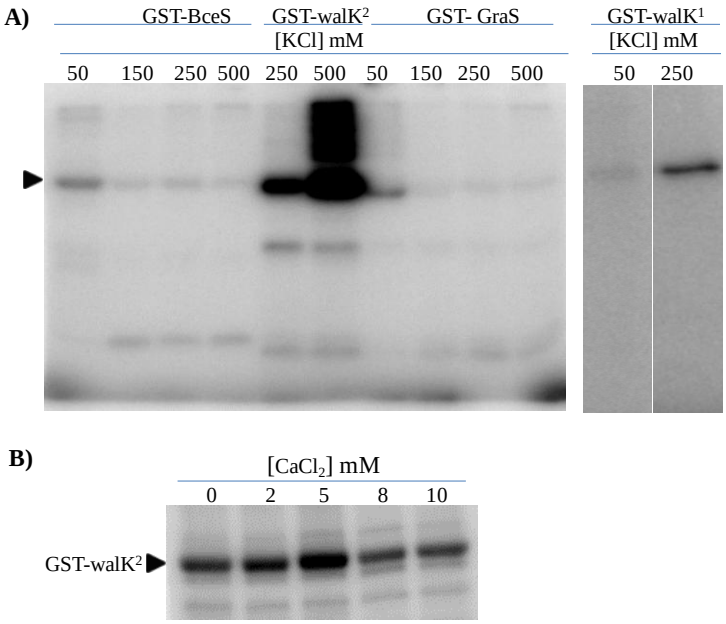

Figure 2.3.7 Effects of metal ions on the autophosphorylation of His-LytS

A) GST-$walK^{1}$, GST-$walK^{2}$,GST-GraS, and GST-BceS all at 2 µM were phosphorylated in PB at varying concentration of KCl for 60 min. B) GST-$walK^{2}$ at 2 µM was phosphorylated in PB at varying concentration of $CaCl_2$ for 60 min. Reactions were quenched and samples were analyzed by 12.5% SDS-PAGE. All gels were exposed to phosphor screen (GE Healthcare) overnight and imaged using a Typhoon $Trio^{+}$ imager (GE Healthcare).

activity of WalK but not of BceS or GraS (Fig 2.3.7A). The optimum concentration of Ca^{2+} ion was found to be 5 mM; any deviation from this resulted in decrease in phosphorylation of GST-$WalK^{2}$ (Fig.2.3.7B). As a control reaction previous members of the lab have shown that under experimental conditions standalone GST is not able to undergo phosphorylation.

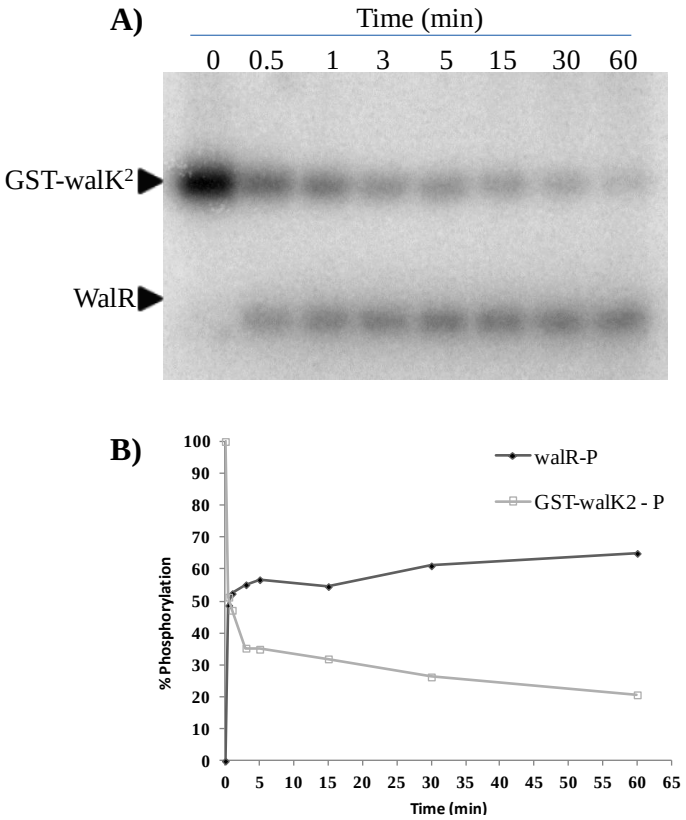

Figure 2.3.8 Phosphotransfer reaction from GST-WalK^2 to WalR
A) Phosphoryalted GST-WalK^2 at 4 µM was incubated with WalR at 15 µM in PB at room temperature. The reaction was quenched after various time intervals and samples were analyzed by 15% SDS-PAGE. B) A graph of relative intensities normalized to phosphoryalted GST-WalK^2 versus time (min). All gels were exposed to phosphor screen (GE Healthcare) overnight and imaged using a Typhoon Trio$^+$ imager (GE Healthcare).

2.3.5 In vitro phosphotransfer from GST-WalK^2 to WalR

As shown in Fig 2.3.8A, a rapid phosphotransfer was observed from GST-WalK^2 to WalR. More than 50% of the phosphoryl group was transferred to walR within the first minute (Fig 2.3.8B). Furthermore, the possibility of crosstalk between GST-WalK^2 and BceR and GraR was investigated. The results showed no apparent crosstalk between GST-WalK^2 and BceR or between GST-WalK^2 and GraR (Fig.2.3.9).

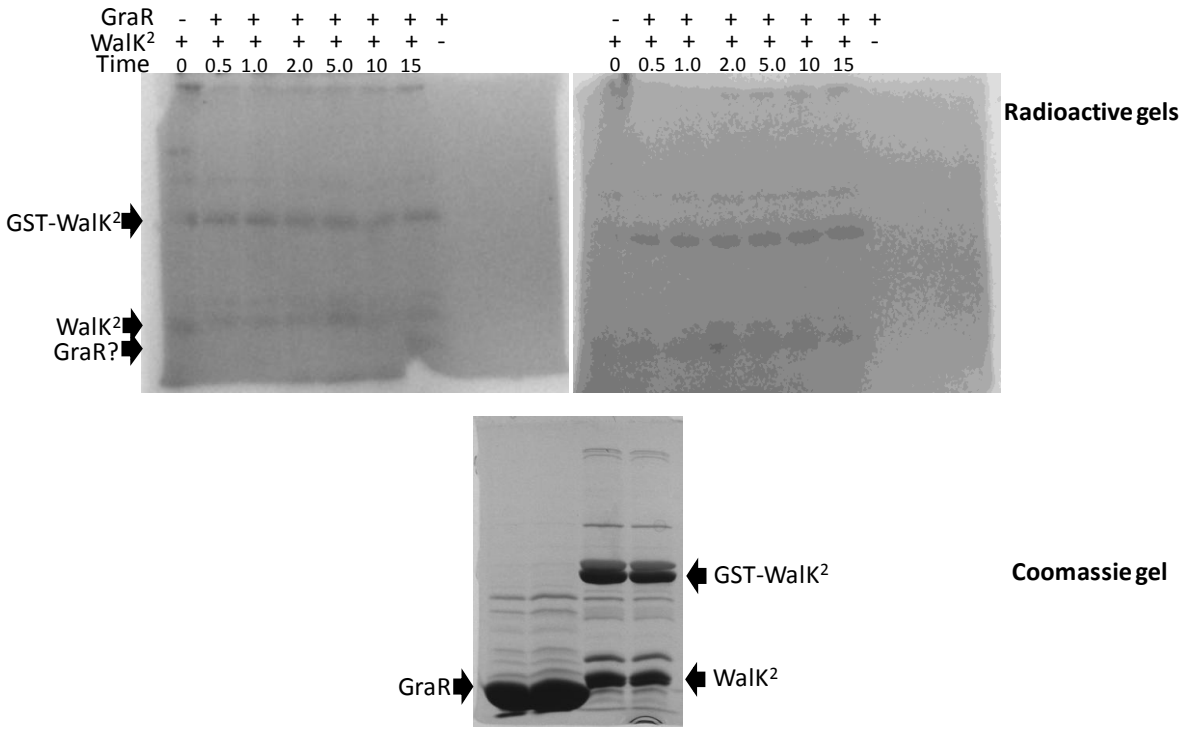

Figure 2.3.9 Phosphotransfer reaction from GST-WalK^1 and GST-WalK^2 to GraR
A) Phosphoryalted GST-WalK^2 at 4 µM was incubated with GraR at 15 µM in PB at room temperature. The reaction was quenched after various time intervals and samples were analyzed by 15% SDS-PAGE. B) Similar phosphotransfer reaction carried out using GST-walK^1. All gels were exposed to phosphor screen (GE Healthcare) overnight and imaged using a Typhoon Trio$^+$ imager (GE Healthcare).

2.4 Discussion

In gram positive bacteria such as *S. aureus*, the WalKR TCS has been proven indispensible due to crucial role plays in maintaining cell viability. It functions like a typical two component system (TCS) whereby an external signal sensed by HK, WalK is propagated though a phosphorylation cascade resulting in phosphorylation of its cognate RR, WalR capable of binding DNA. Since its discovery it has been widely studied both *in vivo* and *in vitro*. *In vitro* studies conducted by Clausen et. al. (2003) have shown the autophosphorylation of WalK and subsequent phosphotransfer to WalR. Furthermore, recent *in vivo* studies have implicated the WalKR system in regulating genes involved in virulence, biofilm formation and most importantly cell metabolism (Dubrac and Msadek 2004, Dubrac, Boneca et al. 2007). Despite the greater part of this system being already characterized, the precise role of the upstream domains in particular, the PAS domain, of WalK was overlooked. Therefore, the goal of this study was to characterize the enzymatic activity of WalK in detail using two truncated versions.

For *in vitro* investigation of the WalKR system, firstly genes of WalR, GST-$WalK^1$ and GST-$WalK^2$ were successfully cloned and purified using previously described methods (Belcheva and Golemi-Kotra 2008). To overcome the issue of protein insolubility, the transmembrane regions of WalK was omitted.

Prior to present study, autophosphorylation of WalK was reported for a highly truncated WalK harboring only the DHp and the CA domain. In corroboration, we showed that GST-$WalK^1$ (0.1809 ± 0.0289 with a $t_{1/2}$ = 6; Fig. 2.3.7) undergoes autophosphorylation at a rate 2-fold higher than GST-$WalK^2$ (0.1127 ± 0.0093 min^{-1} with

a $t_{1/2}$ = 9 min; Fig 2.3.6) at the invariable His385. Although, our results are consistent with previously reported *in vitro* findings by Clausen et. al. (2003) showing that the PAS domain is not required for autophosphorylation of standalone histidine kinase domain, we show that it may facilitate in speeding up the overall signal transduction process. The observed rate of response for WalK was faster compared to that of other HKs involved in vancomycin- resistant such as VraS (Belcheva and Golemi-Kotra 2008) and VanS (Wright, Holman et al. 1993). The saturation time for both versions of WalK was much lower (20 min for GST-$WalK^1$ and 10 min for GST-$WalK^2$) with 50% of GST-$WalK^1$ being phosphorylated within the first 6 min, making it a faster version of kinase. This low response time is in accordance with the essential nature of this system for cell viability and indicates that WalKR can readily transducer the cell wall stress *in vivo*. This is also consistent with *in vivo* finding which demonstrate up regulation of WalKR system and associated genes in the presence of cell wall active antibiotics (Dubrac, Bisicchia et al. 2008).

Furthermore, the effect of metal ions on autophosphorylation of WalK was investigated. Interestingly, in the presence of K^+ ions the autophosphorylation of both GST-$WalK^1$ and GST-$WalK^2$ was significantly enhanced in a concentration dependent manner. On the other hand, the autophosphorylation activity of GST-BceS or GST-GraS, well characterized HK involved in regulating cell wall associated genes, was not affected under similar condition. In the case of WalK, such drastic enhancement in autophosphorylation implied that K^+ ions may act as a stabilizer or as a stress induced activator of WalK (Dubrac, Bisicchia et al. 2008). Evidently, the latter has been proven *in*

vivo in *B. subtilis* TCS systems, where divalent metal ions were used as stress inducer (Moore, Gaballa et al. 2005). However, further investigation is required.

Based on the WalK structure and mathematical modeling, previous studies have designated WalK as bifunctional kinase i.e being able to catalyze both the phosphorylation and dephosphorylation of their cognate response regulator (Alves and Savageau 2003). Many HKs have the inherent ability to phosphorylate their cognate RR. In this regard, we show that the phosphotransfer from GST-WalK^2 to WalR is very efficient with 50% of the transfer taking place within the first minute (Fig.2.3.9). This rapid phosphotransfer suggested that in the presence of cell wall stress this system could be readily activated resulting high levels of phosphoryalted WalR species in cell. However compared to the VraSR system this reaction is slower but comparable to the VanSR system. It is not unusual for RRs to be phosphorylated by non-cognate HK and vise-versa. Studies have already shown physiologically relevant cross-talk between PhoR, a kinase containing PAS domain with WalR from *B. Subtilus* (Howell, Dubrac et al. 2006). In our study we did not observe any cross talk between GST-WalK and BceR; however the results with GraR were inconclusive. It is reported that WalKR and GraSR TCS share extensive regulon properties (Falord, Mader et al. 2011) and the lack of in vitro phosphorylation of GraS one cannot rule out the possibility of GraR phosphorylation by WalK.

Many RRs have an inherent ability to undergo dephosphorylation, however this process is gradual and is usually enhanced by the cognate HK or an auxiliary protein (Bilwes, Alex et al. 1999, Belcheva and Golemi-Kotra 2008). This phenomenon is

referred to as the phosphotase activity of HK (Laub and Goulian 2007). Such mechanisms are needed to modulate the time-scale response of the signal and to control the level of phosphoryalted RR present in cell in response of stress (Dubrac, Bisicchia et al. 2008). Based on the results of *in vitro* studies, positive regulation of WalK phosphotase activity has been attributed to the HAMP – PAS domain (Gutu, Wayne et al. 2010). Unfortunately, further planned work involving the WalKR system was not perused as papers on similar work were published.

To summarize, the essential WalKR system of *S. aureus* plays crucial role in cell viability through regulation of genes associated with cell wall metabolism. In corroboration, we show that the autophosphorylation rate of GST-WalK is higher in the presence of the HAMP-PAS domain. In addition, our results demonstrate that autophosphorylation ability of WalK is highly dependent on the concentration of K^+ ions inferring that they may play a role in constitutively activating this inducible system. Furthermore, we show that GST-WalK^2 can directly phosphorylate WalR, and may phosphorylate GraR, but not BceR.

2.5 References

Alves, R. and M. A. Savageau (2003). "Comparative analysis of prototype two-component systems with either bifunctional or monofunctional sensors: differences in molecular structure and physiological function." Mol Microbiol **48**(1): 25-51.

Belcheva, A. and D. Golemi-Kotra (2008). "A close-up view of the VraSR two-component system. A mediator of *Staphylococcus aureus* response to cell wall damage." J Biol Chem **283**(18): 12354-12364.

Bilwes, A. M., L. A. Alex, B. R. Crane and M. I. Simon (1999). "Structure of CheA, a signal-transducing histidine kinase." Cell **96**(1): 131-141.

Bisicchia, P., D. Noone, E. Lioliou, A. Howell, S. Quigley, T. Jensen, H. Jarmer and K. M. Devine (2007). "The essential YycFG two-component system controls cell wall metabolism in *Bacillus subtilis*." Mol Microbiol **65**(1): 180-200.

Clausen, V. A., W. Bae, J. Throup, M. K. Burnham, M. Rosenberg and N. G. Wallis (2003). "Biochemical characterization of the first essential two-component signal transduction system from *Staphylococcus aureus* and *Streptococcus pneumoniae*." J Mol Microbiol Biotechnol **5**(4): 252-260.

Dubrac, S., P. Bisicchia, K. M. Devine and T. Msadek (2008). "A matter of life and death: cell wall homeostasis and the WalKR (YycGF) essential signal transduction pathway." Mol Microbiol **70**(6): 1307-1322.

Dubrac, S., I. G. Boneca, O. Poupel and T. Msadek (2007). "New insights into the WalK/WalR (YycG/YycF) essential signal transduction pathway reveal a major role in controlling cell wall metabolism and biofilm formation in *Staphylococcus aureus*." J Bacteriol **189**(22): 8257-8269.

Dubrac, S. and T. Msadek (2004). "Identification of genes controlled by the essential YycG/YycF two-component system of *Staphylococcus aureus*." J Bacteriol **186**(4): 1175-1181.

Dubrac, S. and T. Msadek (2008). "Tearing down the wall: peptidoglycan metabolism and the WalK/WalR (YycG/YycF) essential two-component system." Adv Exp Med Biol **631**: 214-228.

Falord, M., U. Mader, A. Hiron, M. Debarbouille and T. Msadek (2011). "Investigation of the *Staphylococcus aureus* GraSR regulon reveals novel links to virulence, stress response and cell wall signal transduction pathways." PLoS One **6**(7): e21323.

Gotoh, Y., A. Doi, E. Furuta, S. Dubrac, Y. Ishizaki, M. Okada, M. Igarashi, N. Misawa, H. Yoshikawa, T. Okajima, T. Msadek and R. Utsumi (2010). "Novel antibacterial compounds specifically targeting the essential WalR response regulator." J Antibiot (Tokyo) **63**(3): 127-134.

Gutu, A. D., K. J. Wayne, L. T. Sham and M. E. Winkler (2010). "Kinetic characterization of the WalRKSpn (VicRK) two-component system of *Streptococcus pneumoniae*: dependence of WalKSpn (VicK) phosphatase activity on its PAS domain." J Bacteriol **192**(9): 2346-2358.

Howell, A., S. Dubrac, D. Noone, K. I. Varughese and K. Devine (2006). "Interactions between the YycFG and PhoPR two-component systems in *Bacillus subtilis*: the PhoR kinase phosphorylates the non-cognate YycF response regulator upon phosphate limitation." Mol Microbiol **59**(4): 1199-1215.

Laub, M. T. and M. Goulian (2007). "Specificity in two-component signal transduction pathways." Annu Rev Genet **41**: 121-145.

Moore, C. M., A. Gaballa, M. Hui, R. W. Ye and J. D. Helmann (2005). "Genetic and physiological responses of *Bacillus subtilis* to metal ion stress." Mol Microbiol **57**(1): 27-40.

Senadheera, D. B., M. Cordova, E. A. Ayala, L. E. Chavez de Paz, K. Singh, J. S. Downey, G. Svensater, S. D. Goodman and D. G. Cvitkovitch (2012). "Regulation of bacteriocin production and cell death by the VicRK signaling system in Streptococcus mutans." J Bacteriol **194**(6): 1307-1316.

Wright, G. D., T. R. Holman and C. T. Walsh (1993). "Purification and characterization of VanR and the cytosolic domain of VanS: a two-component regulatory system required for vancomycin resistance in *Enterococcus faecium* BM4147." Biochemistry **32**(19): 5057-5063.

CHAPTER THREE

IN VITRO CHARACTERIZATION AND PHOSPHORYLATIOIN KINETICS OF THE S. AUREUS LYTSR SIGNAL TRANSDUCTION PATHWAY

3.1 Introduction

One of the major hurdles the *S. aureus* has to overcome during colonization of the host is the host's innate immune system. This defense mechanism relies on the release of a numerous cationic antimicrobial peptides (CAMPs) (Peschel 2002, Voyich, Braughton et al. 2005, Yang, Xiong et al. 2013). CAMPs are amphipathic peptides comprised of less than 50 amino acids, and are found in most of mammalian tissues (Brogden 2005). They have bactericidal activity and their mechanism of action is proposed to involve perturbation of cell membrane as a result alters the electrical potential of the cell membrane (Peschel, Jack et al. 2001, Yang, Xiong et al. 2013). A recent study has shown that the two-component system (TCS), LytSR functions as a sense-response system for detecting such subtle changes in the *S. aureus* cell membrane potential (Patton, Yang et al. 2006, Sharma-Kuinkel, Mann et al. 2009, Yang, Xiong et al. 2009).

LytSR is comprised of a membrane bound sensor histidine kinase (HK) LytS and a response regulator (RR) protein LytR. The domain architecture of LytS and LytR and a schematic of LytSR TCS signal pathway are shown in Fig 3.1.1. LytS belongs to the family of LytS-like HKs (Anantharaman and Aravind 2003), consisting of six transmembrane helices, embedded in to the membrane, a GAF domain, commonly found

in cyclic Guanosine Monophosphate (c*G*MP)-specific phosphodiesterases, *a*denylyl cyclases, and the *F*hlA protein (hence GAF;(Cann 2007), the DHp domain harboring the conserved His390 residue and the ATP catalytic domain.

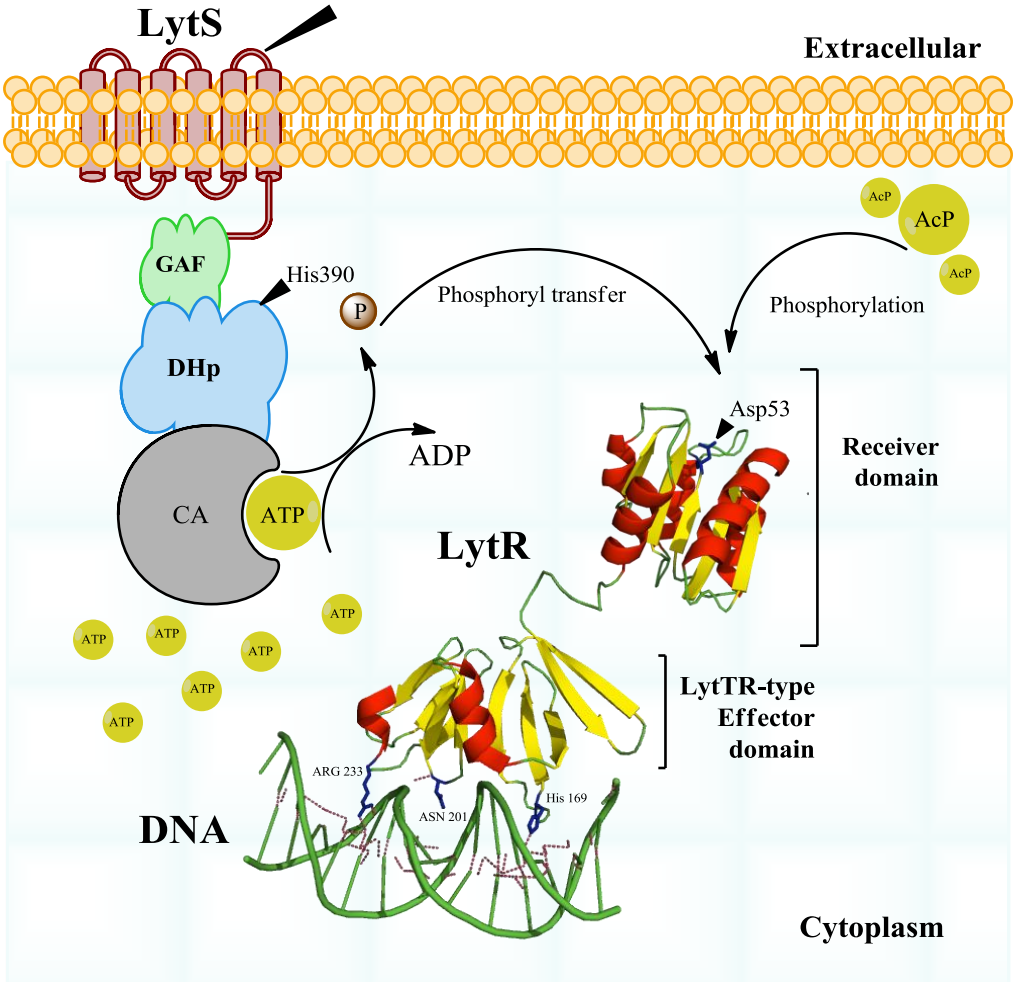

Figure 3.1.1. Architectural design of LytSR TCS and a model of proposed signal propagation

The HK, LytS is consist of a six transmembrane domain and the cytoplasmic N-terminal has a GAF domain linked with the downstream dimerization and histidine phosphotrasnfer domain (DHp). The C-terminal of LytS is the ATP catalytic domain (CA). The RR, LytR is consist of the receiver domain ($LytR^{N}$) and the effector domain ($LytR^{C}$). The crystal structure shown here for the effector domain is of a homologous protein AgrA, a member of LytTR family. A model of signal propagation through a *S.aureus* LytSR TCS shows a cascade of phosphoryl group transfer to elicit a response.

The response regulator protein LytR belongs to the AlgR/AgrA/LytR family of the transcription factors (Sidote, Barbieri et al. 2008) involved in regulation of important virulence factors in pathogenic bacteria (Galperin 2008). It is consists of two domains, the N-terminal Receiver domain ($LytR^{N}$), and the C-terminal Effector domain ($LytR^{C}$). In general the Receiver domain of the RRs harbors a conserved Asp residue that undergoes a reversible phosphorylation by the sensor histidine kinase (Gao, Mack et al. 2007, Gao and Stock, 2010). It is generally accepted that phosphorylation of the Receiver domain initiates a series of conformational changes which ultimately modulate the output response of this proteins (Gao and Stock, 2010). The Effector domain of LytR is a DNA-binding protein that falls into the novel family of non-helix-turn-helix DNA- binding domains, known as LytTR (Nikolskaya and Galperin 2002, Sidote, Barbieri et al. 2008). These groups of effector domains are unique in their ability to bind to DNA and account for ~ 2.7% of all prokaryotic RRs (Galperin 2008). Given that they are not found in any known archeal or eukaryotic systems and their low occurrence in prokaryotic system makes them a suitable target for fighting bacterial infections. The Receiver domains are conserved among the different families of response regulators, OmpR and NarL, unlike the DNA-binding domain, which understandably needs to be variable in order to allow a specific response (Stock, Robinson et al. 2000, Gao, Mack et al. 2007). Nonetheless, there is sufficient variability in the primary structures of the Receiver domains, which limits the cross-talking among two-component systems (Barbieri, Mack et al. 2010).

Recent studies have shown that LytS senses the decrease in transmembrane potential (Sharma-Kuinkel, Mann et al. 2009), which infers that the sensor kinase LytS

may transduce intracellularly this change in membrane potential through phosphorylation of LytR (Fig 3.1.1). LytR is a transcription factor that regulates the *lrgAB* and *cidABC* operons (Brunskill and Bayles 1996). Both operons are involved in the control of apoptosis and cell lysis and in turn regulating the extracellular DNA release during biofilm formation (Groicher, Firek et al. 2000, Rice, Firek et al. 2003). The gene products of the *cid* operon encoding holin like proteins enhances murein hydrolysis activity and trigger cell lysis (Rice, Firek et al. 2003) and antibiotic tolerance, while the *lrg* gene product encoding antiholin like protein, inhibits these processes.

Given the regulatory importance of LytSR TCS, it lacks *in vitro* characterization of the underlying signal transduction mechanism. Herein, we report the kinetic characterization of LytS autophosphorylation; phosphoryltransferase and phosphotase reaction using radiolabel [γ-^{32}P] ATP. Furthermore, we also show acetyl phosphate mediated phosphorylation of the full length LytR and LytR^{N} and investigate phosphorylation induced activation of LytR and its DNA binding efficiency in particular to the *lrgAB* promoter region (Patton, Yang et al. 2006). For the purpose of the above *in vitro* experiments, we have cloned LytS lacking its transmembrane domains along with the full length, C-terminal and N-terminal of LytR.

3.2 Materials and methods

3.2.1 Chemicals

Chemicals and antibiotics were purchased from Sigma (Oakville, Canada) or Thermo-Fisher (Whitby, Canada), unless otherwise stated. Chromatography media and columns were purchased from GE Healthcare (Quebec, Canada). Growth media were purchased from Fisher. *Escherichia coli* strains, NovaBlue and BL21 (DE3), and other expression plasmids were purchased from EMD4 Biosciences (New Jersey, USA). The pGEX-4T-1 vector was purchased from GE Healthcare (Quebec, Canada). The Champion pET Directional TOPO Expression Kit was purchased from Invitrogen (Burlington, Ontario). Restriction enzymes were obtained from New England Biolabs (NEB) Canada (Pickering, Canada) or Thermo-Fisher. The DNA polymerase PfuTurbo® and Phusion High-Fidelity were purchased from Agilent Technologies (Mississauga, Canada) and Thermo Scientific (Whitby, Canada), respectively. The [γ-^{32}P] ATP was purchased from Perkin Elmer LAS Canada Inc. (Toronto, Canada) and the cold ATP was purchased from NEB. The Proteo Extract All-in-One Trypsin Digestion Kit was purchased from EMD4 Bioscience. The genomic DNA of *S. aureus* strain Mu50 was obtained from Cedarlane (Burlington, Canada).

3.2.2 Cloning of the *LytS* gene into an expression plasmid

The gene sequence of *lytS* (SAV0260) containing the cytoplasmic region of the protein (amino acid residues 355-584) was amplified from *S. aureus* MU50 genome using the primers: Dir 5'- *CACC*GCAGAAGGATTGGCAAAT -3' and Rev 5'-

TTATTCCTCCTCTTGTCTTTCA -3'. The *lytS* gene was directionally cloned into pET151/D-TOPO using the Champion™ pET Directional TOPO® Expression Kit. This cloning strategy resulted in introducing an N-terminal 6xHis tag upstream of *lytS*.

To enable directional cloning, the forward PCR primer contained a specific 4 base pair (bp) sequence (italicized) at the 5' end of the primer. The 701 bp *lytS* gene was amplified using Phusion High-Fidelity DNA polymerase with the following PCR conditions: initial denaturation at 98^{o}C for 30s, followed by 30 cycles of denaturation at 98^{o}C for 10s, annealing at 61^{o}C for 20s, extension at 72^{o}C for 20s and final extension at 72^{o}C for 10 min. The blunt ended amplicon was then directly added to the TOPO cloning reaction containing pET151/D-TOPO vector and salt solution (as per instructions in the kit). The ligated *pET151/D-TOPO::lytS* construct was used to transform *E.coli* NovaBlue cells for further amplification. The correct sequence of *lytS* gene was confirmed by DNA sequencing (The Centre for Applied Genomics, the Hospital for Sick Kids, Toronto, Canada; Appendix A Fig A2). And finally the construct *pET151/D-TOPO::lytS* was used to transform the *E. coli* BL21 (DE3) expression cells.

3.2.3 Expression and purification of His-LytS

A frozen glycerol stock of *E. coli* BL21 (DE3) cells carrying the construct *pET151/D-TOPO::lytS* was used to inoculate 5 ml of Luria Bertani (LB) medium in the presence of 100 µg/ml final concentration of ampicillin. An aliquot of 1ml of the overnight grown seed culture was used to inoculate 1 L of Terrific Broth medium supplemented with 100 µg/ml of ampicillin. The cells were allowed to grow to an

OD_{600nm} of 0.6 - 0.8 absorbance unit at 37 ^{o}C, 200 rpm. Once growth was achieved the media was cooled to 4 ^{o}C and protein expression was induced by adding IPTG at a final concentration of 0.1 mM at 18 ^{o}C for 12 hrs. The cells were harvested by centrifugation at 3300 x g for 20 min and the resulting pellet was stored at -80 ^{o}C in aliquots of 3 g until time of purification. All purifications steps were carried out in the cold room at 4 ^{o}C using FPLC. For purification of His-LytS protein, the stored pellet at -80 ^{o}C was resuspended in 50 mM sodium phosphate pH 7.5, supplemented with 300 mM NaCl and 10 mM Imidazole. The cellular contents were liberated by sonication while cooling on ice for 10 min (10s on/15s off) and cell debris was removed by centrifugation at 18,000 x g for 1 hour at 4 ^{o}C. Purification was carried out by loading the supernatant onto a self-assembled affinity column (Generon) packed with 8 mL of Ni-NTA resin. The unbound protein was removed by washing with suspension buffer for 3 CV. The protein of interest was eluted at a flow rate of 1.5 ml/min in 3 CV at each step gradient of 10%, 40% 70% and 100% of the elution buffer (50 mM sodium phosphate pH 7.5 buffer supplemented with 300 mM NaCl and 300 mM imidazole). Collected fractions of 5 mL containing the protein were concentrated using Amicon Ultra- 10K concentrator (Millipore) followed by buffer exchange by dialysis into storage buffer (50 mM Tris pH 7.5, supplemented with 150 mM NaCl and 5 mM $MgCl_2$). The homogeneity of protein was assessed by Coomassie Blue staining of the 15% SDS-PAGE.

3.2.4 Cloning of the *lytR* gene into expression plasmid

The gene sequence of *lytR* (SAV0261) translating into full length protein was amplified from *S. aureus* MU50 genome using the primers: Dir 5'- GGAATTC*CATATG*

AAAGCATTAATCATAGATGATG-3' and Rev 5'-CGG*AATTC* TTATTAAAGTAATCCTATCGACG-'3. The primers were designed to contain *NdeI* and *EcoRI* restriction sites (italicized sequences) at 5' and 3' of *lytR* ends, respectively. PCR amplification of 741 bp *lytR* gene was carried out using Phusion® High-Fidelity DNA polymerase and the thermal cycler conditions included: initial denaturation at 98^{o}C for 30s, followed by 30 cycles of denaturation at 98^{o}C for 10s, annealing at 62^{o}C for 20s, extension at 72^{o}C for 20s and final extension at 72^{o}C for 10 min. Following PCR amplification, the resulting amplicon was purified and both the PCR product and the host vector, pET26b were digested with NdeI and EcoRI. The resulting sticky end products were gel purified from 1% agarose gel using the QIAquick Gel Extraction Kit (Qiagen). Subsequent ligation reaction between *lytR* and pET26b resulted in the construct *pET26b::LytR*. The ligated *pET26b::LytR* construct was used to transform *E. coli* NovaBlue cells for further amplification. The correct sequence of the *lytR* gene was confirmed by DNA sequencing (The Centre for Applied Genomics, the Hospital for Sick Kids, Toronto, Canada; Appendix A, Fig A2). And finally the plasmid harboring the *LytR* gene was used to transform the *E. coli* BL21 (DE3) expression cells. This cloning strategy didn't result in an introduction of any tags or additional amino acids.

3.2.5 Cloning of the *LytR^{N}* gene into expression plasmid

To clone the receiver domain of the LytR protein, LytR^{N} (residues 1-134), a stop codon after the amino acid residue 134 was introduced using the QuikChange® Site-Directed Mutagenesis method. The process of site directed mutagenesis was carried out using the *Pfu* Turbo® DNA polymerase and the following mutagenic primers: 5' -

GCGAATGATATGTCG*TAG*AATTTTGATCAAAGC-3' and 3'-GCTTTGATCAAAATT*CTA*CGACATATCATTCGC- 5' (mutated nucleotides are italicized). The construct *pET26b::LytR* was used as the template DNA. The amplified mutagenic construct, *pET26b::LytR* (A135*) was treated with the restriction endonuclease *DpnI* and used to transform *E. coli* NovaBlue cells. Successful insertion of the stop codon was confirmed by DNA sequencing (The Centre for Applied Genomics, the Hospital for Sick Kids, Toronto, Canada; Appendix A, Fig A2) and the *pET26b::LytR*^{N} construct was used to transform the *E. coli* BL21 (DE3) expression cells.

3.2.6 Cloning of the *LytR*^{C} gene into expression plasmid

To clone the effector domain of LytR (LytR^{C}) spanning the residues 135 - 246 following primers were designed: Dir 5'-GCTATTC*CATATG*GCGAATTTTGATCAAAGC-3' and Rev 5'-CG*GAATTC*TTATTAAAGTAATCCTATCGACG-'3. The primers were designed to contain *NdeI* and *EcoRI* restriction sites (italicized sequences). PCR amplification of the 318 bp long *lytR* gene was carried out using *Taq* DNA polymerase (Thermo scientific) and the construct, *pET26b::lytR* as template. The thermal cycler conditions included: initial denaturation at 95^{o}C for 50s, followed by 30 cycles of denaturation at 95^{o}C for 30s, annealing at 55^{o}C for 60s, extension at 70^{o}C for 50s and final extension at 70^{o}C for 10 min. Following PCR amplification, the resulting amplicon was purified and both the PCR product and the host vector, pET26b were digested with *NdeI* and *EcoRI*. The resulting sticky end products were gel purified from 1% agarose gel using the QIAquick Gel Extraction Kit (Qiagen). Subsequent ligation reaction into pET26b vector resulted in the

construct *pET26b::lytR*^{C}. The ligated *pET26b::lytR*^{C} construct was used to transform *E. coli* NovaBlue cells for further amplification. The correct sequence of *lytR*^{C} gene was confirmed by DNA sequencing (The Centre for Applied Genomics, the Hospital for Sick Kids, Toronto, Canada; Appendix A, Fig A2). And finally the plasmid harboring the *lytR*^{C} gene was used to transform the *E. coli* BL21 (DE3) and C43 (DE3) expression cells. This cloning strategy didn't result in an introduction of any tags or additional amino acids.

3.2.7 Expression and purification of LytR and LytR^{C}

A frozen glycerol stock of *E. coli* BL21 (DE3) cells carrying appropriate constructs were used to inoculate 5 ml of Luria Bertani (LB) medium in the presence of 50 µg/ml final concentration of kanamycin. An aliquot of 1 ml of the overnight grown seed culture was used to inoculate 1 L of Terrific Broth medium supplemented with 50 µg/ml of kanamycin. The cells were allowed to grow to until OD_{600nm} reached 0.6-0.8 absorbance unit with shaking at 200 rpm at 37^{o}C. Once growth was achieved the media was cooled to 4 $^{\circ}$C and protein expression was induced by adding IPTG to a final concentration of 0.1 mM at 18 $^{\circ}$C for 12 hrs. The cells were harvested by centrifugation at 3300 x g for 20 min and the resulting pellet was stored at -80 $^{\circ}$C in aliquots of 5 g until time of purification. To isolate LytR and LytR^{C}, the method of protein precipitation by ammonium sulfate was employed. All purifications steps were carried out in the cold room at 4^{o}C system. As before, the stored pellet at -80^{o}C was suspended in 1:10 (w/v) of 50 mM Tris, pH 8.0, 100 mM NaCl, 5 mM $MgCl_2$ supplemented with 10% glycerol. The cellular contents were liberated by sonication while cooling on ice for 10 min (10s on/15s off) and cell debris was removed by centrifugation at 18,000 x g for 1 hour at 4 ^{o}C. Total

volume of supernatant was adjusted to be 50 ml and 2.67 g of ammonium sulfate ($(NH_4)_2SO_4$) was added gently while stirring, to achieve saturation of 10%. Then the saturated solution was incubated while stirring at 4^oC for 30 mins. Centrifuge at 3300 x g for 15 mins to pellet the precipitated proteins. Completely resuspend the pellet of protein in 10 ml of 50 mM Tris, pH 8.0, 100 mM NaCl, 5 mM $MgCl_2$ supplemented with 10% glycerol and incubate for 5 mins while rotating. Centrifuge again at 3300 x g for 15 mins to pellet the precipitated proteins and collect the supernatant. Repeat this step 5 times to maximize the yield of LytR protein. The collected supernatant was pooled and concentrated using Amicon Ultra-10K concentrator (Millipore) and protein homogeneity was evaluated by 15% SDS-PAGE stained with Coomassie blue.

3.2.8 Identification of His-LytS and LytR by mass spectrometry

After purifying the proteins, the homogeneity of the protein was determined by Coomassie Blue staining of the 15% SDS polyacrylamide gel. The band corresponding to the protein of interest was cut from the gel and was subject to in-gel trypsin digestion carried out using the Trypsin Profile IGD kits (Sigma). Proteins identities were confirmed by liquid chromatography-mass spectrometry (LC-MS/MS) at the Advanced Protein Technology Centre at The Hospital for Sick Children (Toronto, Canada).

3.2.9 Cloning of *lytR* gene to introduce a GST tag

The gene sequence of *lytR* (SAV0261) translating into full length protein was amplified from *S. aureus* MU50 genome using the primers: Dir 5'- AGTCG*GGATCC* ATGAAAGCATTAATCATAGATG-3' and Rev 5'- CG*GAATTC* TTATTAAAGTAATCCTATCGACG -'3. The gene was cloned into pGEX-4T-1 vector

so to introduce an N-terminus GST tag on LytR. The primers were designed to contain *BamHI* and *EcoRI* restriction sites (italicized sequences) at 5' and 3' of *lytR* ends respectively. PCR amplification and thermal cycler conditions was similar to that used for amplification of the $lytR^{C}$. And the cloning strategy was similar to that described for cloning of the *lytR* gene without any tags. Sequencing results shown in Appendix A Fig A2

3.2.10 Site directed mutagenesis of Asp 53 to Ala in GST-LytR

The Asp-53 residue of GST-LytR was mutated to Ala residue by the method of QuikChange® Site-Directed Mutagenesis. Briefly, the process of site directed mutagenesis was carried out using the *Pfu* Turbo® DNA polymerase with the designed mutagenic primers: 5' - ACATTATATTTTTA*GCT*GTCAATTTAATGG -3' and 3'- CCATTAAATTGAC*AGC*TAAAAATATAATGTC - 5' (mutated nucleotides are italicized). The construct, *pGEX-4T1::lytR* was used as a template. The amplified mutagenic construct, *pGEX-4T::lytR* (D53A) was treated with the restriction endonuclease *DpnI* and used to transform *E.coli* NovaBlue cells. Successful mutation of Asp to Ala was confirmed by DNA sequencing (The Centre for Applied Genomics, the Hospital for Sick Kids, Toronto, Canada, Appendix A Fig A2) and the final *pGEX-4T::lytR* (D53A) construct was used to transform the *E.coli* BL21 (DE3) expression cells.

3.2.11 Expression and Purification of GST-LytR and GST-LytR (D53A)

A frozen glycerol stock of *E. coli* BL21 (DE3) cells carrying the desired constructs were used to inoculate 5 mL of Luria Bertani (LB) in the presence of 100 µg/mL final concentration of ampicillin. An aliquot of 1 mL of the overnight grown seed

culture was used to inoculate 1 L of Terrific Broth medium supplemented with 100 µg/mL of ampicillin. The cells were allowed to grow until (OD_{600nm}) reached 0.6-0.8 at 37 ^{o}C, 200 rpm. Once growth was achieved the media was cooled to 4 ^{o}C and protein expression was induced by adding IPTG at a final concentration of 0.5 mM at 18 ^{o}C for 12 hrs. The cells were harvested by centrifugation at 3,300 x g for 20 min and the resulting pellet was stored at -80 ^{o}C in aliquots of 3 g until time of purification. All purifications steps were carried out in the cold room at 4^{o}C using the FPLC (Amersham Bioscience). For purification of the wild type and mutant GST-LytR protein, the stored pellet at -80 ^{o}C was suspended in 1:10 (w/v) of 50 mM Tris pH 7.5, supplemented with 100 mM NaCl and 5 mM $MgCl_2$. The cellular contents were liberated by sonication while cooling on ice for 10 min (10s on/15s off) and cell debris was removed by centrifugation at 18,000 x g for 1 hour at 4 ^{o}C. Purification was carried out by loading the supernatant onto a self-assembled affinity column packed with 5 mL of GST affinity resin (Generon). The protein of interest was eluted at a flow rate of 1.5 mL/min with 100% of elution buffer (50 mM Tris-Cl pH 8.0 supplemented with 10 mM reduced glutathione) over 3 CV. Collected fractions of 5 mL containing the protein were concentrated using Amicon Ultra- 10K concentrator (Millipore) followed by buffer exchange by dialysis into storage buffer (50 mM Tris pH 7.5, supplemented with 100 mM NaCl and 5 mM $MgCl_2$). The homogeneity of protein was assessed by 12.5 % SDS-PAGE stained with Coomassie blue.

3.2.12 Expression and purification of $LytR^N$

A frozen glycerol stock of *E. coli* BL21 (DE3) cells harboring the construct *pET26b::LytR*^{N} was used to inoculate 5 mL of LB media in the presence of 50 µg/mL final concentration of kanamycin. An aliquot of 1 mL of the overnight grown seed culture was used to inoculate 1 L of Terrific Broth medium supplemented with 50 µg/mL of kanamycin. The cells were allowed to grow to until OD_{600nm} reached 0.6-0.8 absorbance unit while shaking at 200 rpm at 37 ^oC. Once growth was achieved the media was cooled to 4 ^oC and protein expression was induced by adding IPTG to a final concentration of 0.5 mM at 25 ^oC for 12 hrs. The cells were harvested by centrifugation at 3,300 x g for 20 min and the resulting pellet was stored at -80 ^oC in aliquots of 5 g until time of purification. All purifications steps were carried out at 4 ^oC using FPLC. To isolate $LytR^N$, the stored pellet at -80 ^oC was suspended in 1:10 (w/v) of 20 mM Tris pH 7.5, supplemented with 5 mM $MgCl_2$. The cellular contents were liberated by sonication while cooling on ice for 10 min (10s on/15s off) and cell debris was removed by centrifugation at 18,000 x g for 1 hour at 4 ^oC. The supernatant was loaded onto a DEAE-Sepharose™ column (GE Healthcare). The protein was eluted over 10 column volumes in a linear gradient of 20 – 500 mM Tris pH 7.5, and 5 mM $MgCl_2$ at a flow rate of 3 ml/min. $LytR^N$ elution peaks were pooled and concentrated by centrifugation using Amicon Ultra-3K concentrator (Millipore) to a final volume of 5 mL. $LytR^N$ was then further purified and buffer exchanged into 100 mM Tris pH 7.5, 5 mM $MgCl_2$ by size exclusion chromatography using HiPrep 26/60 Sephacryl S-200 HR gel-filtration column (GE Healthcare). Ten milliliters fractions corresponding to $LytR^N$ were collected, and

concentrated to 13 mg mL^{-1} (Nanodrop 2000, Thermo Scientific) for crystallization. The homogeneity of the protein was determined using 18% SDS-PAGE. The identity of the protein was confirmed by electrospray ionization mass- spectrometry (ESI-MS) analysis (Advanced Protein Technology Center, Toronto). In collaboration with Dr. Audette's group, crystals trays of $LytR^N$ were setup and screened by Agnesa Shala (Agnesa et al., 2013) and conditions for crystallization were optimized.

3.2.13 Assessment of in-vitro autokinase activity of His-LytS

3.2.13.1 Time dependent autophosphorylation and determination of the rate of autophosphorylation of His-LytS

His-LytS at 5 µM was equilibrated in phosphorylation buffer (PB: 50 mM Tris, pH 7.4, 50 mM KCl, 5 mM $MgCl_2$) supplemented with 10 mM $CaCl_2$. The phosphorylation reaction was initiated by the addition of [γ-^{32}P]-ATP (10 Ci/mmol) mixed with cold ATP at different concentration (10 to 600µM) at room temperature (RT). Samples were removed at different time intervals and the reaction was quenched by adding 5 x SDS sample buffer (125 mM Tris, pH 6.8, 2.5% SDS, 25% glycerol, 100 mM DTT, 0.0025% bromophenol blue). Samples were loaded on to 15% SDS-PAGE. The radioactive gels were washed in ddH_2O containing 2% (v/v) glycerol and gels were exposed to phosphor screen (GE Healthcare) overnight and imaged using a Typhoon $Trio^+$ imager (GE Healthcare). The radioactive gels were stained by Coomassie blue dye.

Each experiment, at different ATP concentration was repeated two times and average intensities were quantified using NIH ImageJ software (Version 1.45s). A graph of intensity versus time was plotted and data were fitted to non-linear fitting curve using

the pseudo first order equation $I = A(1\text{-}e^{-kt})$, where I is the average band intensity, *k* is the rate constant, *t* is the time and A is the proportionality constant relating intensity with concentration of phosphoryalted His-LytS. The data were fitted using Erithacus GraFit software (version 5.0.10). The rate of phosphorylation was calculated for each different ATP concentration. In addition, a graph of rate versus ATP concentration was also plotted and fitted to the Mechalis-Menten equation below:

$$v = Vmax \times \frac{[S]}{Km + [S]}$$

to calculate binding efficiency, K_m and catalytic efficiency, k_{cat}.

3.2.13.2 Effect of salt ions on the phosphorylation of His-LytS

His-LytS at 3 µM was equilibrated in phosphorylation buffer (PB: 50 mM Tris, pH 7.4, 5 mM $MgCl_2$) with varying concentrations of either KCl or $CaCl_2$. The phosphorylation reaction was initiated by the addition of [γ-^{32}P]-ATP (10 Ci/mmol) to final concentration of 20 µM. The reaction was incubated for 90 min at RT then quenched by adding 5X SDS sample buffer. Samples were loaded on to 15% SDS-PAGE. The radioactive gels were washed in ddH_2O containing 2% (v/v) glycerol and gels were exposed to phosphor screen (GE Healthcare) overnight and the screen was imaged using a Typhoon Trio$^+$ imager (GE Healthcare).

3.2.13.3 Investigating stability of phosphoryalted His-LytS

His-LytS at 10 µM was allowed to undergo autophosphorylation for 90 min by adding [γ-^{32}P]-ATP (10 Ci/mmol) to a final concentration of 20 µM. Excess [γ-^{32}P]-ATP

was removed by desalting using the Zeba Spin Desalting column (Pierce, Thermo Scientific) equilibrated with PB. The reaction mixture was further incubated at RT and aliquots were removed at different time interval and quenched by adding 5X SDS sample buffer. Samples were loaded on to 15% SDS-PAGE. The radioactive gels were washed in ddH_2O containing 2% (v/v) glycerol and gels were exposed to phosphor screen (GE Healthcare) overnight and the screen was imaged using a Typhoon Trio$^+$ imager (GE Healthcare). Later the radioactive gels were stained by Coomassie blue dye.

3.2.14 Phosphotransfer reaction from His-LytS to GST-LytR, GST-LytR D53A mutant and LytR^N

His-LytS at 15 µM was phosphorylated for 90 min as described above (3.2.13.1). Excess [γ-^{32}P]-ATP was removed by desalting using the Zeba Spin Desalting column (Pierce, Thermo Scientific) equilibrated in PB (PB: 50 mM Tris, pH 7.4, 50 mM KCl, 5 mM $MgCl_2$). Phosphorylated His-LytS (4 µM) was added to a master mixture containing GST-LytR (10 µM) in the PB buffer so to keep a ratio of 2:5 between HK and RR. The final reaction mixture was incubated at RT (25 ^oC) and aliquots of 10 µL were removed at different time intervals and quenched by adding 10 µL of 5X SDS sample buffer. Samples were loaded on to 15% SDS-PAGE. The radioactive gels were washed in ddH_2O containing 2% (v/v) glycerol and gels were exposed to phosphor screen (GE Healthcare) overnight and imaged using a Typhoon Trio$^+$ imager (GE Healthcare). The radioactive gels were stained by Coomassie blue dye as well. These experiments were repeated multiple times to find optimum reaction conditions. Intensities of two trials were quantified using NIH ImageJ software (Version 1.45s). Phosphorylation intensities were

normalized to phosphoryalted His-LytS and a graph of relative intensity versus time was plotted. The phosphotransfer reaction between mutant GST-LytR (D53A) and $LytR^N$ were carried out similarly.

3.2.15 Investigating the phosphotase activity of His-LytS

A phosphotransfer reaction between His-LytS and GST-LytR was setup as described above. After the phosphotransfer reaction reached completion, fresh His-LytS at 4 µM was added to the reaction mixture and incubated at RT. Aliquots of 10 µL were removed at different time intervals and reaction was quenched by adding 10 µL of 5X SDS sample buffer. Samples were loaded on to 15% SDS-PAGE gels and gels were incubated overnight and phosphotase activity was assessed by scanning using Typhoon $Trio^+$ imager (GE Healthcare)

$LytR^N$ at 20 µM was phosphorylated with 50 mM acetyl phosphate for 90 min in PB and access acetyl phosphate was removed by desalting and fresh His-LytS at 5 µM was added to the reaction mixture and incubated at RT. Reaction was quenched and samples were analyzed by 15 % Phos-tag gel. The gel was stained with Coomassie blue to view the protein bands.

3.2.16 Investigating crosstalk between His-LytS and other response regulators

To investigate crosstalk between His-LytS and GraR and VraR, a phosphotransfer reaction was carried out as described above. The reaction was observed at one time point only and gel was analyzed by autoradiography as above.

3.2.17 Phosphorylation of LytR and LytR^N by acetyl phosphate

LytR and GST-LytR at 10 µM and LytR^N at 20 µM was equilibrated in PB20 buffer (PB: 50 mM Tris, pH 7.4, 50 mM KCl, 20 mM $MgCl_2$) and phosphorylation was initiated by addition of lithium potassium acetyl phosphate to final concentration of 50 mM. The reaction mixture was incubated at 37 ^oC and 15 µL aliquots were removed and quenched by adding 5x SDS sample buffer. The phosphorylated species were separated from unphosphorylated species on 15% Phosphate Affinity SDS-PAGE containing Acrylamide-pendant Phos-tag™ AAL-107 (50 µmol/L) as the active chemical (Wako chemical USA, inc., Cedarlane) (Kinoshita, Kinoshita-Kikuta et al. 2006). From here this gel will be referred to as Phos-tag gel. The gels were stained by Coomassie blue dye and intensities of the phosphoryalted species two trials (only for LytR^N) were quantified using NIH ImageJ software (Version 1.45s) and averaged. A graph of intensity versus time was plotted and data were fitted to non-linear fitting curve using the pseudo first order equation on Erithacus GraFit software (version 5.0.10) and the rate of phosphorylation was determined.

3.2.18 Analysis of the oligomerization state of His-LytS and LytR

Varying concentration of His-LytS and LytR were loaded on to a 10% native polyacrylamide gel electrophoresis (NATIVE -PAGE) and the oligomerization states of protein under native condition was analyzed. The gels were stained with Coomassie blue to visualize any protein bands. Note that internal temperature of the buffer during the gel running process was maintained at 4^oC.

3.2.19 Analysis of the oligomerization state of phosphorylated LytR^N

LytR^N was phosphorylated by acetyl phosphate as described above. Varying concentrations (10 µM, 20 µM and 40 µM) of unphosphorylated and phosphoryalted samples of the LytR^N protein were loaded on to a 10% native polyacrylamide gel electrophoresis (NATIVE-PAGE) and the oligomerization a state of protein was analyzed under native condition. The gels were stained with Coomassie blue to visualize protein bands. Note that internal temperature of the buffer during the gel running process was maintained at 4 ^oC. Similarly, Phosphorylated and unphosphorylated LytR^N at 80 µM was also analyzed using size exclusion chromatography TSKgel G2000SW$_{XL}$ (7.8 x 300mm, 5 µm, TOSOH Biosciences LLC) on HPLC.

3.2.20 Circular dichroism (CD) spectroscopy and thermal melting curves for His-LytS, LytR and LytR^N

Circular Dichroism (CD) spectrum (200-260nm) of LytR (20 µM), heat denatured LytR and LytR supplemented with 10 mM and 50 mM $CaCl_2$ was recorded using a Jasco J-180 instrument at 20 ^oC. The buffer composition in this experiment was 20 mM Tris, 5 mM $MgCl_2$ pH 8.0. Similarly CD spectrum was recorded for sample of non-denatured and heat denatured His-LytS (20 µM) and LytR^N (20 µM) proteins in 50mM sodium phosphate buffer at pH 7.4. CD spectrum of LytR^N phosphoryalted by acetyl phosphate was also recorded. Excess acetyl phosphate was removed by desalting. Two spectra scans were averaged for the sample and the buffer. Later, buffer contribution was subtracted and the buffer corrected data were plotted on a graph using Microsoft Excel.

Thermal melting curves were acquired for His-LytS and $LytR^N$ protein using the Jasco J-180 instrument. 20 µM of respective proteins were buffer exchanged in to 50 mM Sodium phosphate buffer at pH 7.4. The melting spectrum was recorded at by monitoring the change in CD signal at 222 nm by ramping the temperature from 20 ^oC to 90 ^oC at a rate of 3 ^oC min. The obtained data were analyzed on Excel.

3.2.21 Assessment of the DNA-binding activity of LytR by electromobility shift assay (EMSA)

Binding of LytR and phosphorylated LytR to the promoter region of *lrgAB* (P_{lrgAB}), downstream of the *lytSR* operon was assessed by electrophoretic mobility shift assay (EMSA). The promoter region of *lrgAB* (P_{lrgAB}) 120 bp in length was PCR amplified from *S. aureus* MU50 genome using the following primes: Dir 5'-ACAGTAATCCTTTTTTTTATGC -3' and Rev 5'- ACGACCATTGCCTCCTACG -'3. The resulting blunt end amplicon was ligated to pSTblue blunt end vector. The resulting construct, *pSTBlue::*P_{lrgAB} was then used to transform *E. coli* NovaBlue cells. The fidelity of the gene sequence was verified by DNA sequencing (The Centre for Applied Genomics, the Hospital for Sick Kids, Toronto, Canada) and this construct was used as template for all subsequent amplifications.

To perform EMSA experiments, the gel purified P_{lrgAB} DNA fragment was 5' end labeled with [γ-^{32}P]-ATP (3000 Ci/mmol) by T4 polynucleotide kinase for 1 hr at 37^oC. A master mixture containing 5' end labeled P_{lrgAB} (final concentration 2 ng per binding reaction), 1 µg poly (dI-dC) and 200 ng sheared herring sperm DNA, 10X EMSA binding buffer (100 mM Tris, pH 7.5, 500 mM KCl, 10 mM DTT), 5 mM $MgCl_2$ and 2.5% (v/v)

glycerol was prepared and aliquots were added to tube containing the protein of interest to initiate the binding reaction (20 µL final volume). Binding reactions were incubated for 30 mins at 25^{o}C and were loaded on to 8% native polyacrylamide gels, pre-run for 30 mins in 0.5X TBE (Tris-borate-EDTA) buffer at 200V at 4^{o}C. The competition reaction was also carried out by adding 100-fold excess unlabeled DNA. After electrophoresis, the radioactive gels were exposed to phosphor screen (GE Healthcare) for 2 hrs and imaged using a Typhoon Trio^{+} imager (GE Healthcare).

3.3 Results

3.3.1 Sequence alignment of LytR

LytR is a two domain response regulatory protein with a N-terminal receiver domain (residues 1-135) and C-terminal effector domain (residues 135-246, Fig.3.1.1).

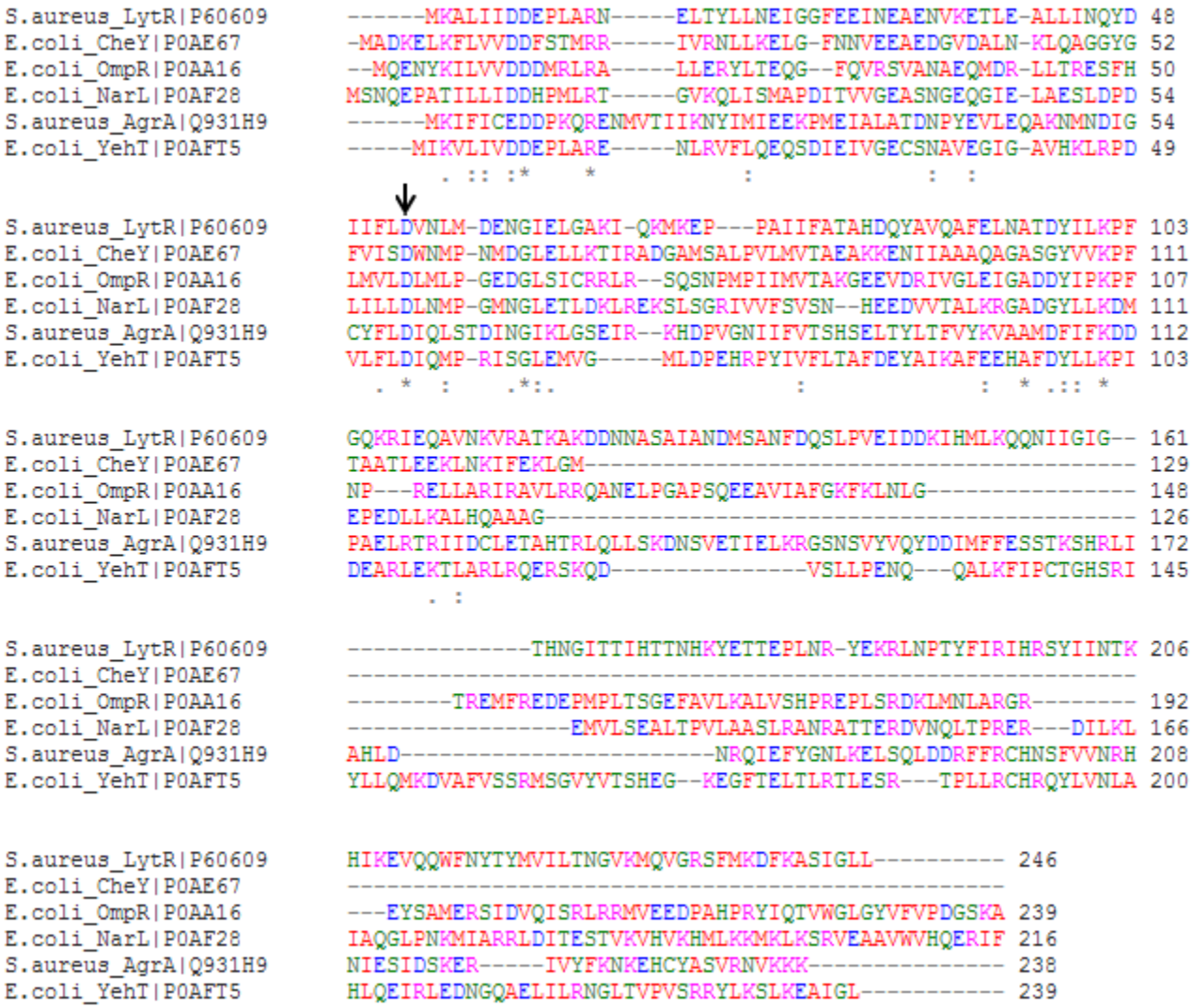

Figure 3.3.1. Sequence alignment of well studied response regulators.

Alignment of LytR protein sequence with some of the CheY, OmpR, NarL, AgrA and YehT. An asterisk indicates conserved residues. A semi colon indicates conservation of strongly similar properties. Hydrophobic residues are highlighted in red and most acidic residues are highlighted in blue. The sequences for each proteins were obtained from Uniprot.

Sequence analysis of LytR reveals that the receiver domain is significantly homologous to other well characterized RRs belonging to the OmpR/NarL family. Based on the sequence alignment in Fig 3.3.1, it is evident that the predicted phosphorylation site Asp53 and other residues in the active site required for phosphotransfer are also highly conserved. The effector domain of LytR, a unique non-helix turn helix DNA binding domain is however not conserved and need to vary to accommodate different DNA binding sites.

3.3.2 Cloning, expression and purifications of His-LytS

Domain organization analyses of LytS (584 amino acid) showed the kinase harbors six transmembrane domains (residues 6 – 206). To overcome the issue of protein insolubility, only the cytoplasmic region (residues 352 – 584) of the kinase was cloned. The desired gene sequence of *LytS* was directly cloned into the pET151/D-TOPO vector and transformed in to *E. coli* BL21 (DE3) expression cells. Protein over expression was optimized for (Fig. 3.3.2) to achieve workable amount of soluble protein. Induction with 0.1 mM IPTG, at 18 ^{o}C for 12 hrs yielded sufficient amount of soluble protein for subsequent purification steps.

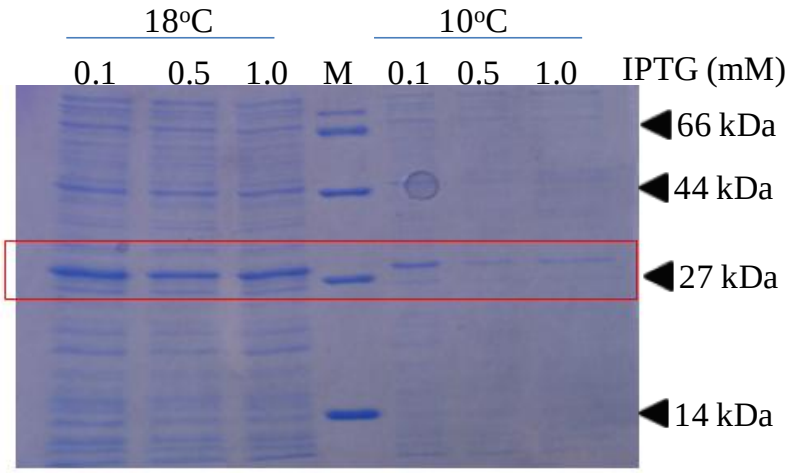

Figure 3.3.2. Optimization of conditions for His-LytS overexpression.

The BL21 (DE3) cells carrying the construct *pET151/D-TOPO:: lytS* were grown to OD_{600} equal to 0.6 in the presence of 100 µg/ml final concentration of ampicillin. The overexpression of His-LytS was probed at three different concentrations of IPTG; 0.1 mM, 0.5 mM and 1.0 mM and at two different temperatures, 10°C and 18°C. The supernatant was analyzed by 15% SDS-PAGE. Overexpression was achieved by induction with 0.1 mM IPTG, at 18°C for 12 hrs yield.

Purification of His-LytS was carried out using a Ni-NTA column attached to the FPLC system. It was aided by the N-terminal 6x His tag. After removal of the cell debris, the soluble fraction of supernatant was loaded on to the Ni-NTA column and the protein of interest was eluted with step gradient of increasing concentration of imidazole (Fig.3.3.3A). It was observed that majority of protein eluted at imidazole concentration of 120 mM and 210 mM (Fig.3.3.3B) with homogeneity and negligible amount of impurities of lower molecular weight. Per liter of cell culture, 9 mg of His-LytS would be obtained on average. Concentrated His-LytS, Fig 3.3.3C, was positively identified by in-gel trypsin digestion followed by LC-MS/MS (Appendix A, Fig A4).

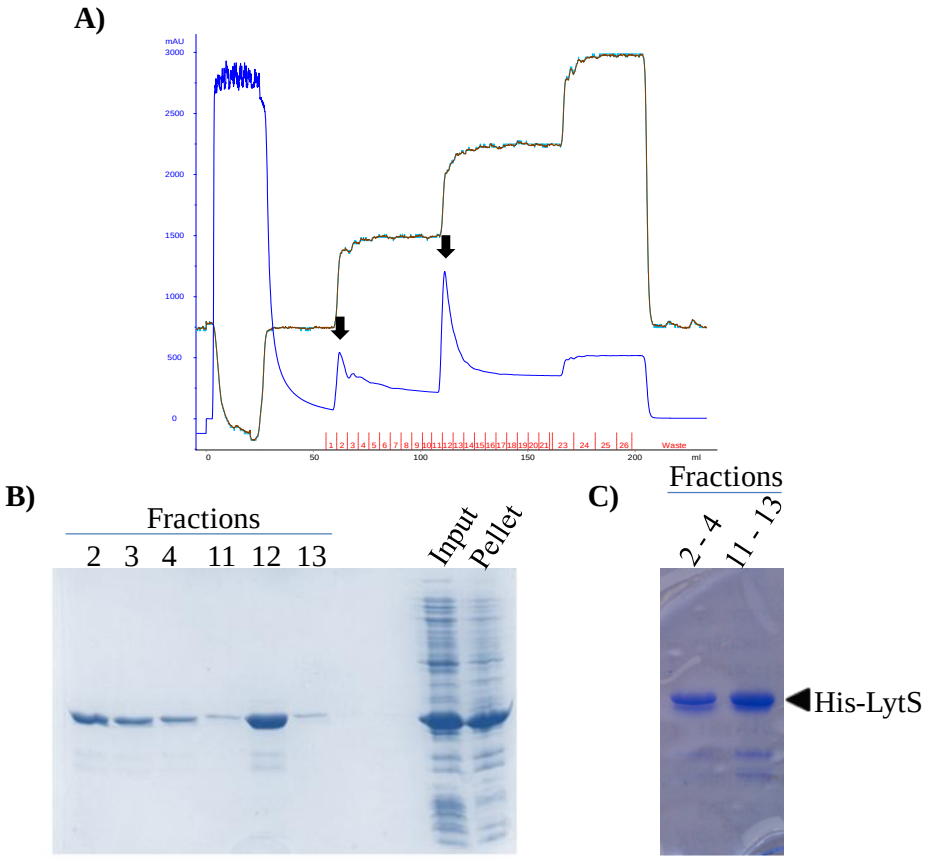

Figure 3.3.3. Purification of His-LytS using Ni-NTA column and subsequent analysis of eluted fractions by SDS-PAGE

A) FPLC chromatogram representing the elution profile of His-LytS from a Ni-NTA column. The blue and brown traces represent absorbance at 280 and conductivity, respectively and the arrows indicate the elution peaks. B) Fractions corresponding to each elution peak loaded on to a 15% SDS-PAGE. C) Fractions 2 – 4 and 11 – 13 containing His-LytS concentrated separately and their homogeneity analyzed by 15% SDS-PAGE. All gels were stained with Coomassie Blue for detection of protein bands

The calculated molecular weight of the recombinant protein with 6x His-V5 epitope tag is 28, 359 Da with a theoretical pI of 6.14. Investigation of protein stability and activity showed His-LytS was most stable with minimum loss in activity when stored at -20^{o}C or -80^{o}C with 40% glycerol.

3.3.3 Cloning, expression and purification of full length LytR and its variants

The full length (residue 1 - 246), the effector domain ($LytR^N$: residues 1 - 135) and the receiver domain ($LytR^C$: residue 135-246) of LytR were successfully cloned in to pET26b vector. The cloning strategy employed resulted in placing the target gene under an inducible T7 promoter. To over express the proteins, several conditions including varying temperatures and concentrations of IPTG were tested. The best expression of LytR and $LytR^C$ was achieved when the cells were induced with 0.1 mM IPTG for 12 hrs at 18°C and 0.5 mM IPTG for 12 hrs at 25°C for $LytR^N$ (Fig.3.3.4).

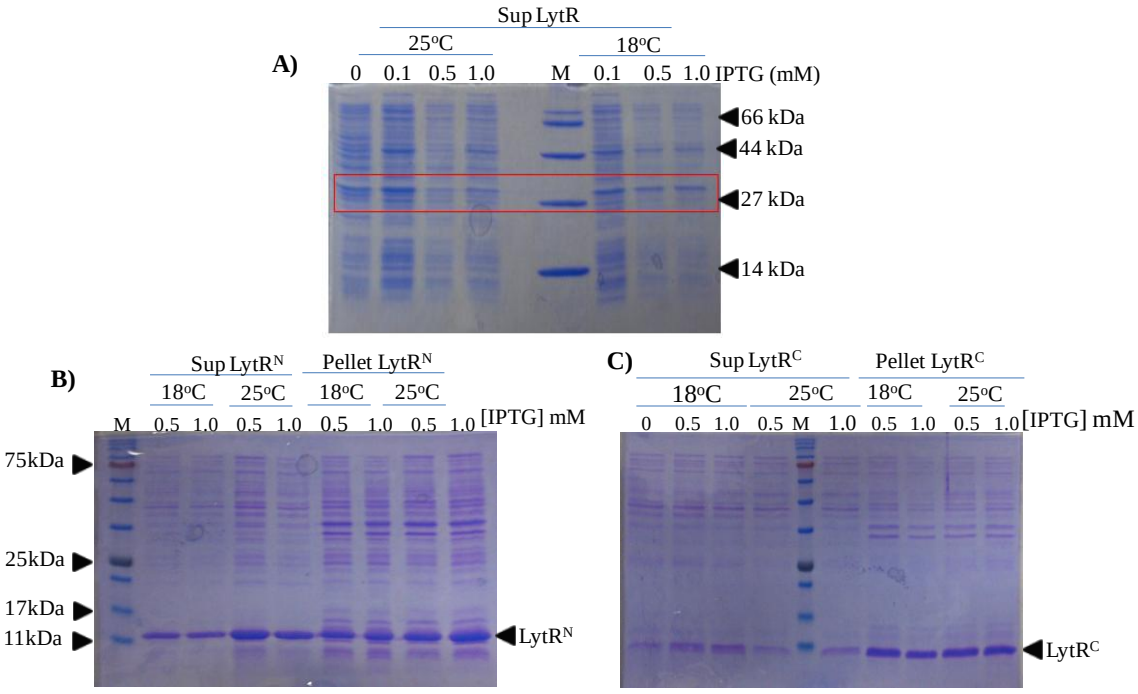

Figure 3.3.4. Optimization of conditions for LytR, $LytR^C$ and $LytR^N$ overexpression.

The BL21 (DE3) cells carrying the appropriate construct were grown to OD_{600} equal to 0.6 in the presence of 50 µg/ml final concentration of kanamycin. The overexpression of protein was probed at different concentrations of IPTG (0.1 mM to 1.0 mM) with two different temperatures, 18°C and 25°C for 12 hrs. The supernatant was analyzed by SDS-PAGE and gels are stained with Coomassie blue. A) and C) Best expression of LytR and $LytR^C$ achieved by induction with 0.1 mM IPTG for 12 hrs at 18°C and B) Best expression of $LytR^N$ is achieved by induction with 0.5 mM IPTG at 25°C for 12 hrs.

It was noted that growth of BL21 (DE3) cells harboring the $LytR^{C}$ protein was retarded, suggesting protein toxicity towards the cells. For this reason, the construct *pET26b::LytR*^{C} was transformed into C43 (DE3) cells used for expression of toxic proteins. Although the protein expressed, the expression was similar to Bl21 (DE3) and the time to reach the desired OD was halved. The overall protein expression of LytR and $LytR^{C}$ was much lower compared to that of $LytR^{N}$ and other expression systems. Unlike a typical RR, purification of LytR didn't prove to be a success using the conventional purification methods. LytR presented a great challenge to purify. LytR interacted very weakly with the resins used in ion exchange chromatography and didn`t bind to the heparin column, widely used technique or purification of transcription factors. After exhausting all purification protocols, successful purification of LytR was achieved by the ammonium sulfate precipitation method (Fig.3.3.5A). Majority of protein precipitated at 10% saturation with ammonium sulfate, suggesting highly hydrophobic nature of the protein. Evidently, the amino acid sequence analysis revealed LytR consisting of 43% hydrophobic residues. The resulting protein pellet was very difficult to redissolve prompting us to investigate several different additives. For example, addition of 0.1% SDS resulted in soluble protein, Fig.3.3.5B, but the protein was rendered biologically inactive, even after through dialysis, because of residual SDS trapped in the individual molecules. For preliminary experiments, we were able to recover sufficient amount of additives free protein. The concentration of the isolated protein was comparatively low and the yield of active protein varied with purification but on average 1 mg of active LytR was obtained per liter of cell culture. The isolated protein was homogenous with

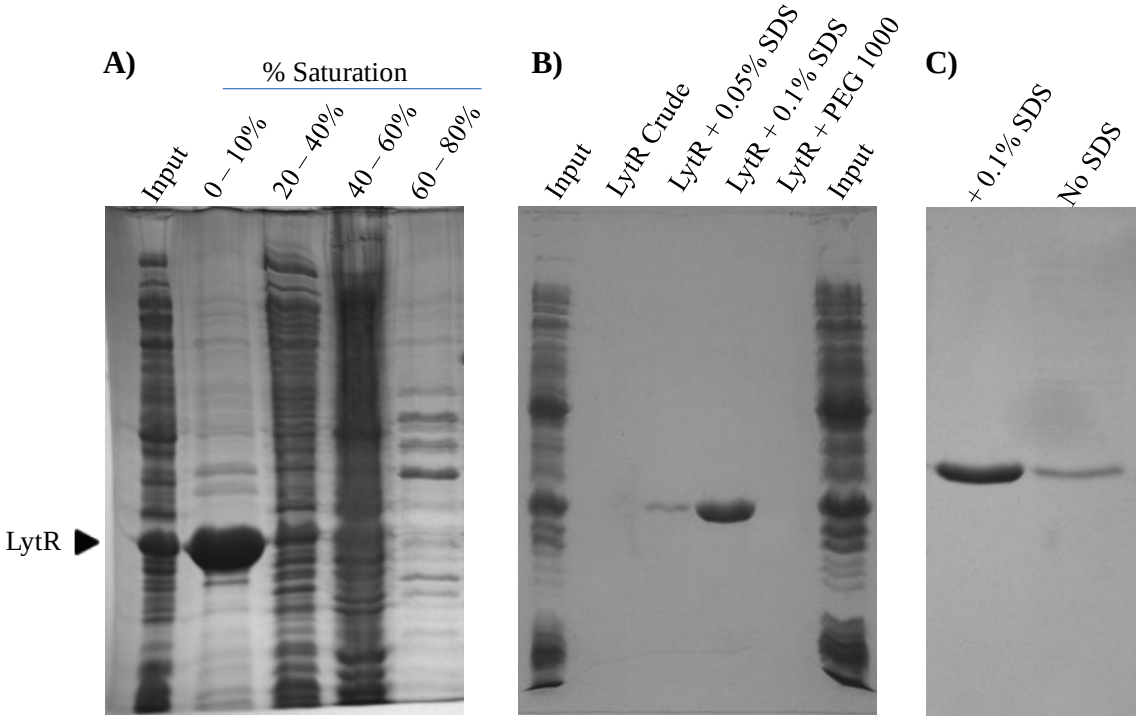

Figure 3.3.5. Purification of LytR by ammonium sulfate precipitation

A) Following removal of cell debris, the supernatant was saturated in steps with ammonium sulfate and sample of precipitated protein pellet was collected and analyzed by 15% SDS-PAGE. Majority of LytR precipitated at10% saturation with ammonium sulfate. B) Resolubility of LytR protein pellet in the presence of different concentration of SDS and PEG 1000 analyzed by 15% SDS-PAGE. C) A 15% SDS-PAGE loaded with concentrated LytR protein with and without SDS. All gels were stained with Coomassie blue staining solution to view the protein bands.

impurities of insignificant amount as assessed by Coomassie Blue staining (Fig 3.3.5C). Identity of protein was positively confirmed by in-gel trypsin digestion followed by LC-MS/MS (Appendix A, Fig A4). The theoretical pI of LytR was calculated to be 5.68 with a molecular weight of 28,221 Da. To overcome the above limitations and in an effort to increase the protein yield, LytR was successfully cloned in to pGEX4T-1 vector. The cloning strategy employed here resulted in a GST tag fused to the N-terminal of LytR. Conditions for over expression of GST-LytR were optimized (Fig 3.3.6). The overall

expression of the protein in the soluble portion was considerably low, contrary to the generally accepted consensus that GST tag aids in protein solubility. The best expression was achieved by induction with 0.5 mM IPTG at 18 °C for 12 hrs.

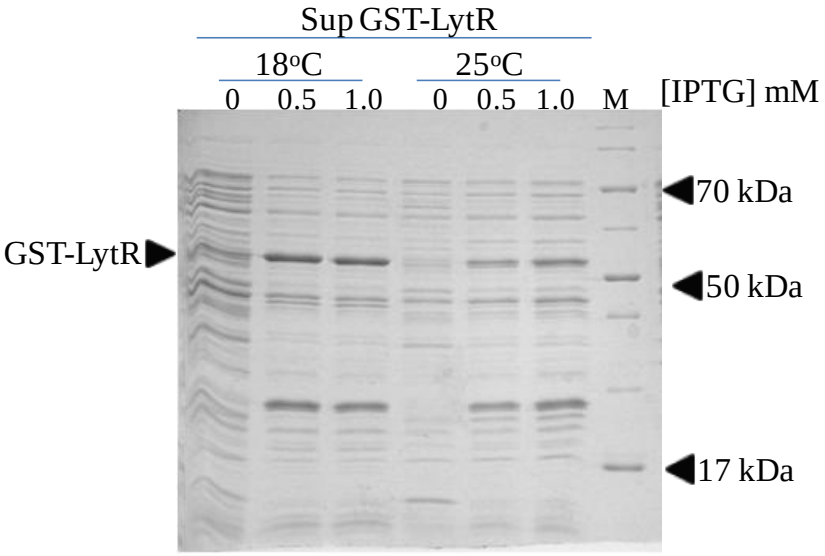

Figure 3.3.6. Optimization of conditions for GST-LytR overexpression.

The BL21 (DE3) cells carrying the construct *pGEX4T-1::lytR* were grown to OD_{600} equal to 0.6 in the presence of 100 µg/ml final concentration of ampicillin. The overexpression of GST-LytR was probed at two different concentrations of IPTG; 0.5 mM and 1.0 mM and at two different temperatures, 18°C and 25°C. The supernatant was analyzed by 12.5 % SDS-PAGE. Overexpression was achieved by induction with 0.5 mM IPTG, at 18°C for 12 hrs .

Similar to His-LytS, purification of GST-LytR was carried out using a GST column attached to FPLC. Fig 3.3.7A shows the collected fractions analyzed by 12.5% SDS-PAGE. Fractions containing the least amount of impurities were pooled and concentrated. On average 3 mg of protein was obtained per liter of culture. The calculated molecular weight is 56, 841 Da.

Using site-directed mutagenesis, the phosphorylation site of GST- LytR, Asp53 was successfully mutated to Ala. The generated mutant, GST-LytR (D53A) was purified using the same protocol as the wildtype (Fig 3.3.7B).

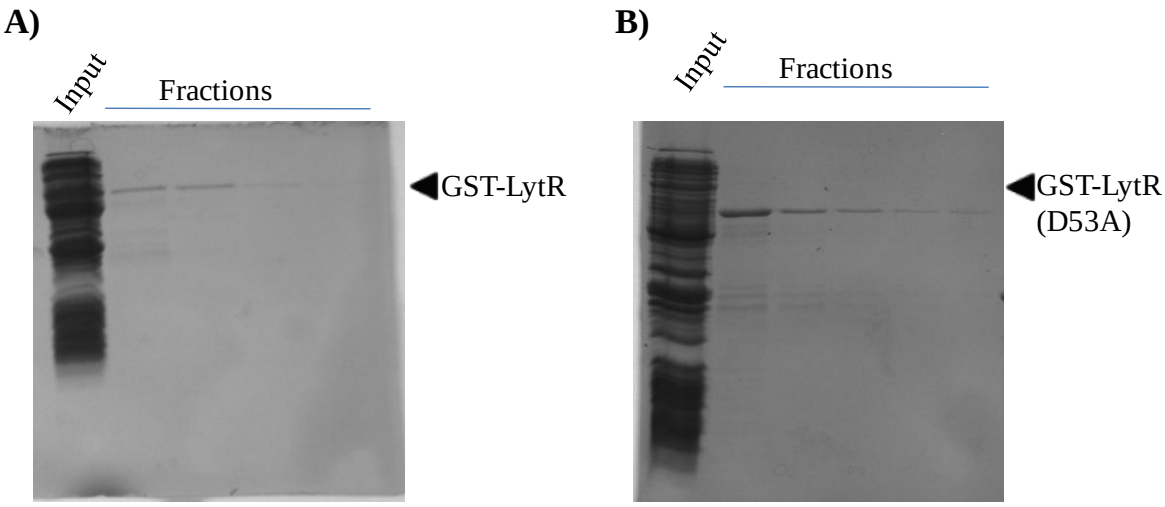

Figure 3.3.7. Purification of wild type and mutant GST-LytR

A) Fractions corresponding to each elution of GST-LytR analyzed by 12.5 % SDS-PAGE. B) Fractions corresponding to each elution of GST-LytR (D53A) analyzed by 12.5 % SDS-PAGE. All gels were stained with Coomassie Blue solution for detection of proteins bands.

Unsuccessful, but once again all attempts to purify $LytR^{C}$ by the conventional method of purification were made. Purification of $LytR^{C}$ by the ammonium sulfate precipitation method revealed similar results (Fig3.3.8) as the full length LytR with low yield of protein, thus hindering us from pursuing further work which involved investigating the DNA binding activity. The theoretical pI of $LytR^{C}$ was calculated to be 9.56 with a molecular weight of 13,342.

Purification of $LytR^{N}$ was carried out by a two step purification protocol involving anion exchange chromatography followed by size exclusion chromatography (SE)

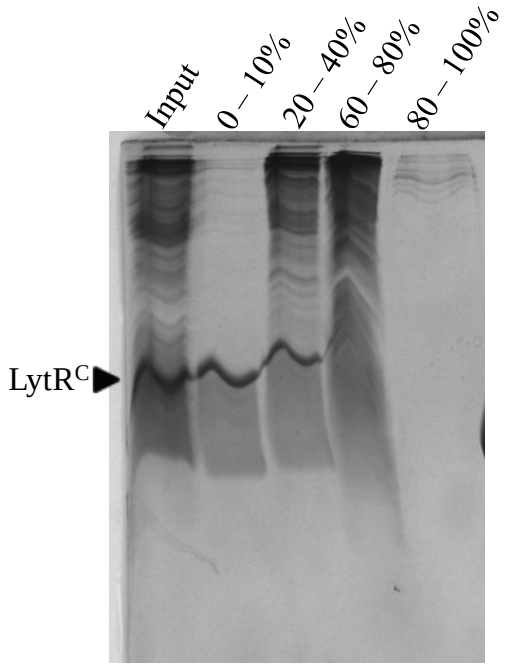

Figure 3.3.8. Ammonium sulfate precipitation of LytR^C

The supernatant was saturated with step gradient of ammonium sulfate and sample of precipitated protein pellet was collected, resuspended and and analyzed by 18 % SDS-PAGE. Majority of LytR^C precipitated at10% saturation with ammonium sulfate.

(Fig.3.3.9). The fact that LytR^N has a pI of 4.44, facilitated with binding of the protein to the positively charged DEAE-Sepharose™ resin equilibrated with 20 mM Tris, pH 7.5, and 5 mM $MgCl_2$ (Fig 3.3.9A). The resulting fractions despite having minor impurities, assessed by 18% SDS-PAGE (Fig 3.3.9B), were further purified by passing through HiPrep 26/60 Sephacryl S-200 HR gel-filtration column (Fig 3.3.9C). Fractions corresponding to LytR^N were collected and concentrated. LytR^N was purified to homogeneity as assessed by Coomassie blue staining of the 18% SDS-PAGE (Fig 3.3.9D). The yield of pure protein was 26 mg per liter of cell culture. The molecular weight of the purified LytR^N protein as determined by ESI-MS was 15, 027 (Appendix A,

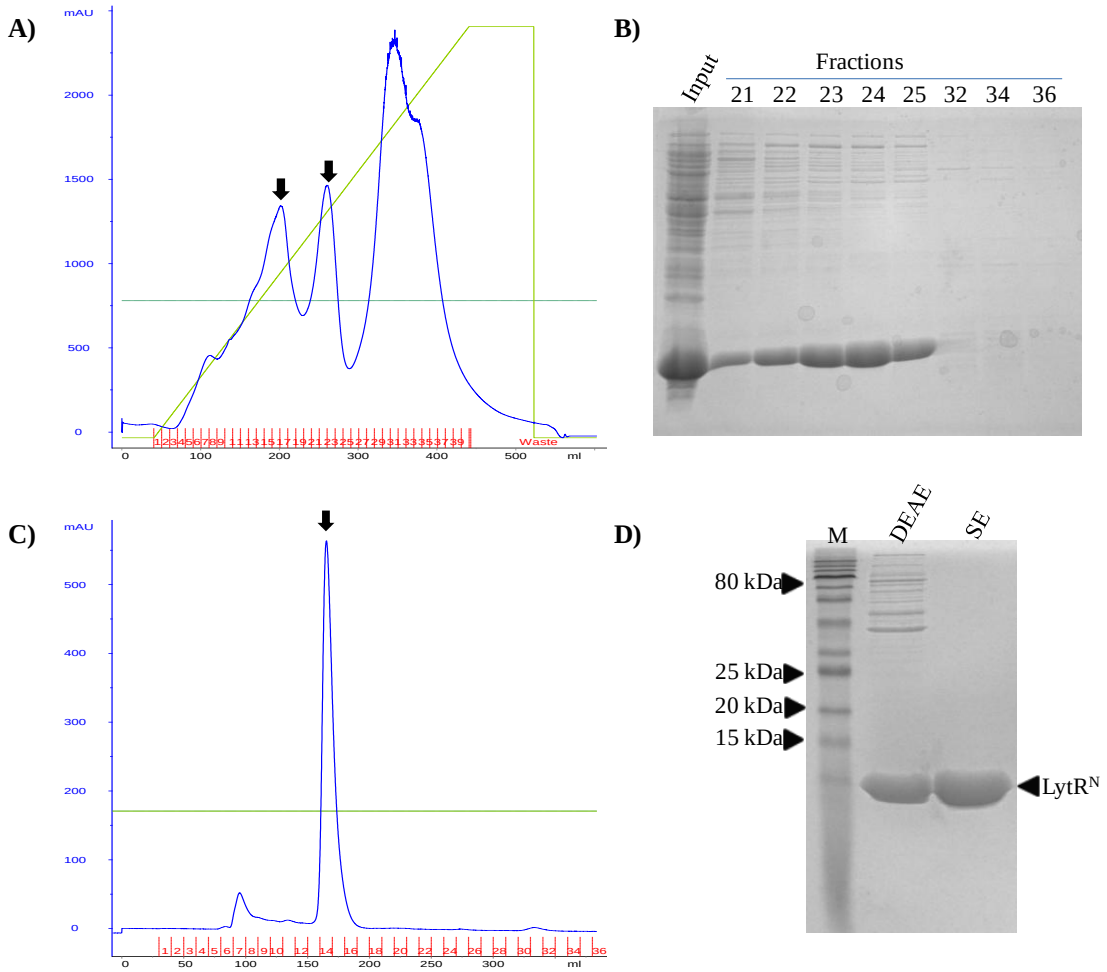

Figure 3.3.9: Purification chromatograms of LytR^N following DEAE column and size exclusion column and analysis of concentrated LytR^N by 18% SDS-PAGE

A) FPLC chromatogram representing the elution profile of LytR^N from 40 mL DEAE column. B) Fractions corresponding to the elution peaks analyzed by 18% SDS-PAGE. C) FPLC chromatogram representing the elution profile of LytR^N from 320 mL size exclusion column (SE). D) Concentrated LytR^N following each purification was separated on an 18% SDS-PAGE to assess homogeneity. All gels were stained with Coomassie Blue for detection of protein bands. A pre-stained broad range protein marker was used from NEB (cat # p7710S).On chromatograms the blue line represents the absorbance at 280 and the arrows indicate the elution peaks.

Fig A4). This is in agreement with the calculated molecular weight of 15, 028. Because of very high yield of LytR^N it was crystallized in collaboration with Dr. Audette`s lab. The purified LytR^N concentrated to 7 mg/ mL was crystallized using the sitting-drop and

hanging-drop vapour-diffusion methods (Shala et. al. 2013). This method yielded a single crystal that diffracted at a resolution of 2.34 Å (Appendix B, Fig B1). The solved structure of $LytR^N$ in collaboration with Dr. Audette's group is shown in Appendix B, Fig B2. The predicted structure using I-TASSER is consistent with the solved structure.

Following purification, attempts to investigate the oligomerization state of His-LytS and LytR were made using a 10% native-PAGE. It should be noted that His-LytS and LytR both have a pI < 7.0. Based on the pI of both proteins, they were expected to enter the gel; however, as observed in Fig.3.3.10 the proteins were unable to enter the separating portion of the gel suggesting that their actual pI differs from the theoretical pI.

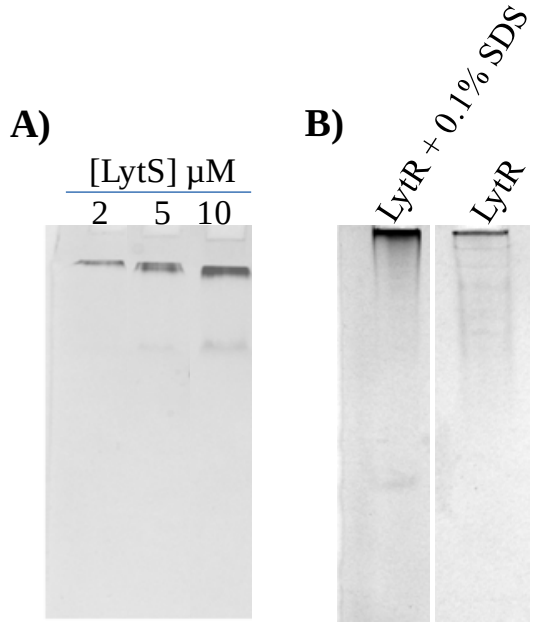

Figure 3.3.10. Analysis of oligomerization state of His-LytS and LytR by native PAGE

A) His-LytS at varying concentrations (2, 5, and 10 µM) was loaded on to a 10% native PAGE.
B) Ammonium sulfate precipitated LytR protein dissolved with and without SDS analyzed by 10% native-PAGE.

3.3.4 Circular dichroism (CD) spectroscopy and thermal melting curves for His-LytS, LytR and $LytR^N$

Before conducting any activity assays, the state of each proteins: folded or unfolded were assessed by obtaining CD spectra and thermal melting curves. Experiments involving CD and thermal melting indicated that His-LytS is highly stable and a well folded protein. Structural analysis of His-LytS based on CD spectrum suggested that His-LytS has a strong α-helical component, indicated by the negative absorbance near 208 nm (Fig.3.3.11A). Furthermore, it was observed that upon boiling, the protein denatured and resembled a spectrum that of an unfolded protein. Melting temperature of His-LytS was estimated to be around 78^{o}C, shown in Fig.3.3.11B, similar to most stable proteins. Close observation of shape of the curve and the first derivative of the CD signal over a range of temperature shows two inflection points (Fig.3.3.11C) suggesting a sequential collapse of the multi-domain kinase, LytS.

The CD spectrum of LytR without any additives (0.1% SDS) resembled that of a folded protein with large amount of beta sheet component (Fig.3.3.12). CD spectrum of LytR also showed protein undergoing conformation changes resulting from boiling and increasing concentration of $CaCl_2$ (Fig 3.3.12). Upon boiling, the protein denatured and resembled a spectrum that of an unfolded protein. Further experiments revealed that increasing concentration of $CaCl_2$ had detrimental effect on the protein resulting in denaturation. Similarly acquired, as shown in Fig.3.3.13A, the CD spectrum of the N-terminal of LytR resembles that of a folded protein consisting of both helices and sheets. Melting temperature of $LytR^N$ is estimated to be 70^{o}C (Fig 3.3.13B&C), indicative of a

highly stable protein.

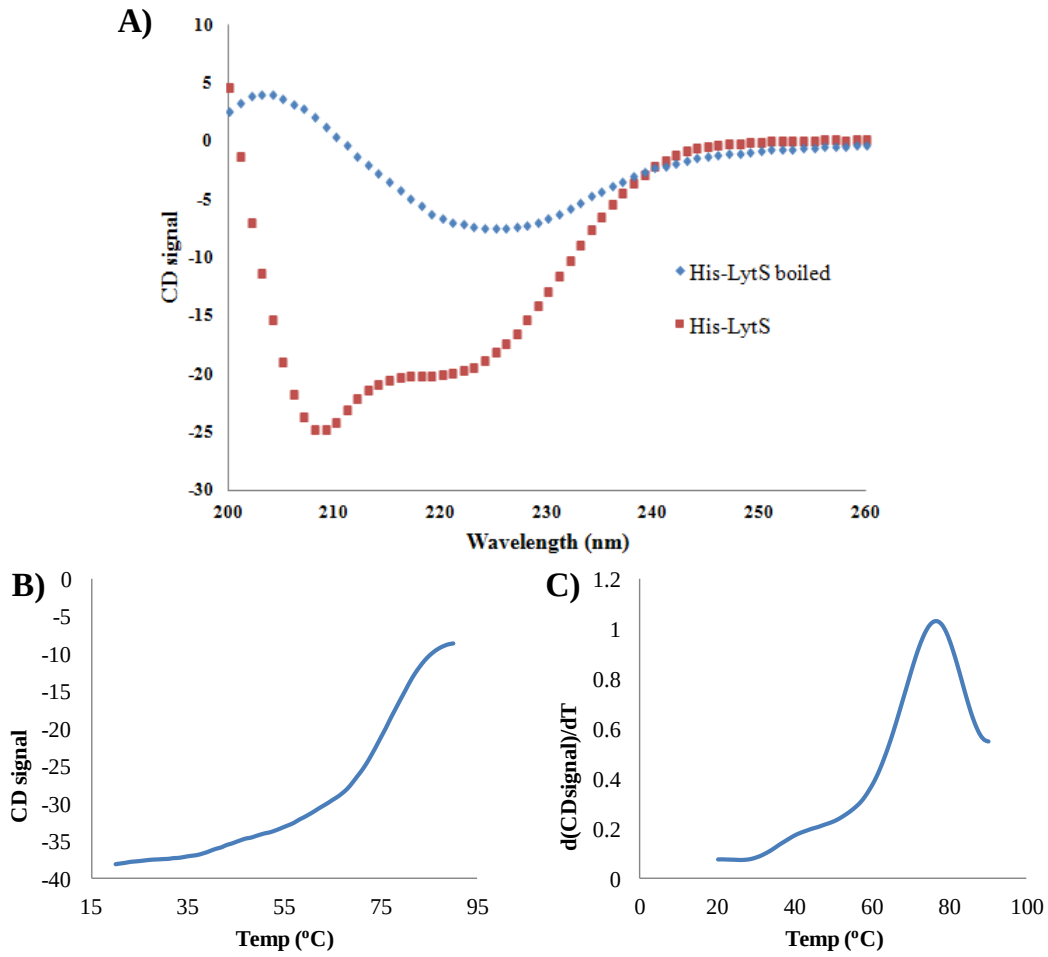

Figure 3.3.11. A circular dichroism (CD) spectra and thermal melting curve of the cytoplasmic domain of His-LytS

A) CD spectra of His-LytS (20 µM, filled squares) and heat denatured His-LytS (20 µM, filled triangles). These spectra were recorded at 22°C in 50 mM sodium phosphate buffer, pH 7.4. B) Thermal melting curve of His-LytS (20 µM) acquired by monitoring the change in ellipcity at 222 nM by ramping the temperature from 20°C to 90°C at a rate of 3°C min in 50 mM sodium phosphate buffer, pH 7.4. C) First derivative plot for melting curve of His-LytS with T_m value of 78°C.

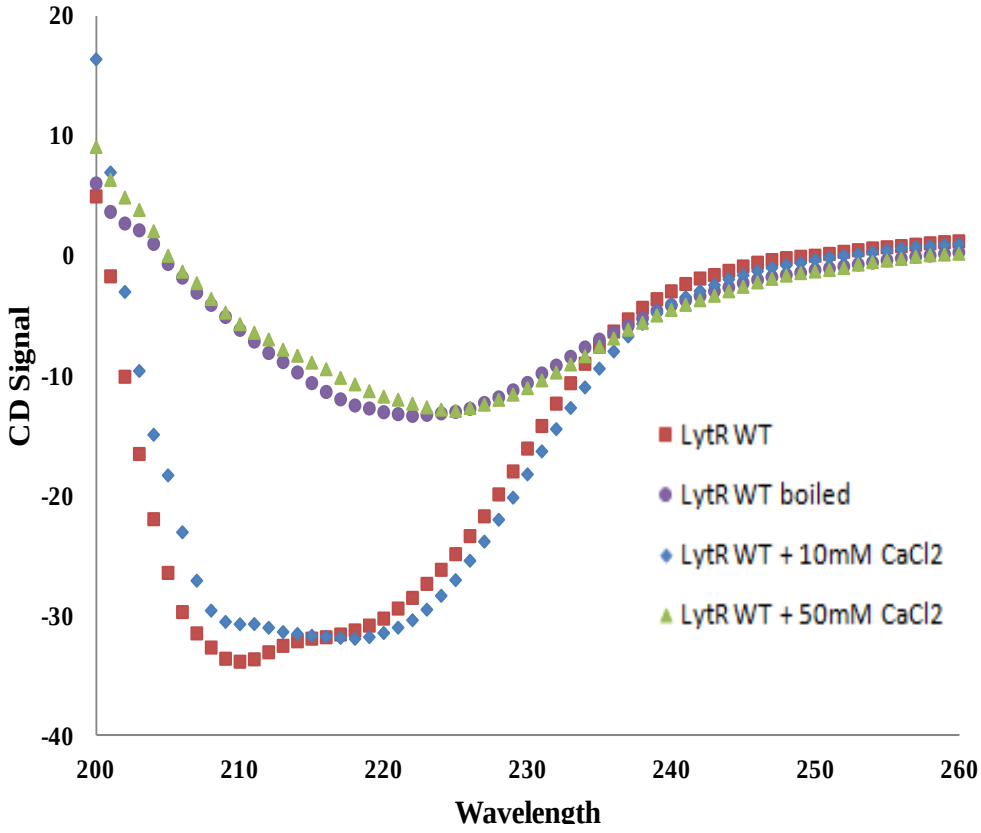

Figure 3.3.12. A circular dichroism (CD) spectra for LytR

CD spectra of LytR (20 µM) , acquired at 22°C in 20mM Tris, 5 mM $MgCl_2$ pH 8.0 buffer shows LytR undergoing conformation changes resulting from boiling (circles) and increasing concentration of $CaCl_2$ (diamond and triangle).

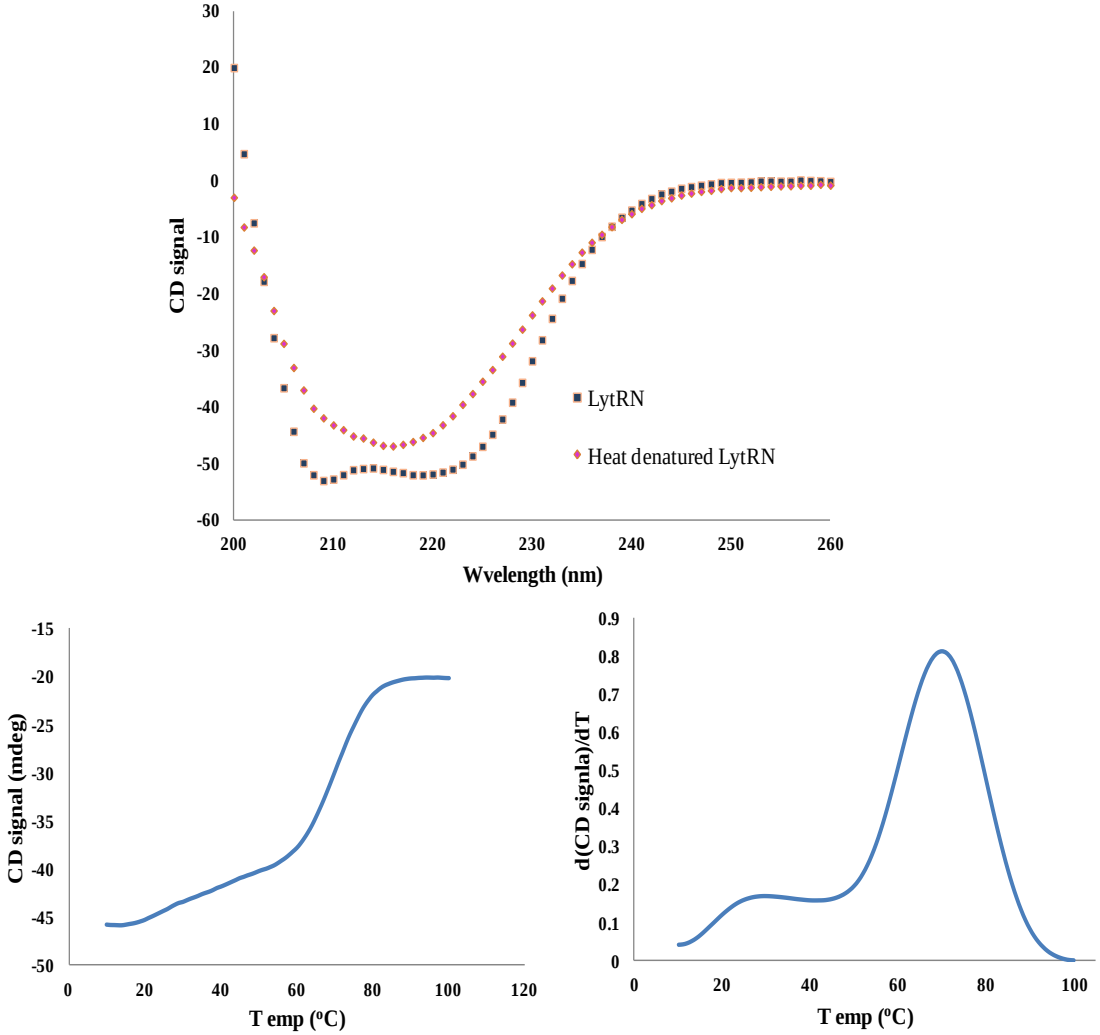

Figure 3.3.13. A circular dichroism (CD) spectra and thermal melting curve of $LytR^N$

A) CD spectra of $LytR^N$ (20 µM) and heat denatured $LytR^N$ (20 µM). These spectra were recorded at 22°C in 50 mM sodium phosphate buffer, pH 7.4. B) Thermal melting curve of $LytR^N$ (20 µM) acquired by monitoring the change in ellipcity at 222 nM by ramping the temperature from 20°C to 90°C at a rate of 3°C min in 50 mM sodium phosphate buffer, pH 7.4 C) First derivative plot for melting curve of $LytR^N$ with two inflection point and T_m value of 70°C.

3.3.5 In-vitro autokinase activity of His-LytS

To assesses the autokinase activity of LytS, a time dependent autophosphorylation of His-LytS was initiated by addition of 100 µM of [γ-^{32}P]-ATP at RT. The results indicated that His-LytS undergoes autophosphorylation in a time-dependent manner (Fig.3.3.14A): a progressive reaction for first 90 min followed by saturation of phosphorylation (Fig.3.3.14B). It was observed that following phosphorylation, the phosphorylated species of His-LytS was stable for over 3 hrs at RT, Fig3.3.14C implying that the phosphate molecule can be transferred anytime within that period to a RR or a phosphotase is required for dephosphorylation.

The pseudo first order rate constant of His-LytS under saturating condition (100 µM ATP) is calculated to be 0.0265 ± 0.0014 min^{-1}. The calculated $t_{1/2}$ time of 30 min suggested relatively slow signal propagation compared to the multiplication time of *S. aureus* (20 min).

Similarly, the pseudo first order rate constant was obtained at different concentration of ATP (ranging from 10 µM to 600 µM, Appendix C, Fig C1). However, it was observed that with increasing concentration of ATP after 100 µM, the rate of reaction started to decrease. This indicated that the enzyme has high affinity for ATP (K_m << [ATP]) and that the maximum rate had been reached requiring more enzyme to drive the reaction faster.

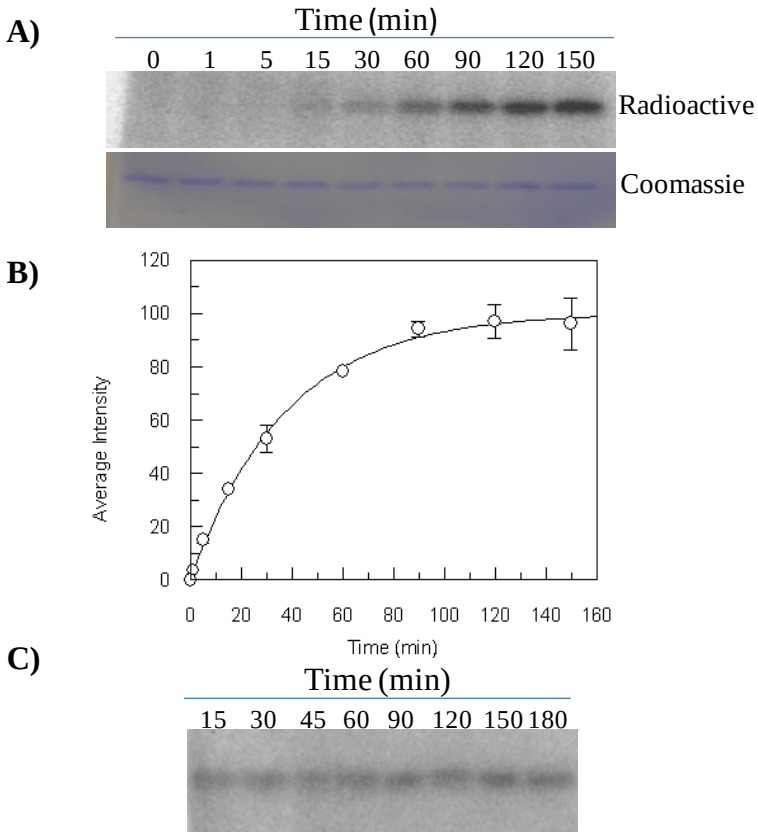

Figure 3.3.14. In vitro autokinase activity of His-LytS

A) Time dependent autophosphorylation of His-LytS . His-LytS at 5 µM was incubated with [γ-^{32}P]-ATP (100 µM) in PB at room temperature. Reaction was quenched at different time intervals and samples were analyzed by 15% SDS-PAGE . B) Progress curve of autophosphorylation reaction. The quantified band intensity of phosphorylation were plotted against time The data were fitted using Origin software to pseudo first order equation to calculate rate constant. The standard deviation represented as errors is averaged over two different trials. C) His-LytS at 5 µM was phosphoryalted for 90 min in PB at room temperature. Excessive ATP was removed by desalting and stability was monitored over 3 hours at different time intervals. Samples were analyzed by 15% SDS-PAGE. All gels were exposed to phosphor screen (GE Healthcare) overnight and imaged using a Typhoon Trio^{+} imager (GE Healthcare). A) was also stained with Coomassie blue staining solution

From the plot of rates versus ATP concentration, Michaelis- Menten kinetics parameters (K_m (ATP) = 7.9 $\pm$ 0.573 µM and k_{cat} = 0.03 ± 0.0005 min^{-1}) were calculated (Fig.3.3.15). The K_m value of 8 µM is very low and it signifies the concentration of ATP

for the enzyme to reach half of the maximum phosphorylation. This result confirms that LytS has high affinity towards ATP.

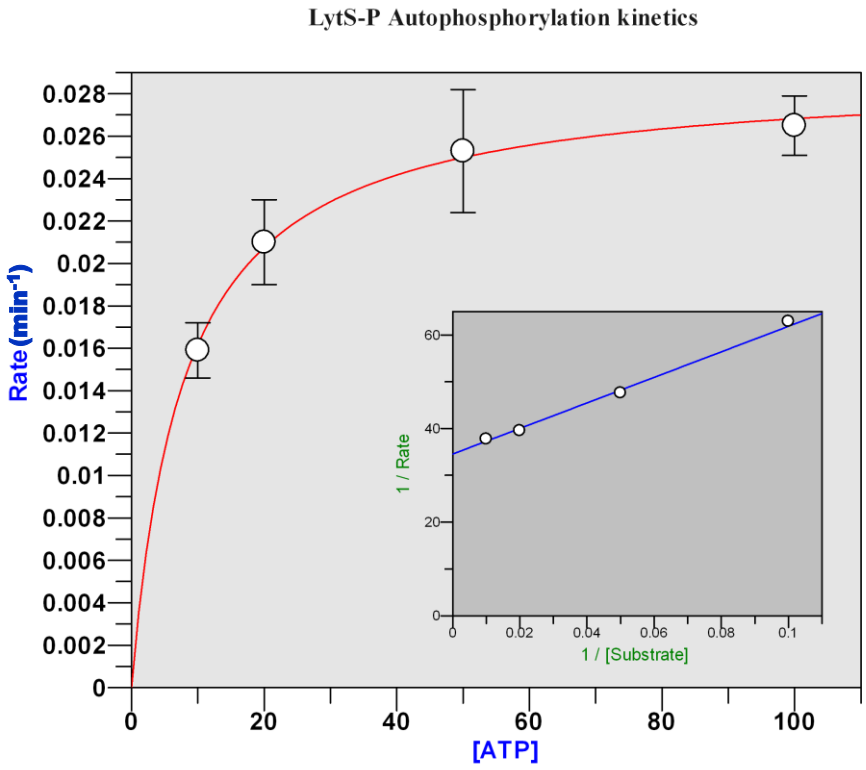

Figure 3.3.15. Determination of His-LytS autophosphorylation kinetics parameters

A plot of rate constant versus [ATP] is fitted to Michaelis - menten equation to determine the ATP binding efficiency, K_m and catalytic efficiency, k_{cat} for autophosphorylation of His-LytS.

Furthermore, the effect of varying concentration of K^+ and Ca^{2+} on autophosphorylation of LytS was investigated (Fig.3.3.16). No significant changes in the autophosphorylation activity of His-LytS were observed with increasing concentration of K^+ and Ca^{2+} ions. In fact contrary to other TCS e.g. WalKR, His-LytS was capable of undergoing phosphorylation in the absence of these ions.

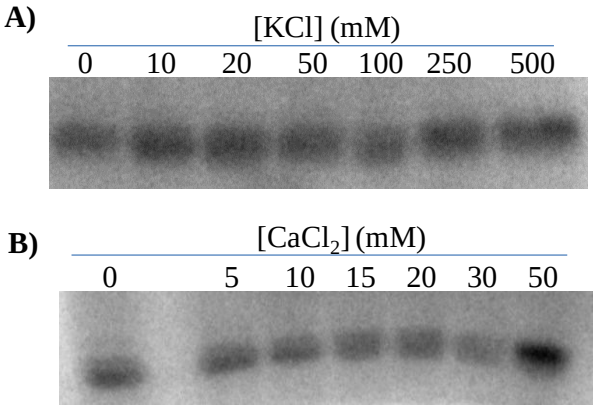

Figure 3.3.16. Effects of metal ions on the autophosphorylation of His-LytS

A) His-LytS at 3 µM was phosphorylated in PB at varying concentration of KCl for 90 min. B) His-LytS at 3 µM was phosphorylated in PB at varying concentration of $CaCl_2$ for 90 min. Reactions were quenched and samples were analyzed by 15% SDS-PAGE. All gels were exposed to phosphor screen (GE Healthcare) overnight and imaged using a Typhoon Trio$^+$ imager (GE Healthcare).

3.3.6 Phosphotransfer reaction from His-LytS to GST-LytR, GST-LytRD53A and $LytR^N$

After establishing the autokinase activity of His-LytS, we proceed to investigate whether phosphorylated LytS (LytS-P) is capable of transferring the phosphoryl group intramolecularly to its cognate RR, LytR. Fig.3.3.17A shows that His-LytS is capable of transferring the phosphoryl group to GST-LytR. It was observed that more than 70% of the phosphate associated with His-LytS was lost within the first 30 mins, but an estimated 30% of it was donated to GST-LytR. It is of note that the quantified intensities at 60 and 90 min time intervals were not considered. Although the transfer was not rapid, it was specific. The specificity of the transfer and the predicted site of phosphorylation, Asp 53, were further confirmed by a transfer reaction to the active site mutant, GST-LytRD53A.

Evidently, as shown in Fig 3.3.17B, the mutant protein failed to undergo phosphorylation by His-LytS. Unexpectedly, no apparent phosphotransfer from His-LytS to $LytR^N$ was observed.

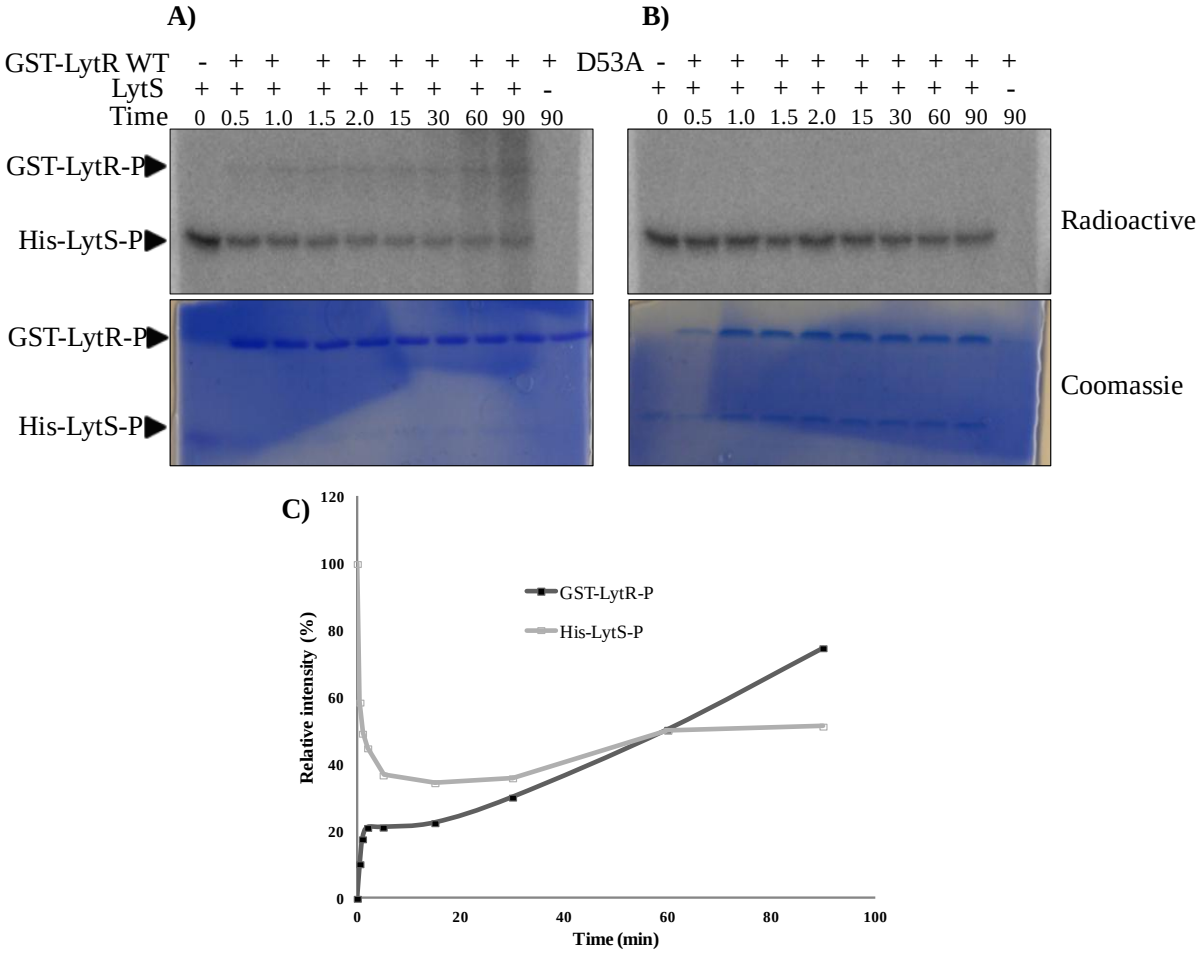

Figure 3.3.17. Phosphotransfer reaction from His-LytS to GST-LytR and its mutant, GST-LytR (D53A)

A) Phosphorylated His-LytS at 4 µM was incubated with GST-LytR at 10 µM in PB at room temperature. The reaction was quenched after various time intervals and samples were analyzed by 15% SDS-PAGE. B) Similar reaction as shown in (A) performed with active site mutant, GST-LytR (D53A). The reaction was quenched after various time intervals and samples were analyzed by 15% SDS-PAGE. C) A graph of relative intensities normalized to phosphoryalted His-LytS versus time (min). All gels were exposed to phosphor screen (GE Healthcare) overnight and imaged using a Typhoon Trio$^+$ imager (GE Healthcare) followed with Coomassie blue staining.

Taking together the slow phosphotransfer kinetics of GST-LytR and no observed transfer between His-LytS and $LytR^N$, it was intriguing to investigate any non-cognate phosphoryl flow between LytS and other well characterized RR, namely VraR and GraR from the lab. It was found that His-LytS was unable to phosphorylate VraR or GraR but this is not to say that cross-talk does not exist. More potential targets can originate from screening of more RRs.

3.3.7 Phosphotase activity of His-LytS

Previous research has shown that most kinases have dual function: one being phosphorylation of their cognate response regulator and the other dephosphorylation (Laub and Goulian 2007). The latter is defined as the phosphotase activity of the kinase. The inefficiencies in the transfer reactions, as shown above, also instigated us to investigate the phosphotase activity of His-LytS. Briefly, phosphoryalted His-LytS was incubated with LytR to allow for a complete phosphotransfer reaction and subsequently unphosphorylated His-LytS was added to the reaction mixture and the phosphotase activity was monitored overtime. Based on Fig 3.3.18, His-LytS completely lacked the phosphotase activity towards both GST-LytR and $LytR^N$

3.3.8 Phosphorylation of LytR and $LytR^N$ by small molecule phosphor-donor and their oligomerization state post-phosphorylation

The ability of LytR and $LytR^N$ to undergo phosphorylation by lithium potassium acetyl phosphate was investigated using the Phos-tag PAGE. In brief, the gel separates the phosphoryalted species from the non-phosphoryalted species based on the principle that the migration of the phosphorylated species is retarded due to charge interaction

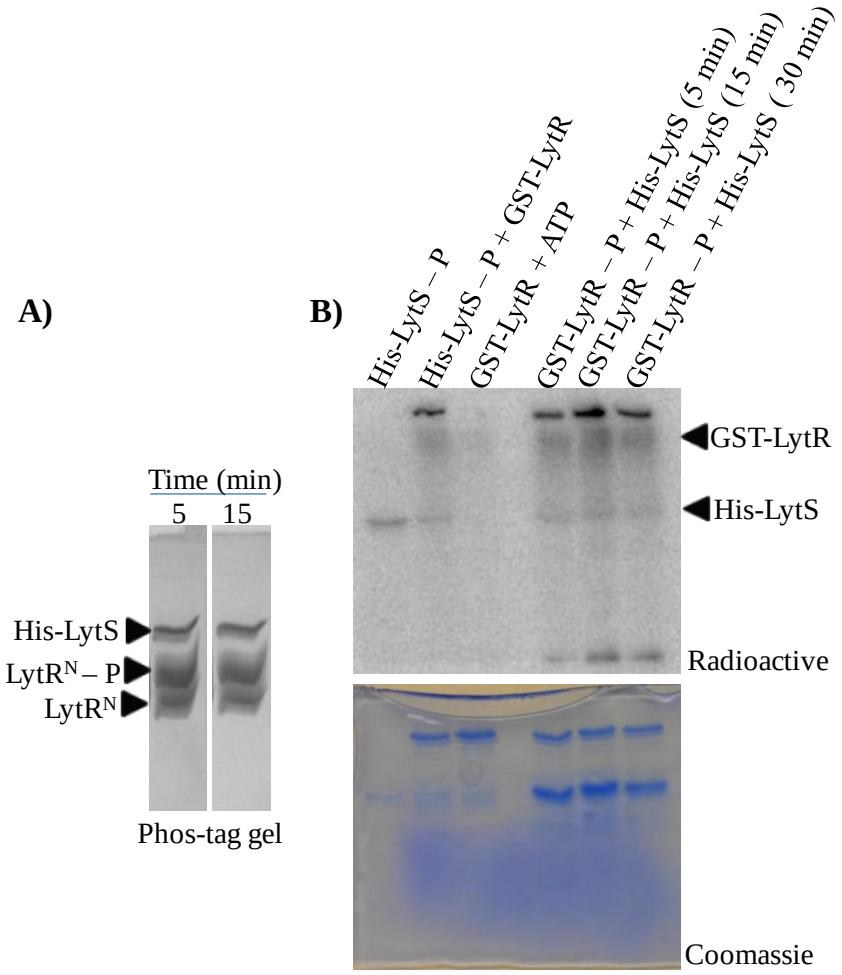

Figure 3.3.18. Investigation of the phosphotase activity of His-LytS

A) $LytR^N$ at 20 µM was phosphoryalted by acetyl phosphate B) GST-LytR was phosphoryalted by His-LytS – ^{32}P. To both reaction mixtures 4 µM of His-LytS was added and reaction was quenched at different time intervals. Samples in (A) were anlayzed by 15 % Phos-tag gel and in (B) by 12.5 % SDS-PAGE. The gel in (B) was first exposed to phosphor screen (GE Healthcare) overnight and imaged using a Typhoon $Trio^+$ imager (GE Healthcare) then both gels were stained with Coomassie blue.

between the negatively charged PO_4^- and the positively charged Mn^{2+} ions chealeted on the Phos-tag chemical. LytR and $LytR^N$ were phosphorylated under the same condition used for phosphorylation of VraR as reported by Belcheva, A and Golemi-Kotra, D

(Belcheva and Golemi-Kotra 2008). As expected, shown in Fig 3.3.19, both the full length LytR and $LytR^N$ undergo phosphorylation and the unphosphorylated species are successfully separated by 12.5 % Phos-tag gel. Herein, samples of phosphoryalted LytR and $LytR^N$ will be referred to as LytR – P and $LytR^N$ – P, respectively, to indicate

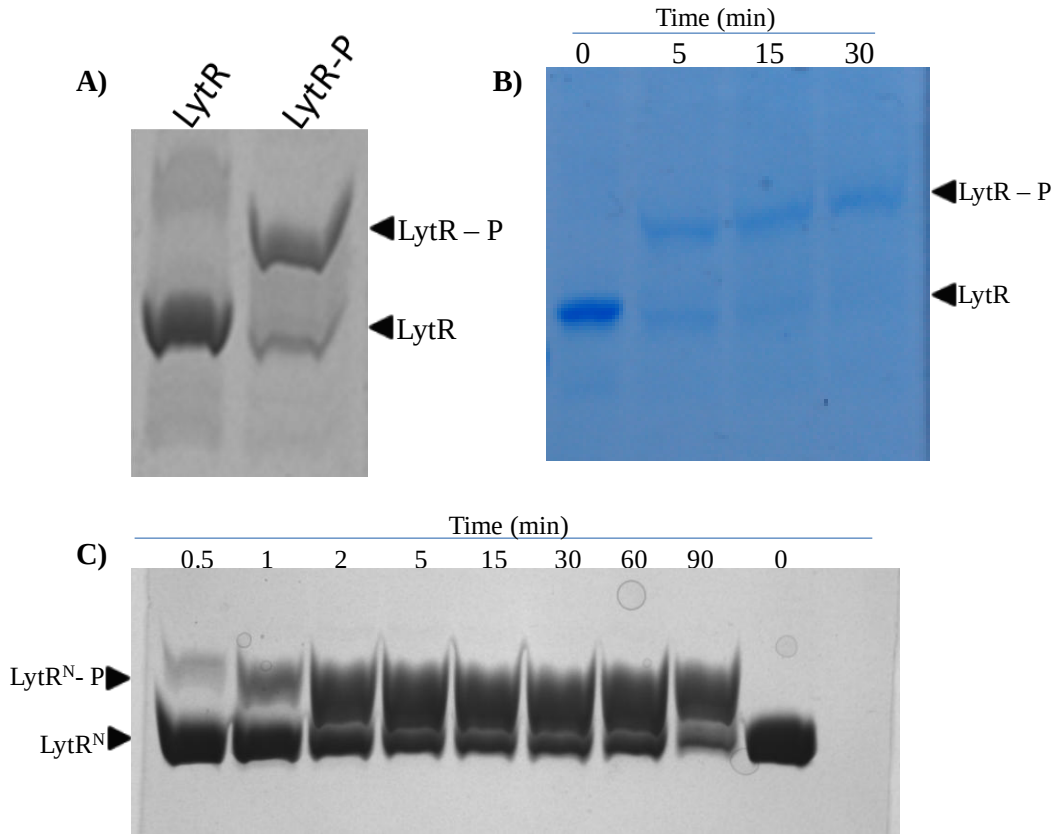

Figure 3.3.19. Phosphorylation of LytR and $LytR^N$ by acetyl phosphate

A) LytR at 10 µM was phosphoryalted by acetyl phosphate (50 mM) in PB for 1 hr at 37°C B) LytR at 5 µM was phosphoryalted by acetyl phosphate (50 mM) in PB by incubating at 37°C and reaction was quenched at various time intervals. C) $LytR^N$ at 20 µM was phosphoryalted by acetyl phosphate (50 mM) in PB at 37°C and reactions was quenched at various time interval. The phosphorylated proteins were separated from the unphosphorylated protein by 15% Phos-tag gel. The gel were stained with Coomassie blue to view the protein bands.

phosphorylation by acetyl phosphate. The gel image in Fig 3.3.19A, acquired after 60 min time point shows that more than 70% LytR is phosphoryalted. The calculated rate of phosphorylation for LytR is 0.3847 min^{-1} (Appendix C, Fig C2). Note that due to difficulty in purifying active LytR protein the rate constant is calculated based on the quantified band intensity of a single trial shown in Fig 3.3.19B. Similar phosphorylation reactions were attempted with GST-LytR; however the separation was not consistent with the accepted principle. As a control, the same reaction was carried out using mutant GST-LytR (D53A) and evidently similar observation was made suggesting possible hindrance caused by the N-terminal GST tag in the active site.

The rate constant for phosphorylation of $LytR^N$ was estimated to be 0.3287 ± 0.0398 min^{-1} (Appendix C, Fig C2), which is not significantly slower, compared to full length LytR. In further experiments the effect of phosphorylation on $LytR^N$ structure was investigated by native PAGE and size exclusion chromatography. The results demonstrate the protein`s ability to form dimers upon phosphorylation (Fig 3.3.20). It was observed that phenomenon of dimerization was concentration dependent (Fig 3.3.20A) and greater than 90% of $LytR^N$ – P species existed in dimeric state after 5 mins of phosphorylation and remained in that state for at least 4 hours. In addition, phosphorylation induced conformational changes were further confirmed by CD (Fig 3.3.21).

Similar experiments to investigate the oligomerization of full length LytR were attempted, but we were unsuccessful due to proteins inability to enter the native-PAGE and the yield of protein was low for analysis by size exclusion chromatography.

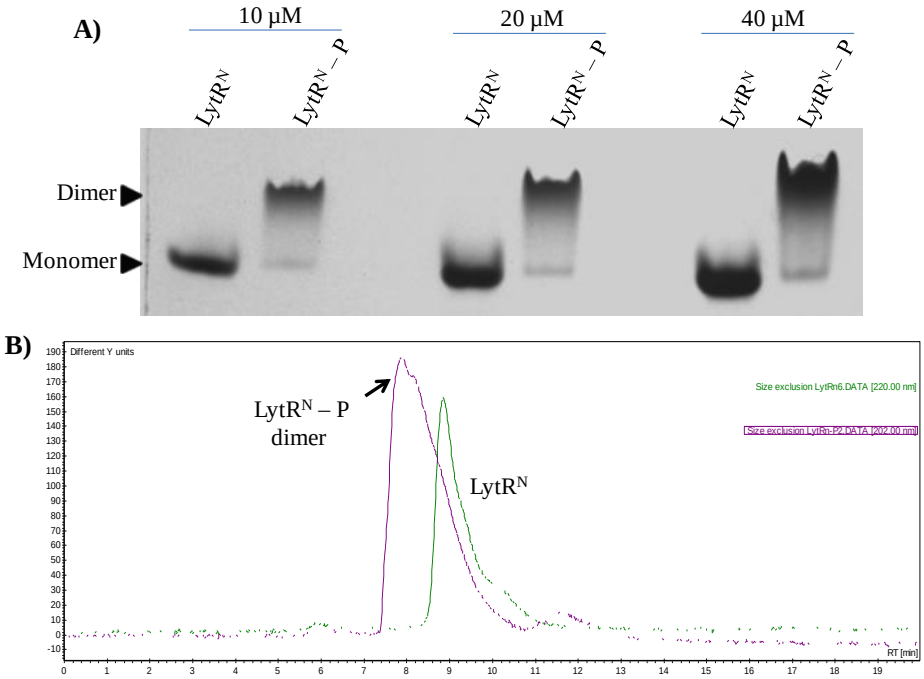

Figure 3.3.20. Phosphorylation induced dimerization of LytR^N

A) LytR^N and LytR^N – P at 10 µM, 20 µM and 40 µM analyzed by 15% native-PAGE and stained with Coomassie blue. B) LytR^N and LytR^N – P at 80 µM were loaded on to HPLC size exclusion column. The retention time of the phosphoryalted LytR^N differed from that of the unphosphorylated protein.

3.3.9 DNA binding activity of LytR

To study the DNA-binding properties of LytR, the end – labeled P$_{lrgAB}$ DNA fragment was incubated with increasing concentration of LytR at RT. The resulting complexes of DNA-protein were separated from the free DNA on an 8% non - denaturing acryl amide gel. Due to low yield of LytR and its inability to enter a non-denaturing gel, these experiments presented a great challenge. EMSA experiments conducted using GST-LytR demonstrated high binding affinity of LytR toward the promoter region of *lrgAB* with a formation of DNA-Protein complex at the top of the gel. The affinity and specificity of binding was further confirmed by competition assay involving unlabeled

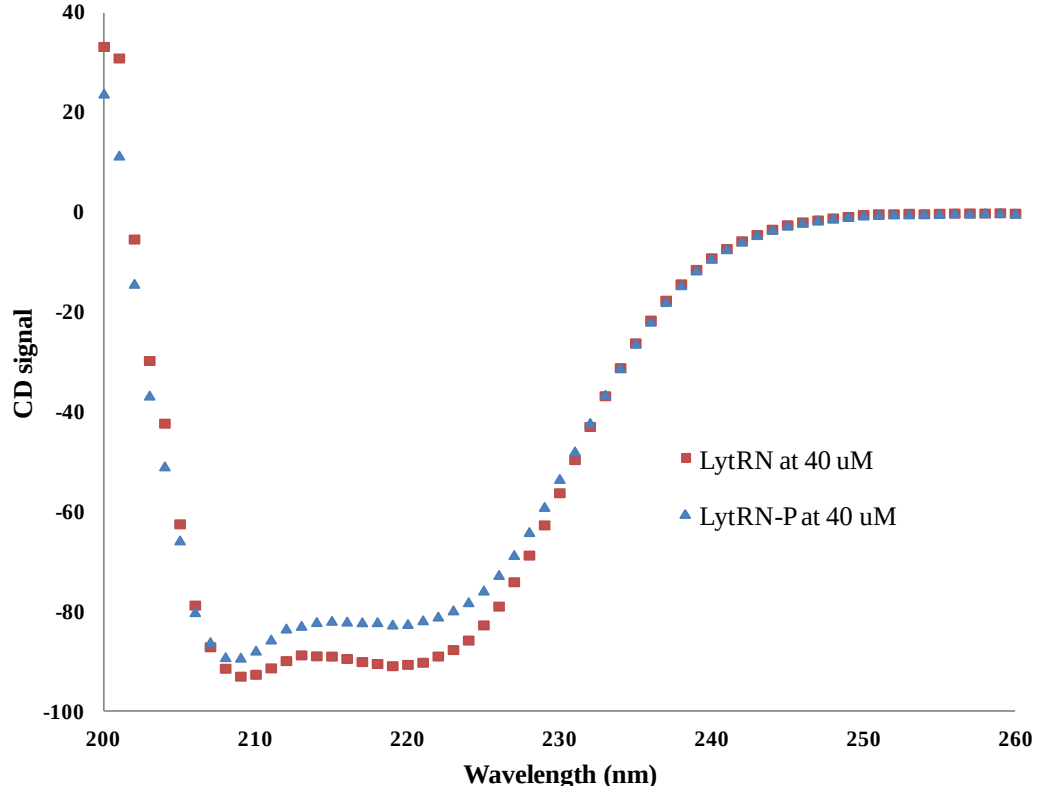

Figure 3.3.21. Phosphorylation induced conformational changes in LytR

CD spectra of $LytR^N$ and $LytR^N$ – P at 40µM. The spectra, acquired at 22°C in 20mM Tris, 5 mM $MgCl_2$ pH 7.4 buffer shows LytR undergoing conformation changes resulting from phosphorylation (triangles).

DNA, as shown in Fig.3.3.22. Based on a single trial the apparent binding reactions dissociation constant K_d was estimated to be around 2 µM for unphosphorylated LytR. We attempted similar experiment using the phosphorylated LytR, however our results are inconclusive.

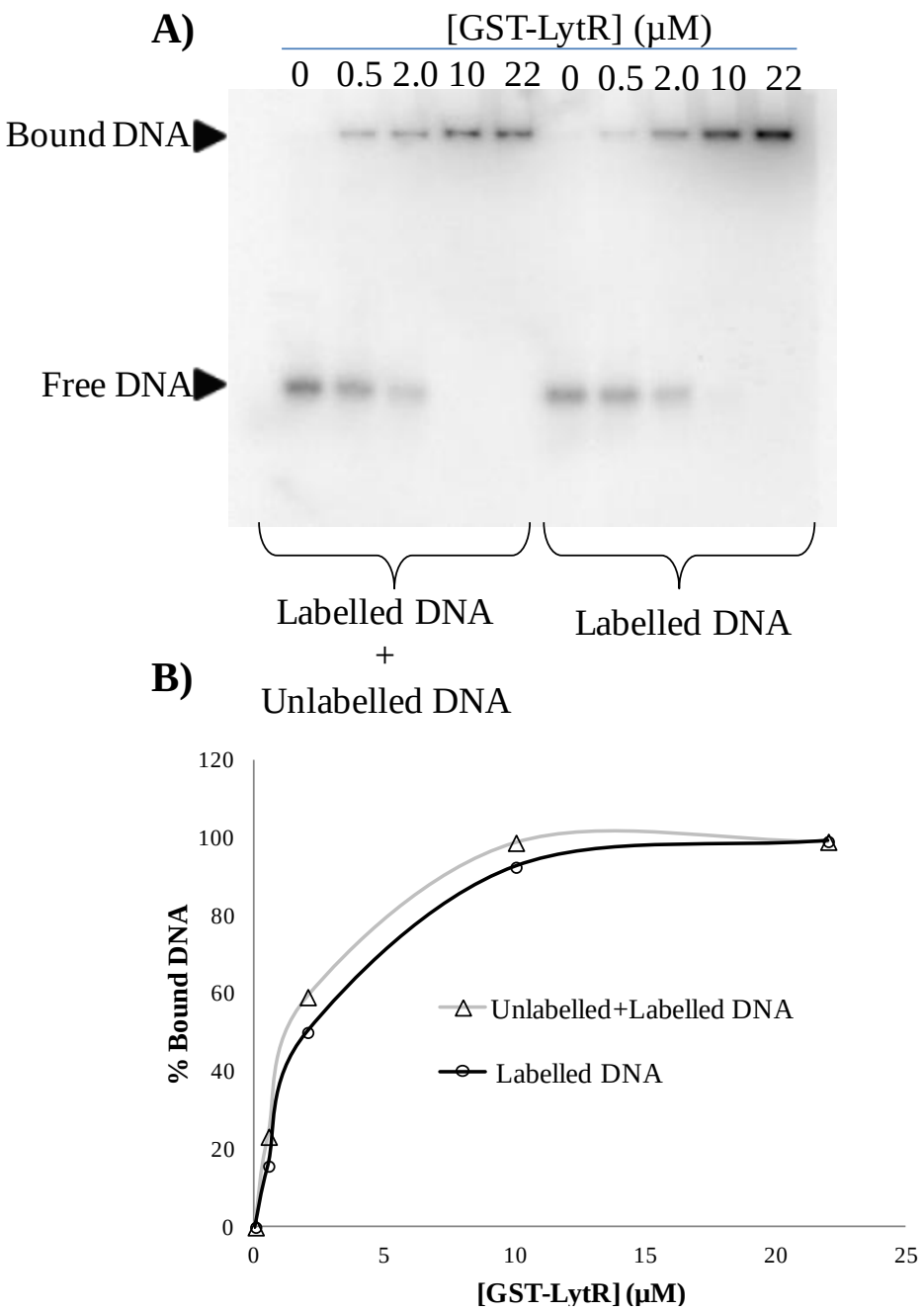

Figure 3.3.22. DNA-binding activity of LytR

A) The end – labeled P_{lrgAB} DNA fragment at 2 ng was incubated with different concentration of LytR for 30 mins at RT. The resulting complex was analyzed by 8% acrylamide gel. The gel was exposed to phosphor screen (GE Healthcare) for two hours and imaged using a Typhoon Trio^{+} imager (GE Healthcare). B) A plot of bound DNA versus protein concentration from which the K_d is estimated to be 2 µM

3.4 Discussion

Two component systems (TCS) are a predominant way for bacteria to sense, response and adapt to their ever-changing environment. In a typical TCS, external cues are sensed by a membrane-bound histidine kinase (HK) triggering a phosphorylation cascade that results in the phosphorylation in turn activation of the response regulator (RR), leading to cellular response through differential expression of target genes.

In *S. aureus,* the LytSR TCS has been shown to regulate genes controlling cell apoptosis, autolysin activity and biofilm formation leading to development of tolerance towards readily available antibiotics. Recent studies have identified the LytSR TCS as a sense-response mechanism for any perturbation of cell membrane resulting in alteration of the membrane potential (Sharma-Kuinkel, Mann et al. 2009, Yang, Xiong et al. 2013) and in turn positively regulating *cid* operon and negatively regulating the *lrgAB* operon.

To present day, molecular details and functionality of LytSR signal transduction pathway leading to over expression of virulence genes has only been presumed but it is lacking *in vitro* evidence. Therefore, this study for the first time provides *in vitro* characterization of the LytSR TCS. For the purpose of our *in vitro* work, we cloned and purified the cytoplasmic histidine kinase domain of LytS and full length LytR, as well as the C-terminal and N-terminal domains, respectively. To overcome the issue of protein insolubility, the N-terminal region of LytS containing six transmembrane regions was omitted. Similar techniques for over expression and purification of histidine kinases have been used for other histidine kinases such as, VraS (Belcheva and Golemi-Kotra 2008) and WalK (Gutu, Wayne et al. 2010).

Purification of full length LytR was quite challenging due to its highly hydrophobic nature. Behavior of LytR was similar to that of AgrA (Sidote, Barbieri et al. 2008), protein from the same family. Based on successful purification and crystallization of the receiver domain of LytR, it was hypothesized that the effector domain contributed to the challenge in purification of the full length protein. LytR interacted very weakly with the resins used in ion exchange chromatography and didn`t bind to the heparin column, which is widely used for purification of transcription factors. This minimal interaction with the ion exchange chromatography could be attributed to the difference in the actual and the theoretical pI of the protein. And a reason for LytR not binding to the heparin column could be that the phosphoryalted state of the protein is required to induce conformational changes in the C-terminal leading to increased affinity for DNA. Nevertheless, we were able to obtain sufficient protein using the ammonium sulfate precipitation method as well as by tagging it with GST.

LytSR mediated regulation of *lrgAB* has been proposed to be initiated by two major events resulting in phosphorylation of LytR (Patton, Yang et al. 2006). In the first phosphorylation event, the HK senses collapse in the cell membrane potential catalyzing its autophosphorylation at the conserved His390 and in a subsequent phosphotransfer reaction the phosphoryl group is transferred to a conserved Asp53 of LytR, in turn activating its DNA binding properties. Studies have shown that the autophosphorylation of HK is the rate limiting step in phosphorylation of RR by HK (Honaker, Leistikow et al. 2009). The results of our study show the quantified kinetic parameters of the autophosphorylation of LytS, and compare the rate of and the level of total

autophosphorylation. From the progress curve in Fig 3.3.14, it is observed that 50% of the kinase is phosphoryalted within the first 30 min of incubation with ATP. This time of response elicitation coincides with the multiplication time of *S. aureus* and it is relatively slower compared to kinases as VraS (Belcheva and Golemi-Kotra 2008) and VanS (Wright, Holman et al. 1993). This is further supported by *in vivo* studies that highlight the secondary role of LytSR system in regulating secondary genes associated with genetic information processing and cell metabolism (Sharma-Kuinkel, Mann et al. 2009).

The kinetics of autophosphorylation of LytS shows saturation of the enzyme after 90 min with rate of phosphorylation to be 0.0265 ± 0.0014 min^{-1} in the presence of excess ATP. These kinetics are slower compare to other the well characterized kinases like VraS (rate constant = 0.07 min^{-1}), however similar to some HK such as nitrate sensing NarQ (rate constant = 0.014 min^{-1}), (Noriega, Schmidt et al. 2008) and citrate sensing Dcus (rate constant = 0.043 min^{-1}), (Janausch, Garcia-Moreno et al. 2002) from *E. coli,* where there exist a correlation between the level of phosphorylation and the rate of phosphorylation (Yamamoto, Hirao et al. 2005). The low rate of phosphorylation is consistent with low level of phosphorylation thus higher time of saturation. Contrary to our finding for WalK, LytS autophosphorylation activity can persist in the absence of K^+ and Ca^{2+} ions.

The calculated K_m value of 8 µM for LytS signified that the affinity of LytS is very high for ATP and a very less concentration of ATP is required to reach half of maximal phosphorylation. And the fact that ATP is present in the range of milimolar *in vivo* (Schneider and Gourse 2004) it will be readily available in saturating concentration.

Moreover, in contrast to kinetics of VraS and WalK, it is observed that the catalytic efficiency of LytS is much lower (k_{cat} = 0.03 ± 0.0005 min^{-1}), hence the very low value of K_m.

Many HKs are known to catalyze both the phosphorylation and dephosphorylation of their cognate response regulator. These are known as bifunctional histidine kinases (Laub and Goulian 2007). The stability of LytS for over 3 hours in the phosphorylated state tempted us to think that a specific phosphotransfer to LytR might be the only way to remove the signal. However under the set conditions, we observed a very slow phosphotransfer from LytS to LytR. The phosphotransfer was not efficient. Our results indicated that it took 30 minutes for 60% of the phosphoryl group to transfer from LytS to LytR, compare to 30 seconds for the VraSR system. Taken together, the slow phosphotransfer kinetics of GST-LytR and no observed transfer activity with $LytR^N$, it was intriguing to investigate any non-cognate phosphoryl flow between LytS and other well characterized RR in the lab. This phenomenon of cross-talk between HKs and RRs has been readily observed *in vitro*. Several *E. coli* TCS have been reported to participate in cross-talk, to name a few, the PhoR-PhoB, the VanS-VanR (Fisher, Jiang et al. 1995) and the EnvZ-OmpR. Albeit the advantage of cross talk in integrating multiple signal and diversifying the response to a specific stimuli, they are usually kept to a minimum so to allow the organism to respond to specific stimuli (Laub and Goulian 2007). In addition, studies have shown the observed rate of phosphoryl flow between two non-cognate pair is significantly less compare to the cognate pair a the correct alignment of the phosphoryl group is hindered which is a key to forming a complex to allow for efficient transfer

(West and Stock 2001). Our results indicate that LytS is unable to phosphorylate VraR or GraR. However, keeping in mind the low efficiency of transfer from LytS to LytR we cannot rule out the possibility of cross talk between LytS and other RRs as well other routes of LytR phosphorylation.

Regarding other means of LytR phosphorylation, it is well established that most RRs are also equipped with the ability to catalyze their own phosphorylation, independently of other proteins, using endogenous low molecular weight phosphor-donors (Lukat, McCleary et al. 1992). In fact, phosphorylation of RRs by low molecular weight phosphor-donors such as acetyl phosphate, carbamyl phosphate or phosphoramide appears to more imperative than phosphorylation by non-cognate HKs (McCleary, Stock et al. 1993). In our study we undertook experiments to investigate acetyl phosphate mediated phosphorylation of LytR. Compare to ATP (ΔG^o = -30.5 kJ mol^{-1}) acetyl phosphate (ΔG^o = -43.1 kJ mol^{-1}) is a high energy molecule with an intracellular concentration ranging from 1 mM to 3 mM, making it as readily available as ATP (Lukat, McCleary et al. 1992, McCleary, Stock et al. 1993, Barbieri, Mack et al. 2010).The results of our study indicated that in the presence of acetyl phosphate LytR undergoes phosphorylation at a rate of 0.3847 min^- and $LytR^N$ at 0.3287 ± 0.0398 min^{-1}. Contrary to the notion that phosphorylation of RRs by cognate HKs is faster than by acetyl phosphate, our results indicate that phosphorylation of LytR by AP is significantly faster and predominant compare to phosphorylation by LytS. Furthermore, there was no significance difference in the rate of phosphorylation of LytR compared to $LytR^N$. Therefore our

findings lead us to believe that *in vivo* phosphorylation induced activation of LytR is mediated by acetyl phosphate to achieve long-term steady state levels of activate RR.

The RRs are also known as the generic molecular switches, turning ON genes in the presence of stimuli and OFF in the absence. It has been well documented that RR phosphorylation is not permanent and is regulated to control the output response. Studies have shown that the aspartate phosphorylation is highly labial and the life span of a phospho species can vary from seconds to hours depending on their physiological function. The dissipation of the phospho species and in turn loss of signal can be attributed to first the inherent self dephosphorylation activity of all RRs and second phosphotase activity of bifunctional HKs. The latter process aids in acceralting the former process as is the case for the VraSR system (Belcheva and Golemi-Kotra 2008). Further studies have shown that the phosphotase activity of a HK can be enhanced by an auxiliary regulatory protein. For example, in the *E. coli* CheA-CheY TCS, CheA lacked phosphotase activity towards its substrate CheY-P in the absence of CheZ, an auxiliary protein (Hess, Oosawa et al. 1988, Bilwes, Alex et al. 1999). Likewise, our results indicated that His-LytS completely lacked the phosphotase activity towards both phosphorylated GST-LytR and $LytR^{N}$ (Fig 3.3.18). This finding implied that an auxiliary protein was required or the GAF domain of LytS, like the PAS domain of walK (Gutu, Wayne et al. 2010) might be a crucial feature for optimal phosphotase activity of LytS.

To elucidate the nature of LytR activation it was necessary to examine the receiver domain of the protein in depth. It has been shown that phosphorylation induced conformational changes propagate from the active site. $LytR^{N}$ harbors the

phosphorylation site (Asp53) therefore we expect to be directly affected by phosphorylation. Our results upon phosphorylation with acetyl phosphate $LytR^N$ underwent phosphorylation induced conformational changes and formed stable dimers. However, the fact the $LytR^N$ has a slower rate of phosphorylation by acetyl phosphate and is unable to receive a phosphoryl group from LytS, suggests that the receiver domain is perhaps held in the intermediate conformation between active and non-active and interdomain contact with the C-terminal is required (Belcheva and Golemi-Kotra 2008) or its lacking the right alignment of the phosphoryl group required for a phosphotransfer (West and Stock 2001). We make these hypothesis based on the fact that RRs catalyze the transfer reaction with maybe a chemical contribution from the HK (West and Stock 2001).

Until recently, structural characterization of RR in their transiently formed covalent phospho species had been a hindrance. After the discovery of BeF_3^-, a non-covalent mimic of a phosphoryl group aiding to form a stable analog of phosphorylated protein, structures of many proteins in their phosphoryalted or otherwise activated state have been determined (Lee, Cho et al. 2001, Leonard, Golemi-Kotra et al. 2013). In collaboration with Dr. Audette group, we have crystallized and determined the structure of unphosphorylated $LytR^N$ and work is underway to determine the structure of $BeF3^-$-activated $LytR^N$. A closer analysis of unphosphorylated $LytR^N$ structure reveals that it is consist of 5 β-sheets all situated in parallel surrounded by 5 amphipathic helices (Appendix B, Fig B2) This folding pattern has been shown to be conserved in receiver domains of at least ten RRs for which structures have been determined (Robinson,

Buckler et al. 2000, Leonard, Golemi-Kotra et al. 2013). Further analysis show that the highly conserved residues including the phosphorylation site Asp 53 are all positioned in the active site cleft formed by loops extending from the C-terminal ends (Appendix B, Fig B3). Similar to that reported for CheY (Guhaniyogi, Robinson et al. 2006) and VraR (Leonard, Golemi-Kotra et al. 2013), $LytR^{N}$ contains a cluster of three acidic Asp residues, Asp 7, Asp 8 and Asp 53 that are involved in coordinating the Mg^{2+} ion required for an efficient phosphoryl transfer (Appendix B, Fig B4). Conserved residues Lys 101, Pro 102 and Phe 103 have been proposed to make up the dimerization interface of $LytR^{N}$; however, this will be further confirmed by determining the $BeF3^{-}$-activated $LytR^{N}$ structure.

The effector domains of RRs are unique with respect to both their structure and function. LytR effector domain falls into the novel family of non-helix-turn-helix DNA-binding domains, known as LytTR. Using EMSA the K_d value of 2 μM was estimated for unphosphorylated LytR. This high affinity of LytR for the promoter region of *lrgAB* is not unusual as similar findings have been reported for AgrA, a transcription component of the quorum sensing ArgCA system and a global regulator of virulence in *S. aureus* harboring the LytTR type effector domain (Sidote, Barbieri et al. 2008). Nevertheless, our work here does not sufficiently characterize the DNA binding properties of LytR and further work is necessary. Ideally, accurate value of K_d for both phosphorylated and unphosphorylated protein would be obtained using a full length protein lacking any tags. And due to the uncanny nature of LytR, an alternative way of estimating K_d using techniques such as Isothermal Titration Calorimetry (ITC) should be considered.

To summarize, the *S.aureus* LytSR TCS acts a sense-response mechanism that responds to any change in membrane potential by regulating the murein hydrolase activity and autolysis. To elicit a response, it follows the phosphoryl mediated TCS signal transduction pathway. In doing so, the HK LytS undergoes autophosphorylation and phosphorylates LytR, which then can bind to the *lrgAB* promoter region and induces transcription. Alternatively, we show that both LytR and $LytR^N$ can catalyze their own phosphorylation by accepting a phosphate from low molecular weight phospho donors to achieve prolonged steady-state levels of active protein for activation of genes involved in cell metabolism. In addition, our result demonstrates that $LytR^N$ forms stable phosphorylation induced dimers and which may enhance or inhibit the DNA binding ability of the effector domain. Finally to end on a positive note, we show that LytR in its unphosphorylated state binds *lrgAB* and facilitates *S. aureus* in developing tolerance towards different antimicrobial drugs.

3.5 References

Anantharaman, V. and L. Aravind (2003). "Application of comparative genomics in the identification and analysis of novel families of membrane-associated receptors in bacteria." BMC Genomics **4**(1): 34.

Barbieri, C. M., T. R. Mack, V. L. Robinson, M. T. Miller and A. M. Stock (2010). "Regulation of response regulator autophosphorylation through interdomain contacts." J Biol Chem **285**(42): 32325-32335.

Belcheva, A. and D. Golemi-Kotra (2008). "A close-up view of the VraSR two-component system. A mediator of *Staphylococcus aureus* response to cell wall damage." J Biol Chem **283**(18): 12354-12364.

Bilwes, A. M., L. A. Alex, B. R. Crane and M. I. Simon (1999). "Structure of CheA, a signal-transducing histidine kinase." Cell **96**(1): 131-141.

Brogden, K. A. (2005). "Antimicrobial peptides: pore formers or metabolic inhibitors in bacteria?" Nat Rev Microbiol **3**(3): 238-250.

Brunskill, E. W. and K. W. Bayles (1996). "Identification of LytSR-regulated genes from *Staphylococcus aureus*." J Bacteriol **178**(19): 5810-5812.

Cann, M. J. (2007). "Sodium regulation of GAF domain function." Biochem Soc Trans **35**(Pt 5): 1032-1034.

Fisher, S. L., W. Jiang, B. L. Wanner and C. T. Walsh (1995). "Cross-talk between the histidine protein kinase VanS and the response regulator PhoB. Characterization and identification of a VanS domain that inhibits activation of PhoB." J Biol Chem **270**(39): 23143-23149.

Galperin, M. Y. (2008). "Telling bacteria: do not LytTR." Structure **16**(5): 657-659.

Gao, R., T. R. Mack and A. M. Stock (2007). "Bacterial response regulators: versatile regulatory strategies from common domains." Trends Biochem Sci **32**(5): 225-234.
Gao, R. and A. M. Stock (2010). "Molecular strategies for phosphorylation-mediated regulation of response regulator activity." Curr Opin Microbiol **13**(2): 160-167.

Groicher, K. H., B. A. Firek, D. F. Fujimoto and K. W. Bayles (2000). "The *Staphylococcus aureus* lrgAB operon modulates murein hydrolase activity and penicillin tolerance." J Bacteriol **182**(7): 1794-1801.

Guhaniyogi, J., V. L. Robinson and A. M. Stock (2006). "Crystal structures of beryllium fluoride-free and beryllium fluoride-bound CheY in complex with the conserved C-

terminal peptide of CheZ reveal dual binding modes specific to CheY conformation." J Mol Biol **359**(3): 624-645.

Gutu, A. D., K. J. Wayne, L. T. Sham and M. E. Winkler (2010). "Kinetic characterization of the WalRKSpn (VicRK) two-component system of Streptococcus pneumoniae: dependence of WalKSpn (VicK) phosphatase activity on its PAS domain." J Bacteriol **192**(9): 2346-2358.

Hess, J. F., K. Oosawa, N. Kaplan and M. I. Simon (1988). "Phosphorylation of three proteins in the signaling pathway of bacterial chemotaxis." Cell **53**(1): 79-87.

Honaker, R. W., R. L. Leistikow, I. L. Bartek and M. I. Voskuil (2009). "Unique roles of DosT and DosS in DosR regulon induction and *Mycobacterium tuberculosis* dormancy." Infect Immun **77**(8): 3258-3263.

Janausch, I. G., I. Garcia-Moreno and G. Unden (2002). "Function of DcuS from *Escherichia coli* as a fumarate-stimulated histidine protein kinase in vitro." J Biol Chem **277**(42): 39809-39814.

Kinoshita, E., E. Kinoshita-Kikuta, K. Takiyama and T. Koike (2006). "Phosphate-binding tag, a new tool to visualize phosphorylated proteins." Mol Cell Proteomics **5**(4): 749-757.

Laub, M. T. and M. Goulian (2007). "Specificity in two-component signal transduction pathways." Annu Rev Genet **41**: 121-145.

Lee, S. Y., H. S. Cho, J. G. Pelton, D. Yan, R. K. Henderson, D. S. King, L. Huang, S. Kustu, E. A. Berry and D. E. Wemmer (2001). "Crystal structure of an activated response regulator bound to its target." Nat Struct Biol **8**(1): 52-56.

Leonard, P. G., Golemi-Kotra, D. and Stock, A.M (2013). "Phosphorylation-dependent conformational changes and domain rearrangements in *Staphylococcus aureus* VraR activation." Proceedings of the National Academy of Sciences **110**(21): 8525-8530.

Leonard, P. G., D. Golemi-Kotra and A. M. Stock (2013). "Phosphorylation-dependent conformational changes and domain rearrangements in *Staphylococcus aureus* VraR activation." Proc Natl Acad Sci U S A **110**(21): 8525-8530.

Lukat, G. S., W. R. McCleary, A. M. Stock and J. B. Stock (1992). "Phosphorylation of bacterial response regulator proteins by low molecular weight phospho-donors." Proc Natl Acad Sci U S A **89**(2): 718-722.

McCleary, W. R., J. B. Stock and A. J. Ninfa (1993). "Is acetyl phosphate a global signal in *Escherichia coli*" J Bacteriol **175**(10): 2793-2798.

Nikolskaya, A. N. and M. Y. Galperin (2002). "A novel type of conserved DNA-binding domain in the transcriptional regulators of the AlgR/AgrA/LytR family." Nucleic Acids Res **30**(11): 2453-2459.

Noriega, C. E., R. Schmidt, M. J. Gray, L. L. Chen and V. Stewart (2008). "Autophosphorylation and dephosphorylation by soluble forms of the nitrate-responsive sensors NarX and NarQ from *Escherichia coli* K-12." J Bacteriol **190**(11): 3869-3876.

Patton, T. G., S. J. Yang and K. W. Bayles (2006). "The role of proton motive force in expression of the *Staphylococcus aureus* cid and lrg operons." Mol Microbiol **59**(5): 1395-1404.

Peschel, A. (2002). "How do bacteria resist human antimicrobial peptides?" Trends Microbiol **10**(4): 179-186.

Peschel, A., R. W. Jack, M. Otto, L. V. Collins, P. Staubitz, G. Nicholson, H. Kalbacher, W. F. Nieuwenhuizen, G. Jung, A. Tarkowski, K. P. van Kessel and J. A. van Strijp (2001). "*Staphylococcus aureus* resistance to human defensins and evasion of neutrophil killing via the novel virulence factor MprF is based on modification of membrane lipids with l-lysine." J Exp Med **193**(9): 1067-1076.

Rice, K. C., B. A. Firek, J. B. Nelson, S. J. Yang, T. G. Patton and K. W. Bayles (2003). "The *Staphylococcus aureus* cidAB operon: evaluation of its role in regulation of murein hydrolase activity and penicillin tolerance." J Bacteriol **185**(8): 2635-2643.

Robinson, V. L., D. R. Buckler and A. M. Stock (2000). "A tale of two components: a novel kinase and a regulatory switch." Nat Struct Biol **7**(8): 626-633.

Schneider, D. A. and R. L. Gourse (2004). "Relationship between growth rate and ATP concentration in *Escherichia coli*: a bioassay for available cellular ATP." J Biol Chem **279**(9): 8262-8268.

Shala, A., Patel, K.H., Golemi-Kotra, D. & Audette, G.F. (2013). "Expression, purification, crystallization and preliminary X-ray analysis of
the receiver domain of *Staphylococcus aureus* LytR protein." Acta Cryst. F69.

Sharma-Kuinkel, B. K., E. E. Mann, J. S. Ahn, L. J. Kuechenmeister, P. M. Dunman and K. W. Bayles (2009). "The *Staphylococcus aureus* LytSR two-component regulatory system affects biofilm formation." J Bacteriol **191**(15): 4767-4775.

Sidote, D. J., C. M. Barbieri, T. Wu and A. M. Stock (2008). "Structure of the *Staphylococcus aureus* AgrA LytTR domain bound to DNA reveals a beta fold with an unusual mode of binding." Structure **16**(5): 727-735.

Stock, A. M., V. L. Robinson and P. N. Goudreau (2000). "Two-component signal transduction." Annu Rev Biochem **69**: 183-215.

Voyich, J. M., K. R. Braughton, D. E. Sturdevant, A. R. Whitney, B. Said-Salim, S. F. Porcella, R. D. Long, D. W. Dorward, D. J. Gardner, B. N. Kreiswirth, J. M. Musser and F. R. DeLeo (2005). "Insights into mechanisms used by *Staphylococcus aureus* to avoid destruction by human neutrophils." J Immunol **175**(6): 3907-3919.

West, A. H. and A. M. Stock (2001). "Histidine kinases and response regulator proteins in two-component signaling systems." Trends Biochem Sci **26**(6): 369-376.

Wright, G. D., T. R. Holman and C. T. Walsh (1993). "Purification and characterization of VanR and the cytosolic domain of VanS: a two-component regulatory system required for vancomycin resistance in *Enterococcus faecium* BM4147." Biochemistry **32**(19): 5057-5063.

Yamamoto, K., K. Hirao, T. Oshima, H. Aiba, R. Utsumi and A. Ishihama (2005). "Functional characterization in vitro of all two-component signal transduction systems from *Escherichia coli*." J Biol Chem **280**(2): 1448-1456.

Yang, S. J., Y. Q. Xiong, P. M. Dunman, J. Schrenzel, P. Francois, A. Peschel and A. S. Bayer (2009). "Regulation of mprF in daptomycin-nonsusceptible *Staphylococcus aureus* strains." Antimicrob Agents Chemother **53**(6): 2636-2637.

Yang, S. J., Y. Q. Xiong, M. R. Yeaman, K. W. Bayles, W. Abdelhady and A. S. Bayer (2013). "Role of the LytSR two-component regulatory system in adaptation to cationic antimicrobial peptides in *Staphylococcus aureus*." Antimicrob Agents Chemother **57**(8): 3875-3882.

CHAPTER FOUR

CONCLUSION AND FUTURE DIRECTIONS

4.1 Conclusion

Since the discovery of the first prokaryotic TCS in 1986, scientists have made great advancement in the field of signal transduction. Many TCSs from different bacteria have been characterized using both in vitro and in vivo studies. The goal of this study was to further that knowledge by studying the following two TCSs in *S. aureus*; the WalKR system and the LytSR system.

In chapter 2, we described the phosphorylation dependent signaling cascade of the essential WalKR system. For this purpose, we successfully cloned, expressed and purified two truncated version of the HK, WalK; GST-WalK^{1} and GST-WalK^{2} and full length RR, WalR. Through in vitro autophosphorylation assays, it was shown that both GST-WalK^{1} and GST-WalK^{2} are biologically active proteins. Furthermore, kinetics of autophosphorylation revealed that GST-WalK^{1} undergoes autophosphorylation at a faster rate compared to GST-WalK^{2}, lacking the HAMP-PAS domain. It was observed that 50 % of phosphorylation was achieved in less than 10 min suggesting a rapid transfer of signal. Our results illustrated that autophosphorylation of WalK was significantly enhanced in the presence of K^{+} ions and this phenomenon was concentration dependent. The fact that similar observation was not made for LytS, BceS or GraS lead us to hypothesize that K^{+} ions may play a stabilizing role or act as stress induced activator of

WalK. Following phosphorylation, we observed that the phosphorylated GST-WalK^2 species was stable for a long period of time, or until WalR was added. We showed that GST-WalK^2 could rapidly transfer this phosphoryl group to its cognate RR, WalR with more than 50% of the phosphate group associated with GST-WalK^2 being transferred to WalR in under one minute. In an attempt to investigate any cross talk, our results showed that GST-WalK^2 is unable to phosphorylate BceR, however results with GraR were inconclusive.

Chapter 3 focuses on the LytSR system of *S. aureus* involved in regulating bacterial autolysis and biofilm formation. The LytSR system was proposed to function via similar phosphorylation dependent signaling cascade. We successfully cloned and purified the His tagged cytoplasmic histidine kinase domain of LytS. Through in vitro autokinase assay we showed His-LytS was biologically active and undergoes autophosphorylation in a time-dependent manner at the invariable His390. The calculated pseudo first order rate constant of 0.0265 ± 0.0014 min^{-1} along with the $t1_{/2}$ time of 30 min suggested relatively slow signal propagation. Furthermore, the calculated Michaelis- Menten kinetics parameters emphasized the high affinity of LytS for ATP (K_m (ATP) = 7.9 $\pm$ 0.573 µM) and low catalytic efficiency (k_{cat} = 0.03 ± 0.0005 min^{-1}). Following phosphorylation, we observed that the phosphorylated His-LytS species was stable for a prolonged time or until LytR is added.

The full length LytR was succefully cloned but the uncanny nature of the protein attributed to its DNA binding domain, made its purification challenging forcing us to place an N-terminal GST tag. The phosphotransfer from His-LytS to the conserved Asp

53 of GST-LytR was inefficient, however specific. The specificity of the transfer was further confirmed with a transfer reaction to D53A mutant of GST-LytR. In an attempt to characterize the individual domains of LytR, the N-terminal receiver domain ($LytR^N$) and the C-terminal effector domains ($LytR^C$) were cloned separately. Using a two step purification protocol we were able to obtained large amount of homogenized $LytR^N$ protein. in collaboration with Dr.Audette's group, we took advantage of the large abundance of $LytR^N$ protein and successfully solved the crystal structure to a resolution of 2.3Å. On the other hand, we were unable to purify structurally stable $LytR^C$ impeding us from further characterizing the DNA binding domain.

Interestingly, there was no phosphotransfer observed from His-LytS to the standalone receiver domain, $LytR^N$. However, as an alternate route to RR phosphorylation in cells and thus activation, we showed that both LytR and $LytR^N$ can catalyze their own phosphorylation by receiving a phosphate group form a small molecule phosphor donor. In comparison to LytR, we showed that $LytR^N$ undergoes phosphorylation by acetyl phosphate at a slower rate. Furthermore, we showed phosphorylation induced conformational changes in $LytR^N$ as well as formation of stable dimers. Lastly, we showed that LytR in its unphosphorylated state has a high affinity for the promoter region of *lrgAB,* as indicated by micromolar K_d, however further work in this area is required. Nonetheless, the work shown here provides important insights into the signaling mechanism involved in *S. aureus* survival and contributes to the development of potent antimicrobial drugs.

4.2 Future Direction

The observation that autokinase activity of Walk is significantly enhanced in the presence of K^+ ions is certainly an interesting one. We have provided concrete evidence that this phenomenon is specific to WalK, however it remains yet to be determined the precise role of K^+ ions in this system. Recent in vivo studies have shown upregulation of WalKR in the presence of metal ion induced stress however K^+ ion was not listed. Therefore, weather K^+ ions stabilize the kinase or it acts as a stress induced activator of the kinase should be addressed as part of the future work. The likelihood of crosstalk between WalK and GraR is strongly supported by in vivo studies (Falord, Mader et al. 2011). As our results were inconclusive, it will be worthwhile to investigate this cross-talk in vitro, which can be accomplished by simply repeating the phosphotransfer experiment with fresh proteins.

With respect to the LytSR system, our results demonstrated that it is an active system. However, the fact that we were unable to purify biologically active LytR free of any tag, limited a lot of our downstream experiments. Firstly, future work will need to focus on purification of the full length protein using multi-step purification approach. Although the highly hydrophobic nature makes the protein form insoluble aggregates, one can investigate other methods to solubilize the protein. Here the use of 0.1% SDS rendered protein biologically inactive, but other non ionic additives can be experimented with. Secondly, our work on DNA-binding ability of LytR is not adequate. Ideally, accurate value of K_d for both phosphoryalted and unphosphorylated protein would be obtained using a full length protein lacking any tags. As an alternative way of estimating

K_d, other techniques such as Isothermal Titration Calorimetry (ITC) should be considered. Future work should also focus on more sensitive method of investigating DNA-binding properties of LytR such as DNase I footprinting. Of particular interest will be the purification of $LytR^C$ as further insight into the mode of LytTR type DNA binding domains can be deduced from structural analysis of $LytR^C$. Lastly, we are in the process of crystallizing and determining the $BeF3^-$-activated $LytR^N$ structure.

4.3 References

Falord, M., U. Mader, A. Hiron, M. Debarbouille and T. Msadek (2011). "Investigation of the *Staphylococcus aureus* GraSR regulon reveals novel links to virulence, stress response and cell wall signal transduction pathways." PLoS One **6**(7): e21323.

Appendix A

Figure A1 : DNA sequencing results for WalR

WalR

ATTGTGAGCGGATAACAATTCCCCTCTAGAAATAATTTTGTTTAACTTTAAGAAGGAGATATACC **pET24d**

ATGGCTAGAAAAGTTGTTGTAGTTGATGATGAAAAACCGATTGCTGATATTTTAGAATTTAACTTAAAAAAA
GAAGGATACGATGTGTACTGTGCATACGATGGTAATGATGCAGTCGACTTAATTTATGAAGAAGAACCAGAC
ATCGTATTACTAGATATCATGTTACCTGGTCGTGATGGTATGGAAGTATGTCGTGAAGTGCGCAAAAAATACG
AAATGCCAATAATAATGCTTACTGCTAAAGATTCAGAAATTGATAAAGTGCTTGGTTTAGAACTAGGTGCAG
ATGACTATGTAACGAAACCGTTTAGTACGCGTGAATTAATCGCACGTGTGAAAGCGAACTTACGTCGTCATT
ACTCACAACCAGCACAAGACACTGGAAATGTAACGAATGAAATCACAATTAAAGATATTGTGATTTATCCAG
ACGCATATTCTATTAAAAAACGTGGCGAAGATATTGAATTAACACATCGTGAATTTGAATTGTTCCATTATTTA
TCAAAACATATGGGACAAGTAATGACACGTGAACATTTATTACAAACAGTATGGGGCTATGATTACTTTGGC
GATGTACGTACGGTCGATGTAACGATTCGTCGTTTACGTGAAAAGATTGAAGATGATCCGTCACATCCTGAA
TATATTGTGACGCGTAGAGGCGTTGGATATTTCCTCCAACAACATGAGTAG **WalR**

TAAGGATCCGAATTCGAGCTCCGTCGACAAGCTTGCGGGCCGCACTCGAGCACCACCACCACCACCACTGA
GATCCGGCTGCTAACAAAGCCCGAAAGGAAGCTGAGTTGGCTGCTGCCACGCTGAGCAATAACTAGCATA **pET24d**

Score	Expect	Identities	Gaps	Strand
1297 bits(702)	0.0	702/702(100%)	0/702(0%)	Plus/Plus

```
Query  66   ATGGCTAGAAAAGTTGTTGTAGTTGATGATGAAAAACCGATTGCTGATATTTTAGAATTT  125
            ||||||||||||||||||||||||||||||||||||||||||||||||||||||||||||
Sbjct  7    ATGGCTAGAAAAGTTGTTGTAGTTGATGATGAAAAACCGATTGCTGATATTTTAGAATTT  66

Query  126  AACTTaaaaaaaGAAGGATACGATGTGTACTGTGCATACGATGGTAATGATGCAGTCGAC  185
            ||||||||||||||||||||||||||||||||||||||||||||||||||||||||||||
Sbjct  67   AACTTAAAAAAAGAAGGATACGATGTGTACTGTGCATACGATGGTAATGATGCAGTCGAC  126

Query  186  TTAATTTATGAAGAAGAACCAGACATCGTATTACTAGATATCATGTTACCTGGTCGTGAT  245
            ||||||||||||||||||||||||||||||||||||||||||||||||||||||||||||
Sbjct  127  TTAATTTATGAAGAAGAACCAGACATCGTATTACTAGATATCATGTTACCTGGTCGTGAT  186

Query  246  GGTATGGAAGTATGTCGTGAAGTGCGCAAAAAATACGAAATGCCAATAATAATGCTTACT  305
            ||||||||||||||||||||||||||||||||||||||||||||||||||||||||||||
Sbjct  187  GGTATGGAAGTATGTCGTGAAGTGCGCAAAAAATACGAAATGCCAATAATAATGCTTACT  246

Query  306  GCTAAAGATTCAGAAATTGATAAAGTGCTTGGTTTAGAACTAGGTGCAGATGACTATGTA  365
            ||||||||||||||||||||||||||||||||||||||||||||||||||||||||||||
Sbjct  247  GCTAAAGATTCAGAAATTGATAAAGTGCTTGGTTTAGAACTAGGTGCAGATGACTATGTA  306

Query  366  ACGAAACCGTTTAGTACGCGTGAATTAATCGCACGTGTGAAAGCGAACTTACGTCGTCAT  425
            ||||||||||||||||||||||||||||||||||||||||||||||||||||||||||||
Sbjct  307  ACGAAACCGTTTAGTACGCGTGAATTAATCGCACGTGTGAAAGCGAACTTACGTCGTCAT  366

Query  426  TACTCACAACCAGCACAAGACACTGGAAATGTAACGAATGAAATCACAATTAAAGATATT  485
            ||||||||||||||||||||||||||||||||||||||||||||||||||||||||||||
Sbjct  367  TACTCACAACCAGCACAAGACACTGGAAATGTAACGAATGAAATCACAATTAAAGATATT  426

Query  486  GTGATTTATCCAGACGCATATTCTATTAAAAAACGTGGCGAAGATATTGAATTAACACAT  545
            ||||||||||||||||||||||||||||||||||||||||||||||||||||||||||||
Sbjct  427  GTGATTTATCCAGACGCATATTCTATTAAAAAACGTGGCGAAGATATTGAATTAACACAT  486

Query  546  CGTGAATTTGAATTGTTCCATTATTTATCAAAACATATGGGACAAGTAATGACACGTGAA  605
            ||||||||||||||||||||||||||||||||||||||||||||||||||||||||||||
Sbjct  487  CGTGAATTTGAATTGTTCCATTATTTATCAAAACATATGGGACAAGTAATGACACGTGAA  546

Query  606  CATTTATTACAAACAGTATGGGGCTATGATTACTTTGGCGATGTACGTACGGTCGATGTA  665
            ||||||||||||||||||||||||||||||||||||||||||||||||||||||||||||
Sbjct  547  CATTTATTACAAACAGTATGGGGCTATGATTACTTTGGCGATGTACGTACGGTCGATGTA  606

Query  666  ACGATTCGTCGTTTACGTGAAAAGATTGAAGATGATCCGTCACATCCTGAATATATTGTG  725
            ||||||||||||||||||||||||||||||||||||||||||||||||||||||||||||
Sbjct  607  ACGATTCGTCGTTTACGTGAAAAGATTGAAGATGATCCGTCACATCCTGAATATATTGTG  666

Query  726  ACGCGTAGAGGCGTTGGATATTTCCTCCAACAACATGAGTAG  767
            |||||||||||||||||||||||||||||||||||||||||||
Sbjct  667  ACGCGTAGAGGCGTTGGATATTTCCTCCAACAACATGAGTAG  708
```

Figure A2 : DNA sequence for LytS, LytR, GST-LytR, GST-LytR (D53A) LytR ^{C} and LytR^{N}

LytS

ggaatTGTGAGCGGataacaaTTCCCCTCTAGAAATAATTTTGTTTAACTTTAAGAAGGAGATATACATATGCATCATC
ACCATCACCATGGTAAGCCTATCCCTAACCCTCTCCTCGGTCTCGATTCTACGGAAAACCTGTATTTTCAGGGAATT
GATCCCTTCACC

pET151 TOPO

GCAGAAGGATTGGCAAATATTTTTAGTAGCCAAATTGAACTTGGTGAAGCCGAAACGCAAAGTAAGTTATTG
AAAGATGCTGAGATTAAGTCATTACAGGCACAAGTGAGTCCACATTTTTTCTTCAATTCAATTAACACGATTTC
AGCTTTAGTTAGAATAAATAGCGAAAAGGCACGAGAGTTACTATTAGAATTGAGTTATTTTTTCAGAGCGAATT
TACAAGGCTCAAAGCAACATACGATTACTTTAGATAAAGAGTTAAGTCAAGTGCGTGCATACTTATCACTCGAAC
AAGCACGTTATCCAGGAAGATTTAATATCAATATTAATGTTGAAGACAAATATCGCGATGTGCTTGTACCACCATTT
TTAATTCAAATTTTAGTTGAAAATGCCATCAAACATGCGTTTACGAATCGAAAGCAAGGTAACGATATTGACGTGT
CAGTGATTAAAGAAACTGCAACACATGTACGTATTAtTGTACAAGATAATGGTCaGGGTATTTCTAAAGATAAAATG
CATTTGTTGGGAGAAACATCTGTAGAA

LytS

Sequence ID: lcl|126191 Length: 1755 Number of Matches: 1

Range 1: 1054 to 1605 Graphics ▼ Next Match ▲ Previous Match

Score	Expect	Identities	Gaps	Strand
1020 bits(552)	0.0	552/552(100%)	0/552(0%)	Plus/Plus

```
Query  169   GCAGAAGGATTGGCAAATATTTTTAGTAGCCAAATTGAACTTGGTGAAGCCGAAACGCAA  228
             ||||||||||||||||||||||||||||||||||||||||||||||||||||||||||||
Sbjct  1054  GCAGAAGGATTGGCAAATATTTTTAGTAGCCAAATTGAACTTGGTGAAGCCGAAACGCAA  1113

Query  229   AGTAAGTTATTGAAAGATGCTGAGATTAAGTCATTACAGGCACAAGTGAGTCCACATTTT  288
             ||||||||||||||||||||||||||||||||||||||||||||||||||||||||||||
Sbjct  1114  AGTAAGTTATTGAAAGATGCTGAGATTAAGTCATTACAGGCACAAGTGAGTCCACATTTT  1173

Query  289   TTCTTCAATTCAATTAACACGATTTCAGCTTTAGTTAGAATAAATAGCGAAAAGGCACGA  348
             ||||||||||||||||||||||||||||||||||||||||||||||||||||||||||||
Sbjct  1174  TTCTTCAATTCAATTAACACGATTTCAGCTTTAGTTAGAATAAATAGCGAAAAGGCACGA  1233

Query  349   GAGTTACTATTAGAATTGAGTTATTTTTTCAGAGCGAATTTACAAGGCTCAAAGCAACAT  408
             ||||||||||||||||||||||||||||||||||||||||||||||||||||||||||||
Sbjct  1234  GAGTTACTATTAGAATTGAGTTATTTTTTCAGAGCGAATTTACAAGGCTCAAAGCAACAT  1293

Query  409   ACGATTACTTTAGATAAAGAGTTAAGTCAAGTGCGTGCATACTTATCACTCGAACAAGCA  468
             ||||||||||||||||||||||||||||||||||||||||||||||||||||||||||||
Sbjct  1294  ACGATTACTTTAGATAAAGAGTTAAGTCAAGTGCGTGCATACTTATCACTCGAACAAGCA  1353

Query  469   CGTTATCCAGGAAGATTTAATATCAATATTAATGTTGAAGACAAATATCGCGATGTGCTT  528
             ||||||||||||||||||||||||||||||||||||||||||||||||||||||||||||
Sbjct  1354  CGTTATCCAGGAAGATTTAATATCAATATTAATGTTGAAGACAAATATCGCGATGTGCTT  1413

Query  529   GTACCACCATTTTTAATTCAAATTTTAGTTGAAAATGCCATCAAACATGCGTTTACGAAT  588
             ||||||||||||||||||||||||||||||||||||||||||||||||||||||||||||
Sbjct  1414  GTACCACCATTTTTAATTCAAATTTTAGTTGAAAATGCCATCAAACATGCGTTTACGAAT  1473

Query  589   CGAAAGCAAGGTAACGATATTGACGTGTCAGTGATTAAAGAAACTGCAACACATGTACGT  648
             ||||||||||||||||||||||||||||||||||||||||||||||||||||||||||||
Sbjct  1474  CGAAAGCAAGGTAACGATATTGACGTGTCAGTGATTAAAGAAACTGCAACACATGTACGT  1533

Query  649   ATTATTGTACAAGATAATGGTCAGGGTATTTCTAAAGATAAAATGCATTTGTTGGGAGAA  708
             ||||||||||||||||||||||||||||||||||||||||||||||||||||||||||||
Sbjct  1534  ATTATTGTACAAGATAATGGTCAGGGTATTTCTAAAGATAAAATGCATTTGTTGGGAGAA  1593

Query  709   ACATCTGTAGAA  720
             ||||||||||||
Sbjct  1594  ACATCTGTAGAA  1605
```

LytR

ggGAtTGTGAGCGgAtaacaaTTCCCCTCTAGAAATAATTTTGTTTAACTTTAAGAAGGAGATATACaT **pET26b**

ATGAAAGCATTAATCATAGATGATGAGCCATTAGCACGTAATGAATTAACATATTTATTAAATGAAAT
TGGTGGTTTTGAAGAAATTAATGAGGCAGAAAATGTAAAAGAAACATTGGAAGCACTACTGATCA
ATCAATATGACATTATATTTTTAGATGTCAATTTAATGGATGAAAATGGGATCGAATTAGGAGCTAAG
ATTCAAAAGATGAAAGAGCCACCTGCGATTATTTTTGCAACTGCACATGACCAATACGCAGTACAG
GCATTTGAATTAAATGCGACAGACTATATTTTGAAACCGTTTGGTCAAAAACGTATTGAACAAGCAG
TCAATAAAGTGCGTGCGACTAAAGCCAAAGATGATAATAACGCAAGTGCAATTGCGAATGATATGTC
GGCGAATTTTGATCAAAGCTTACCTGTTGAAATTGACGATAAAATTCACATGTTAAAGCAACAAAATA
TTATTGGGATTGGCACACATAATGGTATTACAACCATACATACAACGAATCATAAATACGAAACAACAG
AGCCATTGAATCGTTATGAAAAACGATTGAATCCCACTTATTTTATACGTATTCATCGTTCATATATTATTA
ACACGAAACACATTAAAGAAGTGCAACAATGGTTTAACTACaCTTATATGGtAataTTGACAAATGGtGtc

LytR

Sequence ID: lcl|64463 Length: 741 Number of Matches: 1

Range 1: 1 to 681 Graphics ▼ Next Match ▲ Previous Match

Score	Expect	Identities	Gaps	Strand
1258 bits(681)	0.0	681/681(100%)	0/681(0%)	Plus/Plus

```
Query  70   ATGAAAGCATTAATCATAGATGATGAGCCATTAGCACGTAATGAATTAACATATTTATTA  129
            ||||||||||||||||||||||||||||||||||||||||||||||||||||||||||||
Sbjct  1    ATGAAAGCATTAATCATAGATGATGAGCCATTAGCACGTAATGAATTAACATATTTATTA  60

Query  130  AATGAAATTGGTGGTTTTGAAGAAATTAATGAGGCAGAAAATGTAAAAGAAACATTGGAA  189
            ||||||||||||||||||||||||||||||||||||||||||||||||||||||||||||
Sbjct  61   AATGAAATTGGTGGTTTTGAAGAAATTAATGAGGCAGAAAATGTAAAAGAAACATTGGAA  120

Query  190  GCACTACTGATCAATCAATATGACATTATATTTTTAGATGTCAATTTAATGGATGAAAAT  249
            ||||||||||||||||||||||||||||||||||||||||||||||||||||||||||||
Sbjct  121  GCACTACTGATCAATCAATATGACATTATATTTTTAGATGTCAATTTAATGGATGAAAAT  180

Query  250  GGGATCGAATTAGGAGCTAAGATTCAAAAGATGAAAGAGCCACCTGCGATTATTTTTGCA  309
            ||||||||||||||||||||||||||||||||||||||||||||||||||||||||||||
Sbjct  181  GGGATCGAATTAGGAGCTAAGATTCAAAAGATGAAAGAGCCACCTGCGATTATTTTTGCA  240

Query  310  ACTGCACATGACCAATACGCAGTACAGGCATTTGAATTAAATGCGACAGACTATATTTTG  369
            ||||||||||||||||||||||||||||||||||||||||||||||||||||||||||||
Sbjct  241  ACTGCACATGACCAATACGCAGTACAGGCATTTGAATTAAATGCGACAGACTATATTTTG  300

Query  370  AAACCGTTTGGTCAAAAACGTATTGAACAAGCAGTCAATAAAGTGCGTGCGACTAAAGCC  429
            ||||||||||||||||||||||||||||||||||||||||||||||||||||||||||||
Sbjct  301  AAACCGTTTGGTCAAAAACGTATTGAACAAGCAGTCAATAAAGTGCGTGCGACTAAAGCC  360

Query  430  AAAGATGATAATAACGCAAGTGCAATTGCGAATGATATGTCGGCGAATTTTGATCAAAGC  489
            ||||||||||||||||||||||||||||||||||||||||||||||||||||||||||||
Sbjct  361  AAAGATGATAATAACGCAAGTGCAATTGCGAATGATATGTCGGCGAATTTTGATCAAAGC  420

Query  490  TTACCTGTTGAAATTGACGATAAAATTCACATGTTAAAGCAACAAAATATTATTGGGATT  549
            ||||||||||||||||||||||||||||||||||||||||||||||||||||||||||||
Sbjct  421  TTACCTGTTGAAATTGACGATAAAATTCACATGTTAAAGCAACAAAATATTATTGGGATT  480

Query  550  GGCACACATAATGGTATTACAACCATACATACAACGAATCATAAATACGAAACAACAGAG  609
            ||||||||||||||||||||||||||||||||||||||||||||||||||||||||||||
Sbjct  481  GGCACACATAATGGTATTACAACCATACATACAACGAATCATAAATACGAAACAACAGAG  540

Query  610  CCATTGAATCGTTATGAAAAACGATTGAATCCCACTTATTTTATACGTATTCATCGTTCA  669
            ||||||||||||||||||||||||||||||||||||||||||||||||||||||||||||
Sbjct  541  CCATTGAATCGTTATGAAAAACGATTGAATCCCACTTATTTTATACGTATTCATCGTTCA  600

Query  670  TATATTATTAACACGAAACACATTAAAGAAGTGCAACAATGGTTTAACTACACTTATATG  729
            ||||||||||||||||||||||||||||||||||||||||||||||||||||||||||||
Sbjct  601  TATATTATTAACACGAAACACATTAAAGAAGTGCAACAATGGTTTAACTACACTTATATG  660

Query  730  GTAATATTGACAAATGGTGTC  750
            |||||||||||||||||||||
Sbjct  661  GTAATATTGACAAATGGTGTC  681
```

GST- LytR

CTGGTTCCGCGTGGATCC — **pGEX4T-1**

ATGAAAGCATTAATCATAGATGATGAGCCATTAGCACGTAATGAATTAACATATTTATTAAATGAAATTGGTGGT
TTTGAAGAAATTAATGAGGCAGAAAATGTAAAAGAAACATTGGAAGCMCTACTGATCAATCAATATGACATTA
TATTTTTAGATGTCAATTTAATGGATGAAAATGGGATCGAATTAGGAGCTAAGATTCAAAAGATGAAAGAGCC
ACCTGCGATTATTTTTGCAACTGCMCATGACCAATACGCAGTACAGGCATTTGAATTAAATGCGACAGACTATA
TTTTGAAACCGTTTGGTCAAAAACGTATTGAACAAGCAGTCAATAAAGTGCGTGCGACTAAAGCCAAAGATG
ATAATAACGCAAGTGCAATTGCGAATGATATGTCGGCGAATTTTGATCAAAGCTTACCTGTTGAAATTGACGAT
AAAATTCACATGTTAAAGCAACAAAATATTATTGGGATTGGCACACATAATGGTATTACAACCATACATACAACG
AATCATAAATACGAAACAACAGAGCCATTGAATCGTTATGAAAAACGATTGAATCCCACTTATTTTATACGTATT
CATCGTTCATATATTATTAACACGAAACACATTAAAGAAGTGCAACAATGGTTTAACTACACTTATATGGTAATAT
TGACAAATGGTGTCAAGATGCAAGTTGGACGTTCATTTATGAAAGATTTTAAAGCGTCGATAGGATTACTTTAA — **LytR**

TAAGAATTCCCGGGTCGACTCGAGCGGCCGCATCGTGACTGACTGACGATCTGCCTCGCGCGTTTCGGTGAT
GACGGTGAAAACCTCTGACACATGCAGCTCCCGGAGACGGTCACAGCTTGTCTGTAAGCGGATGCCGGGAG
CAKACAAGCCCGTCAGGCGCGTCAGCGGGTGTTGGCGGGTGTCGGGCKCATCATGACCMGTCACGTAG — **pGEX4T-1**

CTCGGATCTGGTTCCGCGTGGATCC — **pGEX4T-1**

ATGAAAGCATTAATCATAGATGA
TGAGCCATTAGCACGTAATGAATTAACATATTTATTAAATGAAATTGGTGGTTTTGAAGA
AATTAATGAGGCAGAAAATGTAAAAGAAACATTGGAAGCACTACTGATCAATCAATATGA
CATTATATTTTTA **GCT** GTCAATTTAATGGATGAAAATGGGATCGAATTAGGAGCTAAGAT
TCAAAAGATGAAAGAGCCMCCTGCGATTATTTTTGCAACTGCACATGACCAATACGCAGT
ACAGGCATTTGAATTAAATGCGACAGACTATATTTTGAAACCGTTTGGTCAAAAACGTAT
TGAACAAGCAGTCAATAAAGTGCGTGCGACTAAAGCCAAAGATGATAATAACGCAAGTGC
AATTGCGAATGATATGTCGGCGAATTTTGATCAAAGCTTACCTGTTGAAATTGACGATAA
AATTCACATGTTAAAGCAACAAAATATTATTGGGATTGGCACACATAATGGTATTACAAC
CATACATACAACGAATCATAAATACGAAACAACAGAGCCATTGAATCGTTATGAAAAACG
ATTGAATCCCACTTATTTTATACGTATTCATCGTTCATATATTATTAACACGAAACACAT
TAAAGAAGTGCAACAATGGTTTAACTACACTTATATGGTAATATTGACAAATGGTGTCAA
GATGCAAGTTGGACGTTCATTTATGAAAGATTTTAAAGCGTCGATAGGATTACTTTAA — **GST-LytR (D53A)**

TAAGAATTCCCGGGTCGACTCGAGCGGCCGCATCGTGACTGACTGACGATCTGCCTCGC
GCGTTTCGGTGATGACGGTGAAAACCTCTGACACATGCAGCTCCCGGAG — **pGEX4T-1**

Bolded and underlined nucleotides show desired mutation

$LytR^N$

AATAATTTTGTTTAACTTTAAGAAGGAGATATACAT — **pET26b**

ATGAAAGCATTAATCATAGATGATGAGCCATTAGCACGTAATGAATTAACATATTTATTAAATGAAATT
GGTGGTTTTGAAGAAATTAATGAGGCAGAAAATGTAAAAGAAACATTGGAAGCACTACTGATCAAT
CAATATGACATTATATTTTTAGATGTCAATTTAATGGATGAAAATGGGATCGAATTAGGAGCTAAGATT
CAAAAGATGAAAGAGCCACCTGCGATTATTTTTGCMACTGCACATGACCAATACGCAGTACAGGCAT
TTGAATTAAATGCGACAGACTATATTTTGAAACCGTTTGGTCAAAAACGTATTGAACAAGCAGTCAAT
AAAGTGCGTGCGACTAAAGCCAAAGATGATAATAACGCAAGTGCAATTGCGAATGATATGTCG**TAG**A
ATTTTGATCAAAGCTTACCTGTTGAAATTGACGATAAAATTCACATGTTAAAGCAACAAAATATTATTG
GGATTGGCACACATAATGGTATTACAACCATACATACAACGAATCATAAATACGAAACAACAGAGCCA
TTGAATCGTTATGAAAAACGATTGAATCCCACTTATTTTATACGTATTCATCGTTCATATATTATTAACAC
GAAACACATTAAAGAAGTGCAACAATGGTTTAACTACACTTATATGGTAATATTGACAAATGGTGTCA
AGATGCAAGTTGGACGTTCATTTATGAAAGATTTTAAAGCGTCGATAGGATTACTTTAATAAGAATTC

— **$LytR^N$ (A135*)**

GAGCTCCGTCGACAAGCTTGCGGCCGCACTCGAGCACCACCACCACCACCACTGAGATCCGGCTGC
TAACAAAGCCCGAAAGGAAGCTGAGTTGGCTGCTGCCACCGCTGAGC — **pET26b**

Bolded and underlined nucleotides show desired mutation

$LytR^C$

GGCTTTGTTAGCAGCCGGATCTCASTGGTGGTGGTGGTGGTGCTCGAGTGCGGCCSCAWKCTTG
TCSACGGAGCTCGAATTCTTA — **pET26b**

TTAAAGTAATCCTATCGACGCTTTAAAATCTTTCATAAATGAACGTCCAACTTGCATCTTGACACC
ATTTGTCAATATTACCATATAAGTGTAGTTAAACCATTGTTGCACTTCTTTAATGTGTTTCGTGTT
AATAATATATGAACGATGAATACGTATAAAATAAGTGGGATTCAATCGTTTTTCATAACGATTCA
ATGGCTCTGTTGTTTCGTATTTATGATTCGTTGTATGTATGGTTGTAATACCATTATGTGTGCCAAT
CCCAATAATATTTTGTTGCTWTAA

— **$LytR^C$ (bp 404-741)**

Figure A3 : Protein sequencing results for WalK and WalR

WalK

>sp|Q7A305|WALK_STAAM Sensor protein kinase WalK OS=Staphylococcus aureus (strain Mu50 / ATCC 700699) GN=walK PE=3 SV=1

MKWLKQLQSLHTKLVIVYVLLIIIGMQIIGLYFTNNLEKELLDNFKKNITQYAKQLEISI
EKVYDEKGSVNAQKDIQNLLSEYANRQEIGEIRFIDKDQIIIATTKQSNRSLINQKANDS
SVQKALSLGQSNDHLILKDYGGGKDRVWVYNIPVKVDKKVIGNIYIESKINDVYNQLNNI
NQIFIVGTAISLLITVILGFFIARTITKPITDMRNQTVEMSRGNYTQRVKIYGNDEIGEL
ALAFNNLSKRVQEAQANTESEKRRLDSVITHMSDGIIATDRRGRIRIVNDMALKMLGMAK
EDIIGYYMLSVLSLEDEFKLEEIQENNDSFLLDLNEEEGLIARVNFSTIVQETGFVTGYI
AVLHDVTEQQQVERERREFVANVSHELRTPLTSMNSYIEALEEGAWKDEELAPQFLSVTR
EETERMIRLVNDLLQLSKMDNESDQINKEIIDFNMFINKIINRHEMSAKDTTFIRDIPKK
TIFTEFDPDKMTQVFDNVITNAMKYSRGDKRVEFHVKQNPLYNRMTIRIKDNGIGIPINK
VDKIFDRFYRVDKARTRKMGGTGLGLAISKEIVEAHNGRIWANSVEGQGTSIFITLPCEV
IEDGDWDE

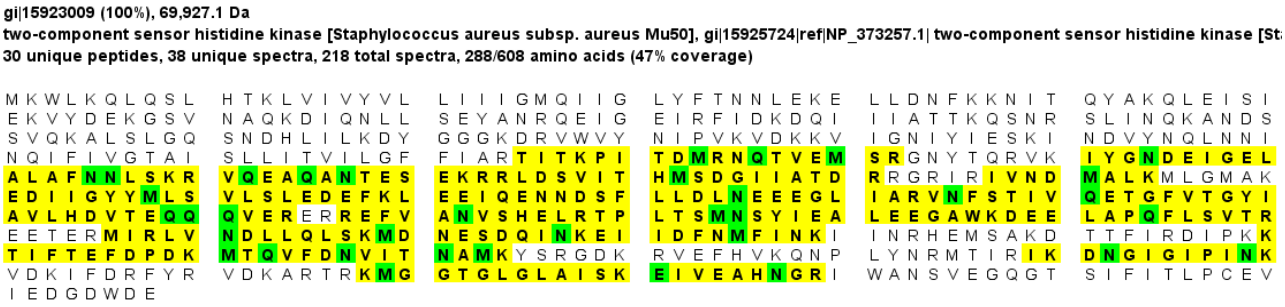

WalR

>sp|Q99XF3|WALR_STAAM Transcriptional regulatory protein WalR OS=Staphylococcus aureus (strain Mu50 / ATCC 700699) GN=walR PE=1 SV=2

MARKVVVVDDEKPIADILEFNLKKEGYDVYCAYDGNDAVDLIYEEEPDIVLLDIMLPGRD
GMEVCREVRKKYEMPIIMLTAKDSEIDKVLGLELGADDYVTKPFSTRELIARVKANLRRH
YSQPAQDTGNVTNEITIKDIVIYPDAYSIKKRGEDIELTHREFELFHYLSKHMGQVMTRE
HLLQTVWGYDYFGDVRTVDVTIRRLREKIEDDPSHPEYIVTRRGVGYFLQQHE

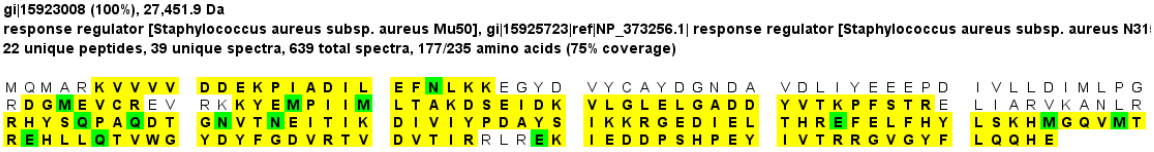

Figure A4 : Protein sequencing results for LytS and LytR and ESI-MS mass anlaysis of $LytR^N$

LytS

>sp|P60612|LYTS_STAAM Sensor protein LytS OS=Staphylococcus aureus (strain Mu50 / ATCC 700699) GN=lytS PE=3 SV=1

MLSLTMLLLERVGLIIILAYVLMNIPYFKNLMNRRRTWKARWQLCIIFSLFALMSNLTGIVIDHQHSLSGSV
YFRLDDDVSLANTRVLTIGVAGLVGGPFVGLFVGVISGIFRVYMGGADAQVYLISSIFIGIIAGYFGLQAQR
RKRYPSIAKSAMIGIVMEMIQMLSILTFSHDKAYAVDLISLIALPMIIVNSVGTAIFMSIIISTLKQEEQMK
AVQTHDVLQLMNQTLPYFKEGLNRESAQQIAMIIKNLMKVSAVAITSKNEILSHVGAGSDHHIPTNEILTSL
SKDVLKSGKLKEVHTKEEIGCSHPNCPLRAAIVIPLEMHGSIVGTLKMYFTNPNDLTFVERQLAEGLANIFS
SQIELGEAETQSKLLKDAEIKSLQAQVSPHFFFNSINTISALVRINSEKARELLLELSYFFRANLQGSKQHT
ITLDKELSQVRAYLSLEQARYPGRFNININVEDKYRDVLVPPFLIQILVENAIKHAFTNRKQGNDIDVSVIK
ETATHVRIIVQDNGQGISKDKMHLLGETSVESESGTGSALENLNLRLKGLFGKSAALQFESTSSGTTFWCVL
PYERQEEE

gi|15923250 (100%), 65,031.3 Da
two-component sensor histidine kinase [Staphylococcus aureus subsp. aureus Mu50]
11 unique peptides, 16 unique spectra, 51 total spectra, 135/584 amino acids (23% coverage)

MLSLTMLLLE	RVGLIIILAY	VLMNIPYFKN	LMNRRRTWKA	RWQLCIIFSL	FALMSNLTGI	
VIDHQHSLSG	SVYFRLDDDV	SLANTRVLTI	GVAGLVGGPF	VGLFVGVISG	IFRVYMGGAD	
AQVYLISSIF	IGIIAGYFGL	QAQRRKRYPS	IAKSAMIGIV	MEMIQMLSIL	TFSHDKAYAV	
DLISLIALPM	IIVNSVGTAI	FMSIIISTLK	QEEQMKAVQT	HDVLQLMNQT	LPYFKEGLNR	
ESAQQIAMII	KNLMKVSAVA	ITSKNEILSH	VGAGSDHHIP	TNEILTSLSK	DVLKSGKLKE	
VHTKEEIGCS	HPNCPLRAAI	VIPLEMHGSI	VGTLKMYFTN	PNDLTFVERQ	LAEGLANIFS	
SQIELGEAET	QSKLLKDAEI	K**SLQAQVSPH**	**FFFNSINTIS**	**ALVR**INSEKA	R**ELLLELSYF**	
FRANLQGSK**Q**	**HTITLDKELS**	**QVR**AYLSLEQ	ARYPGR**FN**IN	**I**NVEDK**YRDV**	**LVPPFLIQIL**	
VENAIKHAFT	NRK**QGNDIDV**	**SVIKETATHV**	**RIIVQDNGQG**	**ISKDKMHLLG**	**ETSVESESGT**	
GSALENLNLR	LKGLFGKSAA	LQFESTSSGT	TFWCVLPYER	QEEE		

Note that the sequence coverage is more than 50% because only the cytoplasmic domain is cloned.

LytR

>sp|P60609|LYTR_STAAM Sensory transduction protein LytR OS=Staphylococcus aureus (strain Mu50 / ATCC 700699) GN=lytR PE=3 SV=1

MKALIIDDEPLARNELTYLLNEIGGFEEINEAENVKETLEALLINQYDIIFLDVNLMDEN
GIELGAKIQKMKEPPAIIFATAHDQYAVQAFELNATDYILKPFGQKRIEQAVNKVRATKA
KDDNNASAIANDMSANFDQSLPVEIDDKIHMLKQQNIIGIGTHNGITTIHTTNHKYETTE
PLNRYEKRLNPTYFIRIHRSYIINTKHIKEVQQWFNYTYMVILTNGVKMQVGRSFMKDFK
ASIGLL

gi|15923251 (100%), 28,222.8 Da
two-component response regulator [Staphylococcus aureus subsp. aureus Mu50]
12 unique peptides, 15 unique spectra, 31 total spectra, 131/246 amino acids (53% coverage)

MK**ALIIDDEP**	**LAR**NELTYLL	NEIGGFEEIN	EAENVKETLE	ALLINQYDII	FLDVNLMDEN	
GIELGAKIQK	**MKEPPAIIFA**	**TAHDQYAVQA**	**FELNATDYIL**	**KPFGQK**RIEQ	AVNKVRATK**A**	
KDDNNASAIA	**NDMSANFDQS**	**LPVEIDDKIH**	**MLKQQNIIGI**	**GTHNGITTIH**	**TTNHKYETTE**	
PLNRYEKRLN	**PTYFIR**IHRS	YIINTKHIKE	VQQWFNYTYM	VILTNGVKMQ	VGR**SFMKDFK**	
ASIGLL						

$LytR^N$ Mass analysis

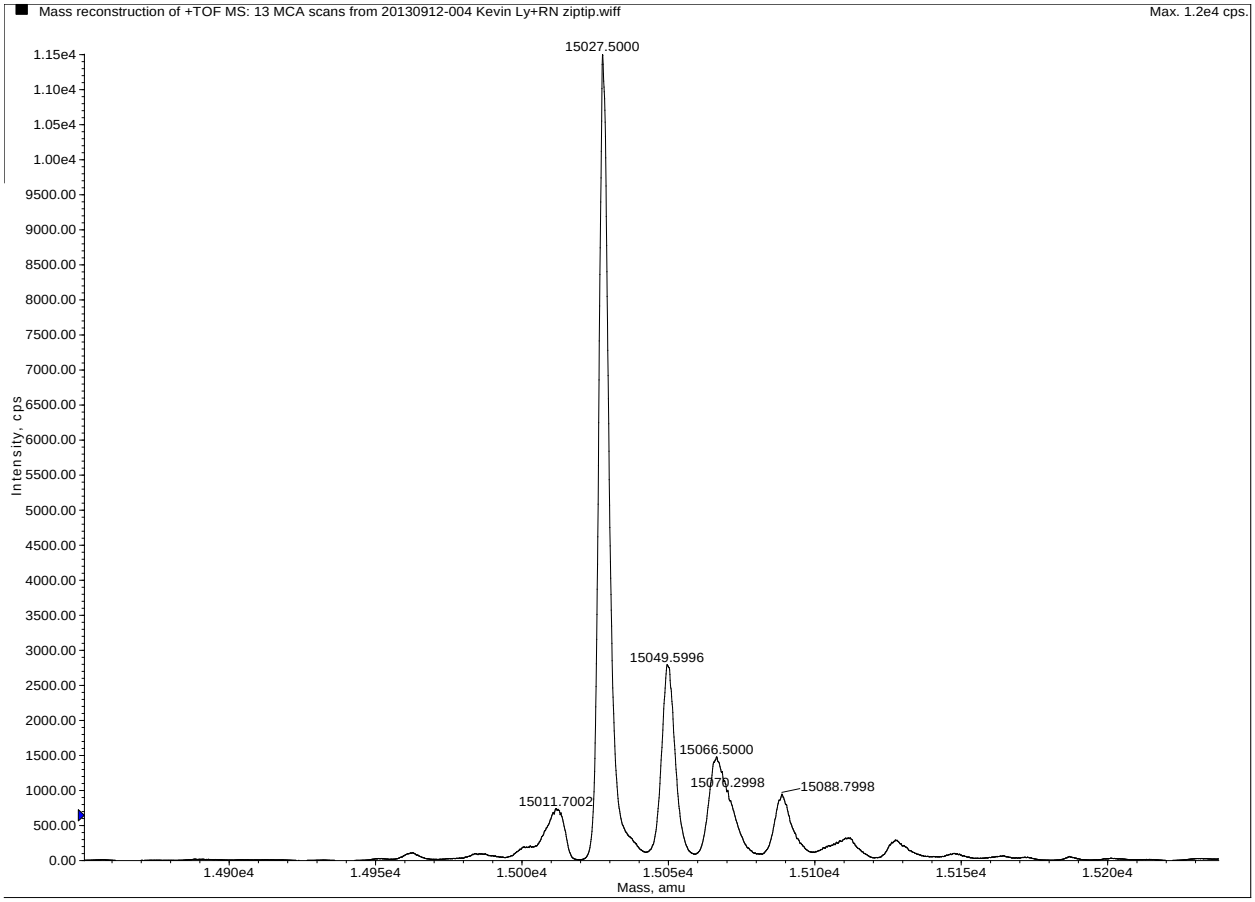

Appendix B

Figure B1 : Crystal structure of $LytR^{N}$, B2: Solved 3D structure of $LytR^{N}$, B3 : Active site residues of $LytR^{N}$, and B4 : $Mg2^{+}$ ion coordination by Asp residues.

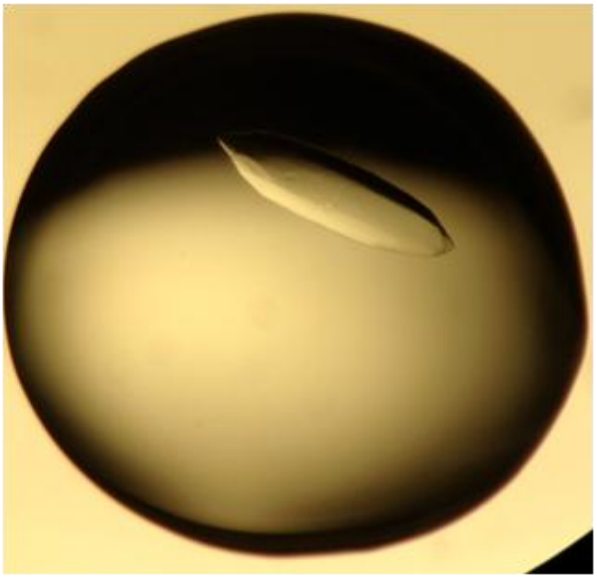

Figure B1

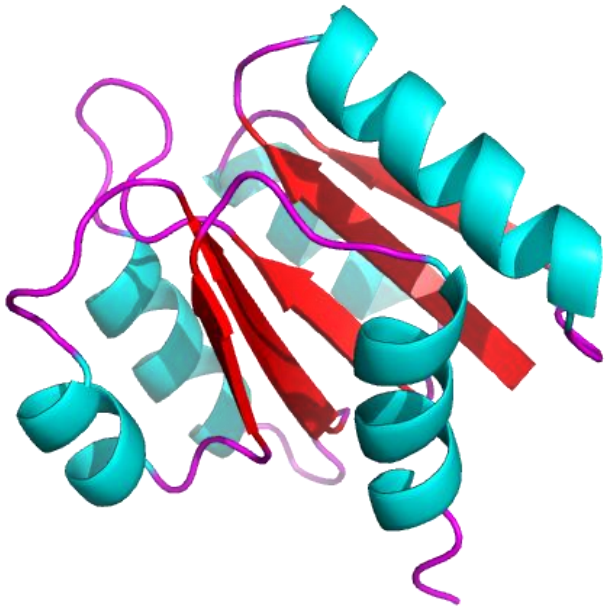

Figure B2

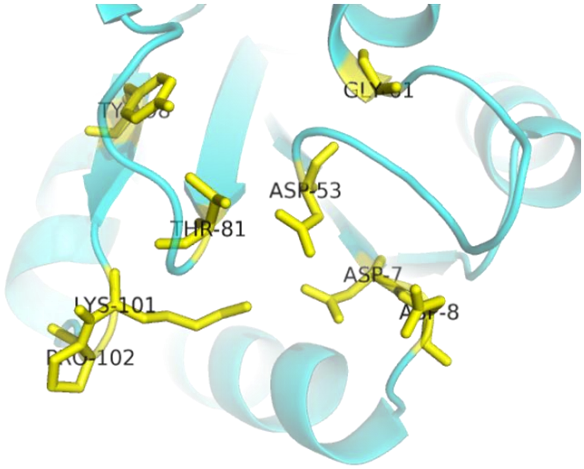

Figure B3

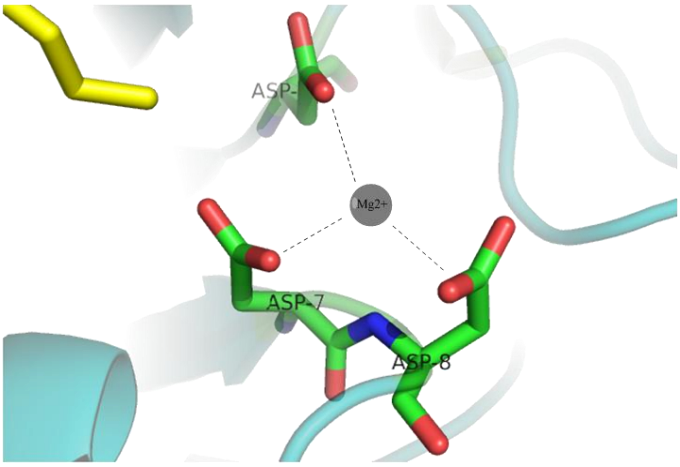

Figure B4

Appendix C

Figure C1 : Band intensity of phosphorylated His-LytS quantified using ImageJ and plotted against time. The data were fitted using Origin software to pseudo first order equation to calculate rate constant.

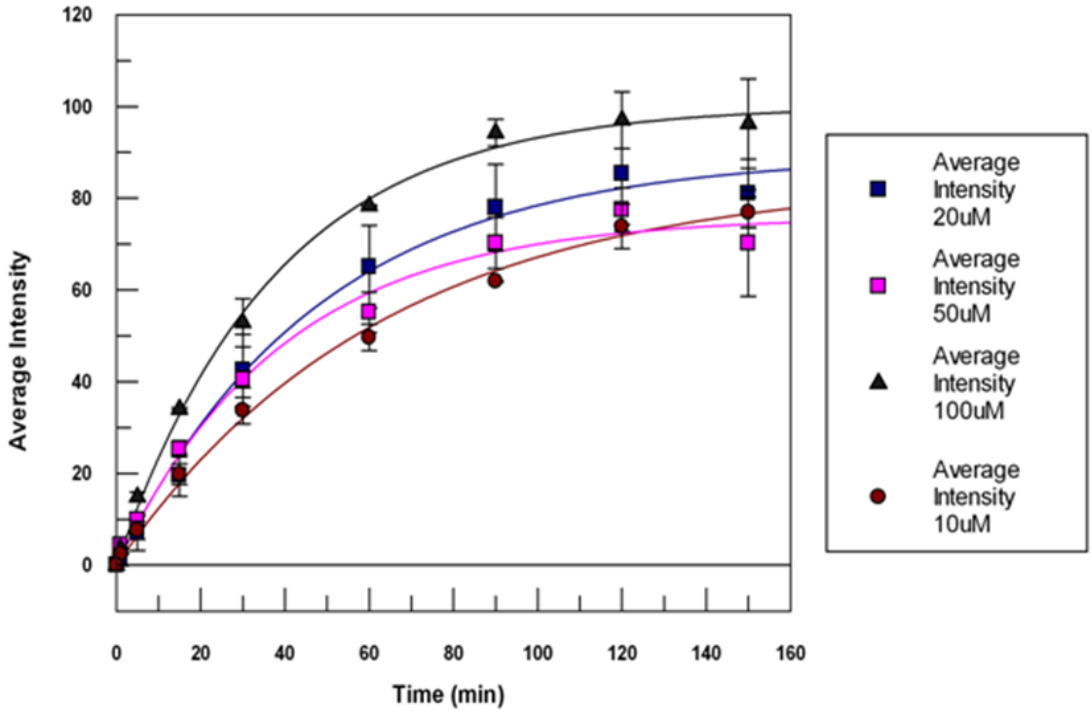

Figure C2 : Band intensity of LytR and LytR^{N} phosphoryalted by acetyl phosphate were quantified using ImageJ and plotted against time. The data were fitted using Origin software to pseudo first order equation to calculate rate constant.

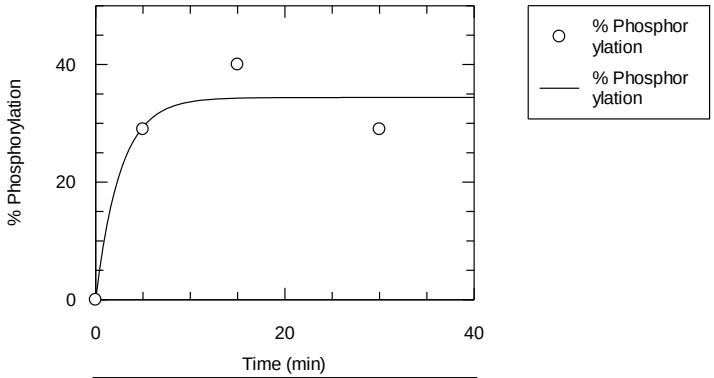

Parameter	Value	Std. Error
rate constant	0.3847	0.2656
proportionality constant	34.3894	4.0528

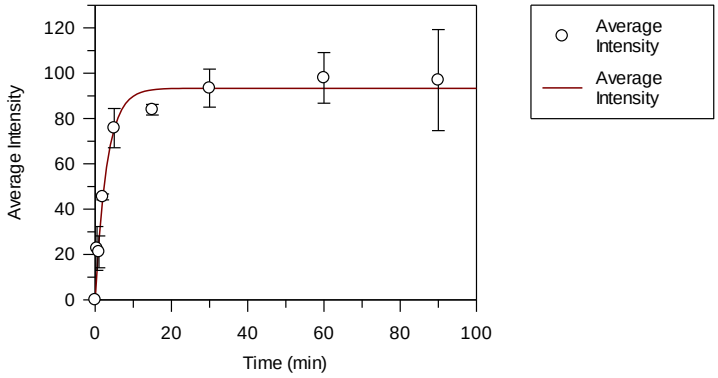

Parameter	Value	Std. Error
Rate sonstant	0.3287	0.0398
Proportionality constant	93.3515	2.7509